Elastohydrodynamic lubrication with mixtures of oil and operating fluids: an industrial challenge

Fan Zhang

▶ **To cite this version:**

Fan Zhang. Elastohydrodynamic lubrication with mixtures of oil and operating fluids: an industrial challenge. Fluids mechanics [physics.class-ph]. Institut National des Sciences Appliquées de Lyon, 2022. English. NNT : . tel-04492782

HAL Id: tel-04492782
https://hal.science/tel-04492782

Submitted on 6 Mar 2024

HAL is a multi-disciplinary open access archive for the deposit and dissemination of scientific research documents, whether they are published or not. The documents may come from teaching and research institutions in France or abroad, or from public or private research centers.

L'archive ouverte pluridisciplinaire **HAL**, est destinée au dépôt et à la diffusion de documents scientifiques de niveau recherche, publiés ou non, émanant des établissements d'enseignement et de recherche français ou étrangers, des laboratoires publics ou privés.

N°d'ordre NNT : 2022ISAL0121

THESE de DOCTORAT DE L'INSA LYON, membre de l'Université de Lyon

Ecole Doctorale N° 162
Mécanique, Energétique, Génie civil, Acoustique (MEGA)

Spécialité/ discipline de doctorat :
Génie Mécanique

Soutenue publiquement le 08/12/2022, par :
Fan ZHANG

Elastohydrodynamic lubrication with mixtures of oil and operating fluids: an industrial challenge

---

Devant le jury composé de :

CAYER-BARRIOZ, Juliette	Directeur de Recherche	École Centrale de Lyon	Présidente de jury
ARGHIR, Mihaï	Professeur	Université de Poitiers	Rapporteur
HARTL, Martin	Professeur	Brno University of Technology	Rapporteur
BRUYERE, Vincent	Docteur	SIMTEC	Examinateur
FILLOT, Nicolas	Maître de conférences HDR	INSA-LYON	Directeur de thèse
MORALES-ESPEJEL, Guillermo	HDR	SKF	Encadrant industriel

Département FEDORA – INSA Lyon - Ecoles Doctorales

SIGLE	ECOLE DOCTORALE	NOM ET COORDONNEES DU RESPONSABLE
CHIMIE	**CHIMIE DE LYON** **https://www.edchimie-lyon.fr** Sec. : Renée EL MELHEM Bât. Blaise PASCAL, 3e étage secretariat@edchimie-lyon.fr	**M. Stéphane DANIELE** C2P2-CPE LYON-UMR 5265 Bâtiment F308, BP 2077 43 Boulevard du 11 novembre 1918 69616 Villeurbanne **directeur@edchimie-lyon.fr**
E.E.A.	**ÉLECTRONIQUE, ÉLECTROTECHNIQUE, AUTOMATIQUE** **https://edeea.universite-lyon.fr** Sec. : Stéphanie CAUVIN Bâtiment Direction INSA Lyon Tél : 04.72.43.71.70 secretariat.edeea@insa-lyon.fr	**M. Philippe DELACHARTRE** INSA LYON Laboratoire CREATIS Bâtiment Blaise Pascal, 7 avenue Jean Capelle 69621 Villeurbanne CEDEX Tél : 04.72.43.88.63 **philippe.delachartre@insa-lyon.fr**
E2M2	**ÉVOLUTION, ÉCOSYSTÈME, MICROBIOLOGIE, MODÉLISATION** **http://e2m2.universite-lyon.fr** Sec. : Bénédicte LANZA Bât. Atrium, UCB Lyon 1 Tél : 04.72.44.83.62 secretariat.e2m2@univ-lyon1.fr	**Mme Sandrine CHARLES** Université Claude Bernard Lyon 1 UFR Biosciences Bâtiment Mendel 43, boulevard du 11 Novembre 1918 69622 Villeurbanne CEDEX **sandrine.charles@univ-lyon1.fr**
EDISS	**INTERDISCIPLINAIRE SCIENCES-SANTÉ** **http://ediss.universite-lyon.fr** Sec. : Bénédicte LANZA Bât. Atrium, UCB Lyon 1 Tél : 04.72.44.83.62 secretariat.ediss@univ-lyon1.fr	**Mme Sylvie RICARD-BLUM** Institut de Chimie et Biochimie Moléculaires et Supramoléculaires (ICBMS) - UMR 5246 CNRS - Université Lyon 1 Bâtiment Raulin - 2ème étage Nord 43 Boulevard du 11 novembre 1918 69622 Villeurbanne Cedex Tél : +33(0)4 72 44 82 32 **sylvie.ricard-blum@univ-lyon1.fr**
INFOMATHS	**INFORMATIQUE ET MATHÉMATIQUES** **http://edinfomaths.universite-lyon.fr** Sec. : Renée EL MELHEM Bât. Blaise PASCAL, 3e étage Tél : 04.72.43.80.46 infomaths@univ-lyon1.fr	**M. Hamamache KHEDDOUCI** Université Claude Bernard Lyon 1 Bât. Nautibus 43, Boulevard du 11 novembre 1918 69 622 Villeurbanne Cedex France Tél : 04.72.44.83.69 **hamamache.kheddouci@univ-lyon1.fr**
Matériaux	**MATÉRIAUX DE LYON** **http://ed34.universite-lyon.fr** Sec. : Yann DE ORDENANA Tél : 04.72.18.62.44 yann.de-ordenana@ec-lyon.fr	**M. Stéphane BENAYOUN** Ecole Centrale de Lyon Laboratoire LTDS 36 avenue Guy de Collongue 69134 Ecully CEDEX Tél : 04.72.18.64.37 **stephane.benayoun@ec-lyon.fr**
MEGA	**MÉCANIQUE, ÉNERGÉTIQUE, GÉNIE CIVIL, ACOUSTIQUE** **http://edmega.universite-lyon.fr** Sec. : Stéphanie CAUVIN Tél : 04.72.43.71.70 Bâtiment Direction INSA Lyon mega@insa-lyon.fr	**M. Jocelyn BONJOUR** INSA Lyon Laboratoire CETHIL Bâtiment Sadi-Carnot 9, rue de la Physique 69621 Villeurbanne CEDEX **jocelyn.bonjour@insa-lyon.fr**
ScSo	**ScSo*** **https://edsciencessociales.universite-lyon.fr** Sec. : Mélina FAVETON INSA : J.Y. TOUSSAINT Tél : 04.78.69.77.79 melina.faveton@univ-lyon2.fr	**M. Bruno MILLY** Université Lumière Lyon 2 86 Rue Pasteur 69365 Lyon CEDEX 07 **bruno.milly@univ-lyon2.fr**

*ScSo : Histoire, Géographie, Aménagement, Urbanisme, Archéologie, Science politique, Sociologie, Anthropologie

Abstract

The fluid that separates the contacting elements in many industrial applications is often a mixture of oil and operating fluids. This work aims to provide a better understanding of lubrication with mixtures in elastohydrodynamic contacts in order to anticipate appropriate lubrication system performance. The oil/refrigerant mixture and the oil/water mixture, representing respectively miscible fluids and immiscible fluids, are thoroughly investigated in this study. The essential questions differ depending on the characteristics of the mixtures.

The main issue for oil/refrigerant solution is at the contact outlet, where the refrigerant may evaporate. An original cavitation modeling with thermal effects for oil/refrigerant solutions is reported in this work. A comparison with other cavitation models from the literature is made, highlighting the necessity of considering the refrigerant solubility in oil for such problems. Indeed oil/refrigerant mixtures may dramatically reduce the amount of liquid oil for the next contact compared to the case of pure oil cavitation.

Besides this, the problem of water droplets in oil emulsion is addressed at the contact inlet to evaluate the risks of water droplet contamination. A micro-sized water-in-oil emulsion flow is directly observed at the EHL point contact inlet. In parallel, a numerical approach was developed to investigate the impacts of various operating parameters on the flow of water-in-oil emulsion. The results of this work give a possible explanation for the contradictory findings in the literature and reveal the critical conditions under which water-in-oil emulsion would influence the EHL contacts.

Keywords— Computational Fluid Dynamics, Fluid mechanics, Two-phase flow, Thermal effects, Numerical modeling, Emulsion, Mixture lubricant, Cavitation, Lubrication, Elastohydrodynamic

Résumé

Le fluide qui sépare les éléments en contact dans de nombreuses applications industrielles est souvent un mélange d'huile et de fluides environnants. Ce travail vise à fournir une meilleure compréhension de la lubrification avec des mélanges dans les contacts élastohydrodynamiques afin d'anticiper les performances du système. Le mélange huile/réfrigérant et le mélange huile/eau, représentant respectivement des fluides miscibles et des fluides non miscibles, sont étudiés de manière approfondie dans cette étude. Les questions essentielles diffèrent en fonction des caractéristiques des mélanges.

Dans le cas d'une solution huile/réfrigérant, la principale question se pose à la sortie du contact, où le réfrigérant peut s'évaporer. Une modélisation originale de la cavitation incluant des effets thermiques est rapportée dans ce travail. Une comparaison avec d'autres modèles de cavitation de la littérature est proposée, soulignant la nécessité de considérer la solubilité du réfrigérant dans l'huile pour de tels problèmes. En effet, les mélanges huile/réfrigérant peuvent réduire considérablement la quantité d'huile liquide pour le prochain contact par rapport à la cavitation de l'huile pure.

De manière tout à fait différente, le problème des gouttelettes d'eau dans l'émulsion d'huile est abordé à l'entrée du contact pour évaluer les risques de contamination. Des gouttelettes d'eau dans l'huile de tailles microscopiques sont observées directement à l'entrée du contact EHL. Une approche numérique a été développée pour étudier les impacts de divers paramètres de fonctionnement sur l'écoulement de l'émulsion. Les résultats de ce travail donnent une explication possible aux conclusions parfois contradictoires de la littérature, et révèlent les conditions critiques dans lesquelles l'émulsion «eau-dans-huile» influencerait les contacts EHD.

Mots-clés— Dynamique des fluides numérique, Mécanique des fluides, Ecoulement diphasique, Effets thermiques, Modélisation numérique, Emulsion, Mélange lubrifiant, Cavitation, Lubrification, Elastohydrodynamique

Remerciements

Je tiens à exprimer ma profonde reconnaissance à mes encadrants de thèse, Nicolas FILLOT et Guillermo MORALES-ESPEJEL, pour leur soutien indéfectible et leur disponibilité tout au long de cette aventure de thèse. Leur guidance et leurs conseils précieux ont été essentiels à la réalisation de ce travail.

Je tiens également à remercier chaleureusement tous les membres de mon jury, Juliette CAYER-BARRIOZ, Mihaï ARGHIR, Martin HARTL et Vincent BRUYERE pour leur temps et leur engagement dans l'évaluation de ma thèse. Leurs remarques et suggestions ont été précieuses et ont contribué à améliorer significativement mon travail.

Je suis également reconnaissant envers mes collègues de recherche, pour leur soutien et leur camaraderie durant cette période de travail intense. Leur présence et leurs encouragements ont été précieux pour moi.

Enfin, je tiens à remercier toutes les personnes qui, de près ou de loin, ont contribué à la réalisation de cette thèse.

Je termine en remerciant ma famille et mes amis pour leur soutien constant et leur patience durant cette période de ma vie. Je n'aurais pas pu y arriver sans eux.

Contents

List of Figures

List of Tables

Nomenclature

α	Piezo-viscosity coefficient	1/Pa
α_g	Volume fraction of gaseous phase in total mixture	–
α_{ml}	Volume fraction of liquid oil/refrigerant solution in total mixture	–
α_{rg}	Volume fraction of gaseous refrigerant in total mixture	–
β	Thermal expansion coefficient	1/K
$\boldsymbol{v_d}$	Velocity vector of droplets	m/s
$\boldsymbol{v_{oil}}$	Velocity vector of oil	m/s
$\boldsymbol{v_r}$	Relative velocity vector of droplets	m/s
$\boldsymbol{F_B}$	Buoyancy force vector	N
$\boldsymbol{F_D}$	Drag force vector	N
$\boldsymbol{F_G}$	Gravitational force vector	N
$\boldsymbol{F_{st}}$	Surface tension force vector	N
$\boldsymbol{G}$	Chemical potential	Pa
$\boldsymbol{q}$	Conductive heat flux vector	W/m^2
$\boldsymbol{U}$	Displacement vector	m
$\boldsymbol{u}$	Velocity vector	m/s
χ	Mobility tuning parameter	$m \cdot s/kg$

δ	Elastic displacement of the surface	m
$\dot{m}_d$	Mass flow rate of droplets	kg/s
$\dot{\gamma}$	Shear strain rate	1/s
ϵ	Interface thickness	m
ϵ_s	strain tensor	–
γ	Mobility parameter	$m^3 \cdot s/kg$
γ_{ls}	Interfacial free energies of solid/liquid	N/m
γ_{lv}	Interfacial free energies of liquid/vapor	N/m
γ_{sv}	Interfacial free energies of solid/vapor	N/m
λ	Mixing energy density	N
$\mathcal{H}$	Enthalpy per unit mass	J/kg
$\mathcal{H}_{ml}$	Enthalpy per unit mass of the liquid oil/refrigerant solution	J/kg
$\mathcal{H}_{rg}$	Enthalpy per unit mass of the gaseous refrigerant	J/kg
μ	Viscosity	$Pa \cdot s$
μ_m	Viscosity of the total mixture	$Pa \cdot s$
μ_0	Atmospheric viscosity of oil	$Pa \cdot s$
μ_{ml}	Viscosity of the liquid oil/refrigerant solution	$Pa \cdot s$
μ_{ol}	Viscosity of the liquid oil	$Pa \cdot s$
μ_{rg}	Viscosity of the gaseous refrigerant	$Pa \cdot s$
μ_{rl}	Viscosity of the liquid refrigerant	$Pa \cdot s$

μ_w	Viscosity of water	$\mathrm{Pa} \cdot \mathrm{s}$
Ω_i	Solid domain i	–
Ω_R	Reynolds contact area	–
ϕ	Phase field parameter	–
ρ_m	Density of the total mixture	$\mathrm{kg/m^3}$
ρ_0	Atmospheric density of oil	$\mathrm{kg/m^3}$
ρ_c	Density of the continuous phase	$\mathrm{kg/m^3}$
ρ_{ml}	Density of the liquid oil/refrigerant solution	$\mathrm{kg/m^3}$
ρ_{rg}	Density of the gaseous refrigerant	$\mathrm{kg/m^3}$
ρ_w	Density of water	$\mathrm{kg/m^3}$
σ	Surface tension	N/m
τ	Viscous stress tensor	$\mathrm{N/m^2}$
θ	Proportion of lubricant in the gap	–
θ_w	Contact angle	$^\circ$
υ_i	Poisson's ratio of solid i	–
a	Hertzian radius or semi-minor axis	m
c_g	Velocity of sound in the pure refrigerant gas	m/s
C_p	Specific heat capacity	J/kg/K
$C_{p,i}$	Specific heat capacity of solid i	J/kg/K
$C_{p,ml}$	Specific heat capacity of the oil/refrigerant solution	J/kg/K

$C_{p,ol}$	Specific heat capacity of oil	J/kg/K
$C_{p,rg}$	Specific heat capacity of gaseous refrigerant	J/kg/K
$C_{p,rl}$	Specific heat capacity of liquid refrigerant	J/kg/K
D_d	The mean water droplet diameter	m
e	Internal energy per unit mass	J/kg
$E^{'}$	Reduced elastic modulus	Pa
E_i	Young's modulus of solid i	Pa
h	Film thickness	m
h_0	Initial central film thickness	m
h_c	Central film thickness	m
h_m	Minimum film thickness	m
k_i	Thermal conductivity of solid i	W/m/K
k_{ml}	Thermal conductivity of the oil/refrigerant solution	W/m/K
k_{ol}	Thermal conductivity of oil	W/m/K
k_{rg}	Thermal conductivity of gaseous refrigerant	W/m/K
k_{rl}	Thermal conductivity of liquid refrigerant	W/m/K
L	Distance between the centers of two successive rolling elements	m
m_d	Mass of droplets	kg
m_{ml}	Mass of the liquid oil/refrigerant solution	kg
m_{ol}	Mass of the liquid oil	kg

m_{rg}	Mass of the gaseous refrigerant	kg
m_{rl}	Mass of the liquid refrigerant	kg
N_d	Number of water droplets	–
p	Pressure	Pa
p_{cav}	Cavitation pressure	Pa
p_h	Maximum Hertzian pressure	Pa
p_{ml}	Pressure at bubble point	Pa
p_{sat}	Thermodynamic saturation pressure of oil/refrigerant solution	Pa
p_s	Pressure in the compressor sump	Pa
p_{vm}	Pressure at wet point	Pa
Q_{comp}	Heat source terms generated from compression	W/m^3
Q_{shear}	Heat source terms generated from shear	W/m^3
R	Curvature radius	m
R_{ell}^{eq}	Equivalent radius of curvature	m
R_x	Reduced curvature radius	m
S_d	Cross section surface of water droplets at the inlet	m^2
S_{in}	Surface of inlet area	m^2
t	Time	s
T_s	Temperature in the compressor sump	K
u_i	Velocity of solid i	m/s

u_m	Entrainment speed	m/s
$V_{f,o}$	Volume fraction of oil in water/oil mixture	–
$V_{f,w}$	Volume fraction of water in water/oil mixture	–
w	External load	N
w^{eq}	Equivalent normal load	N/m
w_d	Mass fraction of water in oil	–
w_{ol}	Mass fraction of liquid oil in the liquid oil/refrigerant solution	–
$w_{rl,in}$	Initial mass fraction of liquid refrigerant in the liquid oil/refrigerant solution	–
w_{rl}	Mass fraction of liquid refrigerant in the liquid oil/refrigerant solution	–
w_{sat}	Solubility of refrigerant in oil	–
X_{ol}	Mole fraction of liquid oil in the liquid oil/refrigerant solution	–
x_{rg}	Mass fraction of gaseous refrigerant in the total mixture	–
X_{rl}	Mole fraction of liquid refrigerant in the liquid oil/refrigerant solution	–
x_w	Inlet distance of water droplets	m

Dimensionless numbers

X_w	Dimensionless water inlet distance parameter	$\frac{x_w}{a}$
X_c	Dimensionless critical inlet distance parameter	$1 + 3.06((\frac{R_x}{a})^2 H_c)^{0.58}$
H_c	Dimensionless central film thickness	$1.2G^{0.53}U^{0.67}W_2^{-0.067}$
U_m	Dimensionless velocity parameter	$\frac{u_m}{u_{ref}}$
W	Dimensionless applied load parameter	$\frac{w}{w_{ref}}$
$\bar{\eta}$	Dimensionless viscosity parameter	$\frac{\mu_0}{\mu_{0ref}}$
Re_r	Relative Reynolds number	$\frac{\rho_{oil} D_d \boldsymbol{v_r}}{\mu_{oil}}$
We	Weber number of droplet	$\frac{\rho_c U^2 d}{\sigma}$

List of Abbreviations

ALE	**A**rbitrary **L**agrangian **E**ulerian
EHD	**E**lasto**H**ydro**D**ynamic
EHL	**E**lasto**H**ydrodyamic **L**ubrication
FSI	**F**luid **S**tructure **I**nteraction
HL	**H**ydrodyamic **L**ubrication
LaMCoS	**Co**ntact and **S**tructure **M**echanics **La**boratory
PRL	**P**ure **R**efrigerant **L**ubrication

REB	**R**olling **E**lement **B**earing
VOF	**V**olume **O**f **F**luid

Résumé étendu

a Introduction

La lubrification est reconnue depuis longtemps comme une solution prometteuse pour réduire le frottement en séparant les surfaces en contact par un film lubrifiant. Elle est actuellement employée dans presque tous les systèmes d'ingénierie modernes. De nombreux efforts ont été consacrés à ce sujet au cours des dernières décennies, amenant des progrès significatifs dans la connaissance des mécanismes de lubrification en film mince. Cependant, l'interaction du lubrifiant avec d'autres fluides environnants, en particulier autour de la zone de contact, est encore largement inexplorée. Or, dans de nombreuses applications impliquant par exemple des roulements, le fluide qui sépare les pièces en contact n'est pas uniquement le lubrifiant (une huile ou une graisse) mais est souvent un mélange incluant le fluide environnant (eau, liquide de refroidissement, carburant, etc.). Les conséquences de la lubrification avec de tels mélanges sont complexes et nécessitent une attention particulière, car la capacité de lubrification du mélange peut différer considérablement de celle du lubrifiant pur. Pour assurer la performance d'une large gamme d'applications industrielles pertinentes, une compréhension approfondie de la lubrification avec des mélanges est essentielle.

Ce travail étudie la lubrification avec des mélanges d'huile et de fluides environnants. C'est pour répondre à ce défi industriel que le mélange huile/réfrigérant et le mélange huile/eau sont étudiés ici. Ils représentent respectivement deux types d'états mixtes, les fluides miscibles et les fluides non miscibles. Tout au long de ce travail, un double problème est abordé et, par conséquent, des méthodologies de recherche distinctes sont proposées pour relever les défis pertinents.

b Etat de l'art

b.1 Mélange huile/réfrigérant

Le mélange huile/réfrigérant est problématique pour le compresseur du système de réfrigération. Dans les applications pratiques, le lubrifiant utilisé dans

le compresseur doit être miscible avec le réfrigérant du système pour garantir que l'huile retournera dans le compresseur après avoir traversé le cycle du système de réfrigération [1]. Comme l'huile est en contact avec le réfrigérant et qu'elle est miscible avec lui, le système de roulement du compresseur de réfrigération est en fait lubrifié par une solution, qui est un mélange homogène d'huile et de réfrigérant dissous [2]. Pour comprendre les conséquences de la lubrification du contact avec le mélange huile/réfrigérant dans les compresseurs de réfrigération, une attention particulière a été portée à ce type de mélange depuis le début des années 1990. Il a été démontré expérimentalement que la dilution du réfrigérant dans l'huile a pour effet de réduire la viscosité et la piézo-viscosité de la solution, et d'augmenter la compressibilité, diminuant ainsi les capacités de lubrification des contacts [2–4]. De nombreuses études ont été réalisées pour mesurer l'épaisseur du film EHL avec une solution huile/réfrigérant afin de quantifier l'effet de la dilution du réfrigérant dans l'huile dans les contacts EHL [1, 5, 6].

Un autre problème avec les mélanges huile/réfrigérant est que le fluide réfrigérant est très volatile. Par conséquent, la concentration de réfrigérant dans l'huile n'est pas toujours constante, car le réfrigérant dissous dans l'huile peut s'évaporer ou se condenser lorsque la température et la pression locales changent [7].

Bien que des études extensives sur les contacts EHL dans les solutions huile/réfrigérant aient été menées, elles se sont limitées à l'investigation de la zone de forte pression. Peu d'attention a été accordée au phénomène de cavitation se produisant à la sortie des contacts EHL, qui est pourtant crucial pour les solutions huile/réfrigérant.

b.2 Mélange huile/eau

Les effets de l'eau sur les systèmes lubrifiés ont été largement étudiés et peuvent être classés en effets à long terme et à court terme [8, 9]. Les effets à court terme comprennent les impacts immédiats de l'eau sur l'huile lubrifiante, tels que certains changements de la viscosité et de la piézo-viscosité [9–11], qui ont tous deux une influence majeure sur la capacité de formation de film. Les effets de l'eau dans l'huile sous forme d'émulsion sur la capacité de lubrification instantanée de la zone de contact ont été étudiés expérimentalement ; cependant, les résultats publiés présentent certaines divergences. Il a été constaté que l'épaisseur du film central $h_{c,mix}$ formée par l'émulsion eau dans l'huile est plus grande que celle formée par l'huile de base seule $h_{c,oil}$ lorsque la taille moyenne des particules de l'émulsion D_d est inférieure ou du même ordre que l'épaisseur du film central $h_{c,mix}$ [12, 13]. Les études précédentes sont toutefois contradictoires lorsque la taille moyenne des gouttelettes est supérieure à l'épaisseur du

film. Certaines études [12, 14, 15] ont constaté que les émulsions «eau-dans-huile» se comportent comme de l'huile pure en termes de capacité à former un film et ont suggéré que les gouttelettes d'eau de grande taille étaient repoussées avant de pénétrer dans la zone de contact. Liu et al. [16], au contraire, ont suggéré que l'eau peut former les grandes zones d'eau dans la région de contact et peut diminuer l'épaisseur du film.

c Méthodologie de recherche

Basé sur l'étude bibliographique précédente, on peut conclure qu'il est nécessaire de développer des méthodologies de recherche distinctes pour différents types de mélanges.

Le mélange huile/réfrigérant impliqué dans l'application du compresseur de réfrigération est en fait une solution, qui est un mélange homogène d'huile et de réfrigérant volatil. Le mélange huile/eau étudié dans ce travail, par contre, est une émulsion avec des gouttelettes d'eau dans l'huile. En raison des caractéristiques différentes de ces deux mélanges, les recherches sur le contact EHL dans les solutions huile/réfrigérant et les gouttelettes d'eau dans l'émulsion d'huile diffèrent significativement.

Deux problèmes majeurs se posent avec les solutions huile/réfrigérant dans les contacts EHL. Premièrement, la dilution du réfrigérant dans l'huile peut réduire la capacité de lubrification de l'huile. Deuxièmement, en raison de sa volatilité, le réfrigérant peut s'évaporer de manière spectaculaire à la sortie du contact, ce qui affecte la situation de lubrification pour le contact suivant [17]. Par conséquent, les études du contact EHD doivent se concentrer sur la capacité de formation de film des solutions d'huile/réfrigérant dans la zone pressurisée et sur l'évaporation/condensation du réfrigérant dans la région de cavitation.

D'autre part, le problème des gouttelettes d'eau dans l'émulsion d'huile est abordé à l'entrée en contact, où l'on cherche à mettre en évidence l'hypothèse selon laquelle les gouttelettes d'eau seraient expulsées du contact sous pression [8, 15, 18]. Le mouvement des gouttelettes d'eau à l'entrée est donc critique dans les études EHL pour évaluer les risques de contamination des gouttelettes d'eau dans l'huile. Puisque cette thèse aborde un double défi, deux méthodologies de recherche distinctes sont proposées pour traiter de la lubrification avec des fluides miscibles et immiscibles.

c.1 Fluides miscibles

Au meilleur de la connaissance d'auteur, aucune étude expérimentale n'a réussi à observer la cavitation à la sortie des contacts EHL pour les systèmes huile/réfrigérant en raison des limites de l'approche expérimentale. Par conséquent, la présente étude vise à étudier la zone de cavitation des systèmes huile/réfrigérant en utilisant l'approche numérique.

Une analyse numérique de la lubrification élastohyrodynamique incluant les effets thermiques (Thermo-EHD) est développée pour un système huile/réfrigérant afin de prédire la capacité de formation de film dans la zone de contact et les risques potentiels de l'évaporation du réfrigérant à la sortie du contact [17].

Une configuration de contact ponctuel lubrifié est considérée dans cette étude, en condition de roulement pur. Un régime permanent est supposé puisque le système dans la présente étude est considéré comme atteignant l'équilibre thermodynamique instantanément.

Les procédures numériques proposées par Habchi [19] pour un fluide monophasique sont ici adaptées à la solution huile/réfrigérant. Une approche de l'écoulement diphasique homogène est développée sur la base de la résolution par éléments finis des différentes équations régissant le contact Thermo-EHD en considérant les conditions d'équilibre [17]. La distribution de la pression dans le film lubrifiant est décrite par l'équation de Reynolds généralisée. Elle est complétée par le nouveau modèle de cavitation présenté dans la section suivante pour tenir compte à la fois de la région pressurisée et de la région de cavitation. La déformation élastique des éléments en contact est calculée par les équations d'élasticité linéaire. La variation de température dans le contact lubrifié est régie par l'équation de conservation de l'énergie. Enfin, l'égalité entre la force appliquée et la pression générée par le film lubrifiant est assurée par l'équation d'équilibre de charge. Les équations mentionnées ci-dessus sont discutées en détail dans les sections suivantes.

Nouveau modèle de cavitation pour les solutions huile/réfrigérant

Un nouveau modèle de cavitation pour les solutions d'huile/de réfrigérant est présenté dans cette section. Il a donné lieu à la publication [17]. La phase gazeuse est supposée être formée uniquement de gaz réfrigérant et la phase liquide est une solution d'huile et de réfrigérant dissous. Pour coupler avec l'équation de Reynolds généralisée, la densité et la viscosité du mélange sont calculées en fonction de la solubilité du réfrigérant.

La fraction massique du réfrigérant liquide dans la solution w_{rl} peut être exprimée comme suit :

$$w_{rl} = \begin{cases} w_{rl,in}, & \text{si} \quad w_{sat}(p,T) > w_{rl,in} \\ w_{sat}(p,T), & \text{si} \quad w_{sat}(p,T) \leq w_{rl,in} \end{cases} \tag{1}$$

La fraction massique du gaz réfrigérant x_{rg}, qui représente le rapport de la masse du gaz réfrigérant m_{rg} sur la masse totale du mélange, est donnée par [20] :

$$x_{rg} = \frac{m_{rl,in} - m_{rl}}{m_{rl,in} - m_{rl} + m_{ml}} = \frac{w_{rl,in} - w_{rl}}{1 - w_{rl}} \tag{2}$$

La fraction volumique du gaz réfrigérant α_{rg}, qui est définie comme le rapport entre le volume du gaz réfrigérant et le volume total du mélange, peut être exprimée en fonction de la fraction massique du gaz réfrigérant x_{rg} et des densités du liquide et du gaz, respectivement ρ_{ml} et ρ_{rg} :

$$\alpha_{rg} = \frac{x_{rg}\rho_{ml}}{x_{rg}\rho_{ml} + (1 - x_{rg})\rho_{rg}} \tag{3}$$

En conséquence, la densité du mélange diphasique peut être écrite comme suit :

$$\rho_m = \alpha_{rg}\rho_{rg} + (1 - \alpha_{rg})\rho_{ml} \tag{4}$$

La corrélation de viscosité de Dukler a été utilisée par de nombreux auteurs [21–24] pour calculer la viscosité moyenne du mélange homogène liquide-gaz. Elle est également adoptée dans le présent travail :

$$\mu_m = \alpha_{rg}\mu_{rg} + (1 - \alpha_{rg})\mu_{ml} \tag{5}$$

Equation de Reynolds généralisée

L'équation de Reynolds généralisée [25] adaptée à un écoulement diphasique en introduisant les propriétés du mélange définies dans la section précédente est résolue sur la zone de contact bidimensionnelle Ω_R, dont la dimension est $16a \times 6a$, définie pour $x \in [-4.5a, 11.5a]$ et $y \in [-3a, 3a]$, avec a le rayon de contact hertzien (voir Figure 1 (a)).

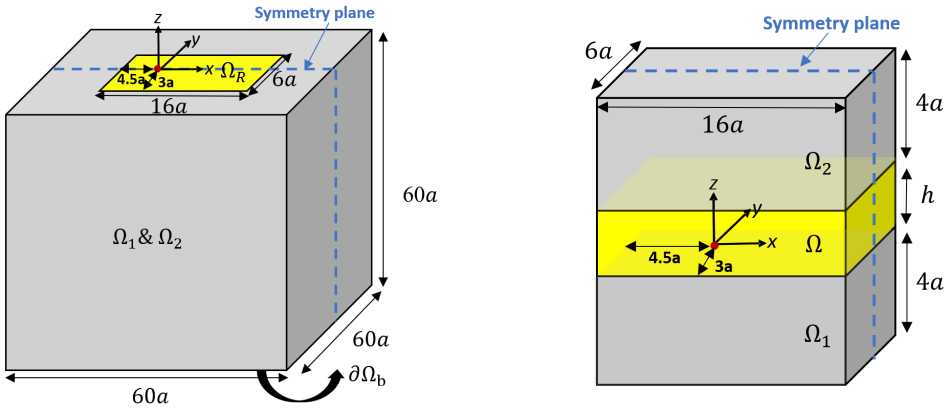

Figure 1: Géométries utilisées pour (a) le calcul de la pression et des déplacements élastique des surfaces et (b) le calcul de la température dans le lubrifiant et les surfaces

La résolution de l'équation de Reynolds généralisée permet le calcul du champ de pression p dans le fluide en prenant en compte les variations de viscosité et de densité à travers le film :

$$-\frac{\partial}{\partial x}\left[\left(\frac{\rho_m}{\mu_m}\right)_e \frac{\partial p(x,y)}{\partial x}\right] - \frac{\partial}{\partial y}\left[\left(\frac{\rho_m}{\mu_m}\right)_e \frac{\partial p(x,y)}{\partial y}\right] + \frac{\partial \rho^*_{x,m}}{\partial x} + \frac{\partial \rho^*_{y,m}}{\partial y} = 0 \quad (6)$$

La condition de limite pour l'équation précédente est :

$$p = p_s \quad \text{sur } \partial\Omega_R \quad (7)$$

Il convient de noter que, dans la présente étude, la pression dans le compresseur de réfrigération p_s appliquée autour de la zone de contact $\partial\Omega_R$ est supérieure à la pression atmosphérique car un réservoir de compresseur pressurisé est utilisé [26].

De plus, une condition de symétrie sur le plan $x - z$ à $y = 0$ est appliquée pour réduire les efforts de calcul.

Equation d'élasticité linéaire et équation d'équilibre de charge

L'épaisseur du film prends en compte le déplacement élastique de la surface $\delta(x, y)$, la séparation des corps solides h_0 et la courbure originale des surfaces non déformées:

$$h(x,y) = h_0 + \frac{x^2 + y^2}{2R} - \delta(x,y) \quad (8)$$

Le déplacement élastique $\delta(x, y)$ dans la direction z des éléments en contact résulte de l'équation d'élasticité linéaire:

$$div(\sigma) = 0 \quad avec \quad \sigma = C : \epsilon_s(\boldsymbol{U}) \tag{9}$$

où $\boldsymbol{U}$ représente les déplacements dans le massif équivalent (Ω_1&Ω_2 sur Figure 1 (a)).

Les conditions aux limites associées sont présentées comme suit :

$$\begin{aligned} &\boldsymbol{U} = 0 \quad \text{à la surface inférieure } \partial\Omega_b \\ &\sigma_n = -p \quad \text{à la zone de contact } \Omega_R \\ &\sigma_n = 0 \quad \text{ailleurs} \end{aligned} \tag{10}$$

Enfin, l'équation d'équilibre de la charge s'écrit :

$$\int_{\Omega_R} p(x, y)\, d\Omega = F \tag{11}$$

De plus, une condition de symétrie sur le plan $x - z$ à $y = 0$ est appliquée pour réduire les efforts de calcul.

Equation de conservation de l'énergie

L'équation de l'énergie est résolue sur la géométrie schématisée dans la Figure 1 (b) :

$$\rho_m C_{p,m} \left(u_x \frac{\partial T}{\partial x} + u_y \frac{\partial T}{\partial y} \right) = \frac{\partial}{\partial z} \left(k_m \frac{\partial T}{\partial z} \right) + Q_{comp} + Q_{shear} \tag{12}$$

Où C_p et k_m sont la capacité thermique spécifique et la conductivité thermique du mélange, u_x et u_y sont les composantes du champ de vitesse du lubrifiant le long de x et y et T le champ de température.

Avec

$$Q_{comp} = [\alpha_{rg} - (1 - \alpha_{rg}) \frac{T}{\rho_{ml}} \frac{\partial \rho_{ml}}{\partial T}] \left(u_x \frac{\partial p}{\partial x} + u_y \frac{\partial p}{\partial y} \right) \tag{13}$$

$$Q_{shear} = \mu_m \left(\left(\frac{\partial u_x}{\partial z} \right)^2 + \left(\frac{\partial u_y}{\partial z} \right)^2 \right) \tag{14}$$

Et

$$\rho_m = \alpha_{rg}\rho_{rg} + (1-\alpha_{rg})\rho_{ml} \tag{15}$$
$$\mu_m = \alpha_{rg}\mu_{rg} + (1-\alpha_{rg})\mu_{ml} \tag{16}$$
$$k_m = \alpha_{rg}k_{rg} + (1-\alpha_{rg})k_{ml} \tag{17}$$

Des conditions aux limites de continuité du flux de chaleur sont imposées aux interfaces solide/lubrifiant pour assurer l'équilibre énergétique du système :

$$\begin{aligned} k_m \left.\frac{\partial T}{\partial z}\right|_{z=0^+} &= k_1 \left.\frac{\partial T}{\partial z}\right|_{z=0^-} \\ k_m \left.\frac{\partial T}{\partial z}\right|_{z=h^-} &= k_2 \left.\frac{\partial T}{\partial z}\right|_{z=h^+} \end{aligned} \tag{18}$$

La température est fixée à la température dans le compresseur de réfrigération T_s sur les frontières supérieures et inférieures du solide, ainsi que sur les frontières d'entrée des solides.

La condition limite à l'entrée (x_{in}) du domaine du fluide [19] est:

$$T(x_{in}, y, z) = T_s \quad \text{si} \quad u_f(x_{in}, y, z) \geq 0 \tag{19}$$

Les autre conditions limités représentent un flux nul: $\frac{\partial_T}{\partial_n} = 0$.

De plus, une condition de symétrie sur le plan $x - z$ à $y = 0$ est appliquée pour réduire les efforts de calcul.

c.2 Fluides immiscibles

Peu de recherches dans la littérature se concentrent sur l'écoulement eau dans l'huile à l'entrée des contacts EHD, en particulier sur les trajectoires des gouttelettes d'eau. Par conséquent, cette étude vise à contribuer à une meilleure compréhension de ce problème en utilisant à la fois des approches expérimentales et numériques pour explorer le comportement d'une émulsion «eau-dans-huile» à l'entrée du contact. Afin d'imiter la situation d'un roulement d'une installation industrielle (informations fournies par le groupe de référence SKF), une émulsion eau dans l'huile a été préparée à partir de l'huile Morlina S1 B 320 (viscosité dynamique à 25°C = $0,781$ Pa $\cdot$ s), de 10 % en poids d'eau distillée, contenant 5 % de liquide de refroidissement dilué (Quakerol TWN). Un agitateur magnétique chauffant FB15001 à 855 rev/min mélange à 25°C pendant 90 min. Le liquide de refroidissement évoqué est un tensioactif, qui se compose de 1 % de tensioactif, $0,5$ à 3 % d'huile (Morlina S1 B 320), et d'eau.

Observation directe à l'entrée d'un contact EHD

Le dispositif expérimental pour l'observation directe peut être schématisé comme dans Figure 2.

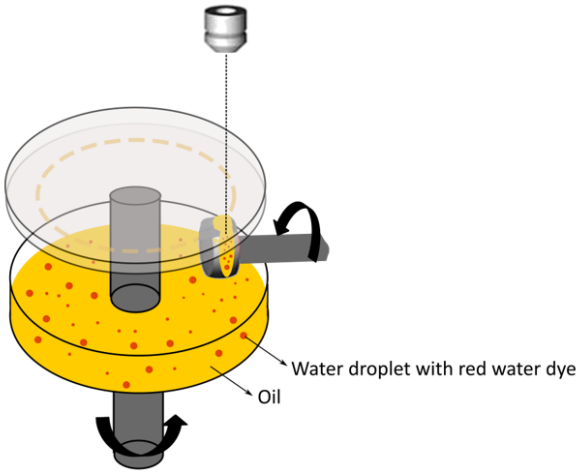

Figure 2: Schéma du banc d'essai reproduisant le contact bille - disque.

Dans l'expérience, un réservoir de lubrifiant composé de 20 ml d'émulsion eau dans huile a été utilisé, et la température a été maintenue à 25 °C avec un thermostat. Une bille d'acier de 25.4 mm a été immergée dans le réservoir et a été mise en contact avec un disque en verre par une charge de 40 N, ce qui a donné une pression hertzienne maximale de 0.57 GPa et un rayon de contact de Hertz a de 0.18 mm. La taille caractéristique initiale des gouttelettes d'eau était d'environ 8 µm. La condition de roulement pur a été appliquée. L'observation directe a été faite à l'entrée du contact par microscopie à lumière blanche. Le processus complet par lequel des gouttes d'eau s'approchent de la zone de contact a été filmé par la caméra haute vitesse Micro Ex4 à travers un disque en verre transparent. Les expériences ont été réalisées en augmentant la vitesse de roulement de $0,015$ m/s à 3 m/s et chaque palier de vitesse a été maintenue pendant 15 s.

Modèles numériques

Un couplage unidirectionnel entre les gouttelettes d'eau et les champs est supposé, ce qui signifie que seuls les effets de l'huile sur le mouvement des gouttelettes d'eau sont considérés. Les effets des gouttelettes d'eau sur l'huile, ainsi que les interactions entre les gouttelettes d'eau, sont négligés. En utilisant cette approche, le champ de vitesse de la phase continue (huile) et celui de la phase dispersée (gouttelettes d'eau) peuvent être évaluées l'une après

l'autre [27]. L'épaisseur de film $h(x, y)$ est calculée par la méthode précédente (Ryenolds) dans une étape initiale. Elle permet de construire une géométrie tridimensionnelle au niveau de la zone d'entrée du contact avec une surface supérieure définie par $z = h(x, y)$.

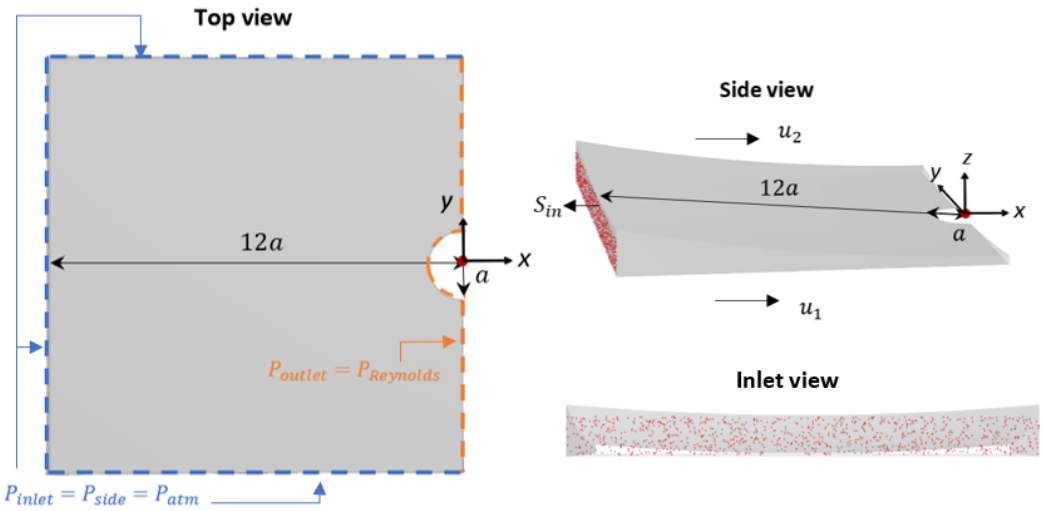

Figure 3: Géométries utilisées pour le calcul de l'écoulement des fluides et du traçage des gouttelettes d'eau et conditions limites

L'équation de Navier-Stokes est d'abord résolue pour tracer l'écoulement du fluide dans le régime laminaire (avec $Re < 1$) sur le domaine de calcul 3D généré (voir Figure 3) :

$$\begin{aligned} \rho_{oil}\frac{\partial \boldsymbol{u_{oil}}}{\partial t} + \rho_{oil}(\boldsymbol{u_{oil}} \cdot \nabla)\boldsymbol{u_{oil}} &= \nabla \cdot [-p\boldsymbol{I} + \mu_{oil}(\nabla \boldsymbol{u_{oil}} + (\nabla \boldsymbol{u_{oil}})^T)] + \rho_{oil}\boldsymbol{g} \\ \nabla \cdot (\rho_{oil}\boldsymbol{u_{oil}}) &= 0 \end{aligned} \tag{20}$$

Le mouvement des gouttelettes d'eau dans le fluide était décrit par la deuxième loi de Newton comme suit [27] :

$$\frac{d}{dt}(m_d \boldsymbol{v_d}) = \boldsymbol{F_D} + \boldsymbol{F_G} + \boldsymbol{F_B} \tag{21}$$

Où $\boldsymbol{v_d}$ est la vitesse de la gouttelette, $\boldsymbol{F_D}$ est la force de traînée, $\boldsymbol{F_G}$ et $\boldsymbol{F_B}$ sont la force de gravité et la force de flottabilité. m_d est la masse de la gouttelette.

En supposant que les gouttelettes d'eau sont uniformément réparties dans l'huile en amont de la zone d'entrée, la vitesse initiale des gouttelettes d'eau a été

fixée égale à celle de l'huile. Le débit massique $\dot{m}_d$ et le nombre de gouttelettes d'eau N_d à l'entrée peuvent être calculés avec l'expression ci-dessous :

$$\begin{aligned} \dot{m}_d &= S_{in} w_d \boldsymbol{u_{oil}} \rho_d \\ N_d &= \frac{S_{in} w_d}{S_d} \end{aligned} \tag{22}$$

Avec w_d la fraction massique d'eau dans l'huile, S_{in} la surface de l'entrée (voir Figure 3) et S_d la surface de la section transversale des gouttelettes d'eau à l'entrée.

d Cavitation du mélange huile/réfrigérant au niveau de la zone de sortie des contacts EHD

Une solution huile/réfrigérant de référence, RL68H et HFC-R134a a été utilisée. La condition de roulement pur a été employée, et une charge w de $F = 10.95$ N a été appliquée sur une bille d'acier de 19.05 mm, donnant une pression hertzienne maximale de 0.7 GPa. La pression et la température dans la chambre d'essai étaient de $p_s = 1,171$ MPa et $T_s = 65$°C, ce qui a donné une fraction massique initiale de réfrigérant $w_{in} = 23,7$ % dans la solution huile/réfrigérant. Les profils de pression, de fraction massique de réfrigérant liquide dans la solution huile/réfrigérant et une carte de la fraction volumique du gaz réfrigérant dans le mélange total α_{rg} sont représentés sur les figures 4, 5 et 6 pour une vitesse de roulement de 1 m/s.

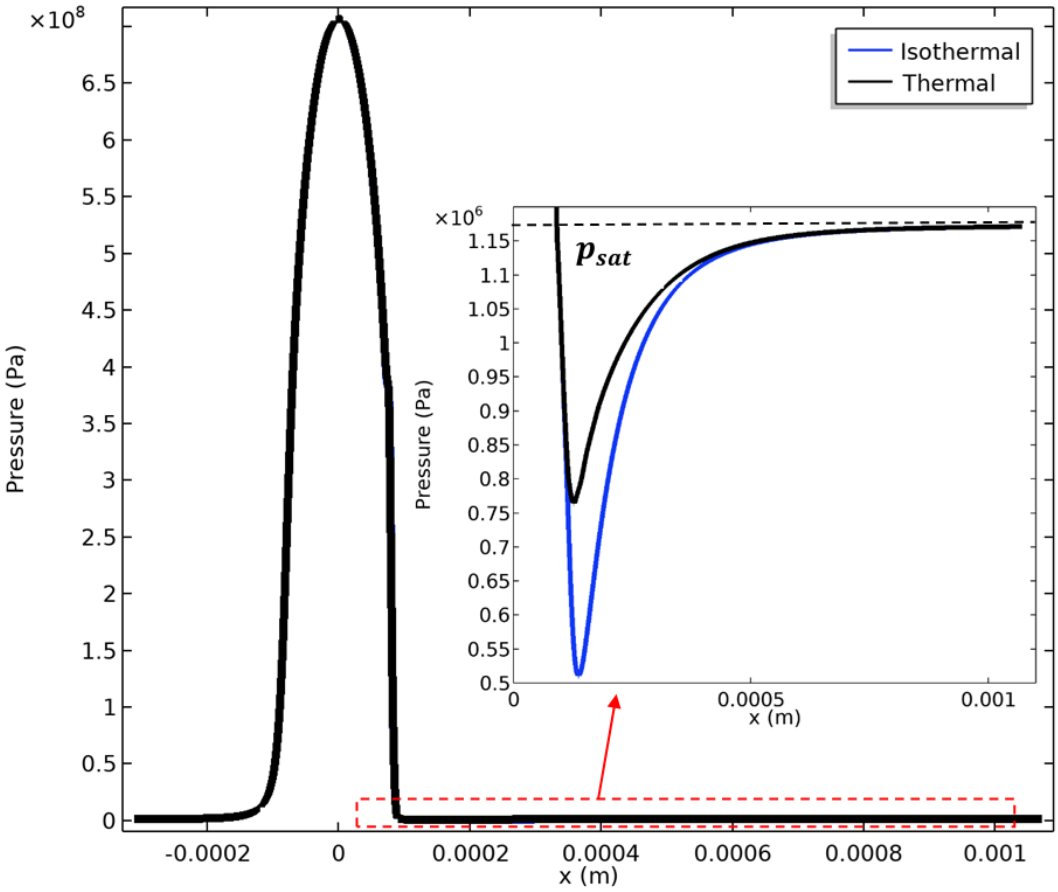

Figure 4: Pression du mélange huile/réfrigérant le long x à $y = 0$ (ligne centrale) et $z = h$ (surface supérieure) obtenue en résolvant le problème EHD et Thermo-EHD avec la présente modélisation de la cavitation basée sur la solubilité (voir Figure 1 pour le système de coordonnées).

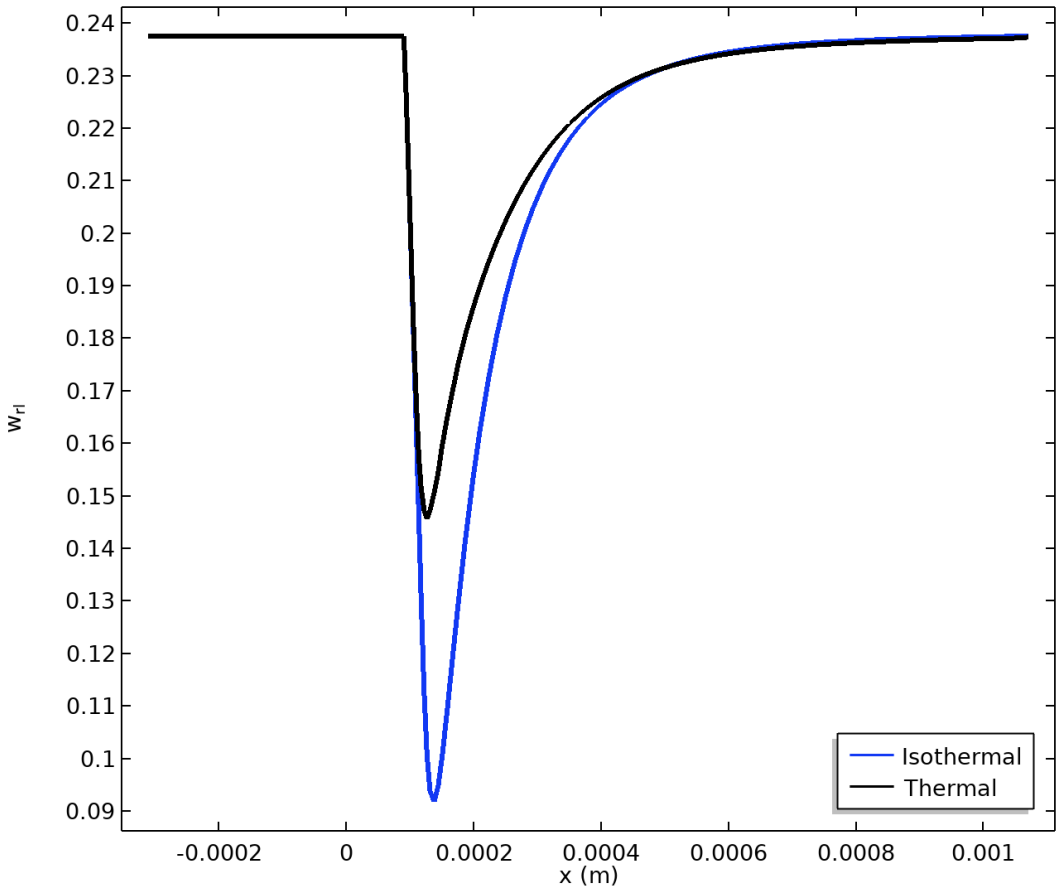

Figure 5: Fraction massique du réfrigérant liquide dans la solution huile/réfrigérant le long de x à $y = 0$ (ligne centrale) et $z = h$ (surface supérieure) obtenue en résolvant le problème EHD et Thermo-EHD avec la présente modélisation de la cavitation basée sur la solubilité (voir Figure 1 pour le système de coordonnées).

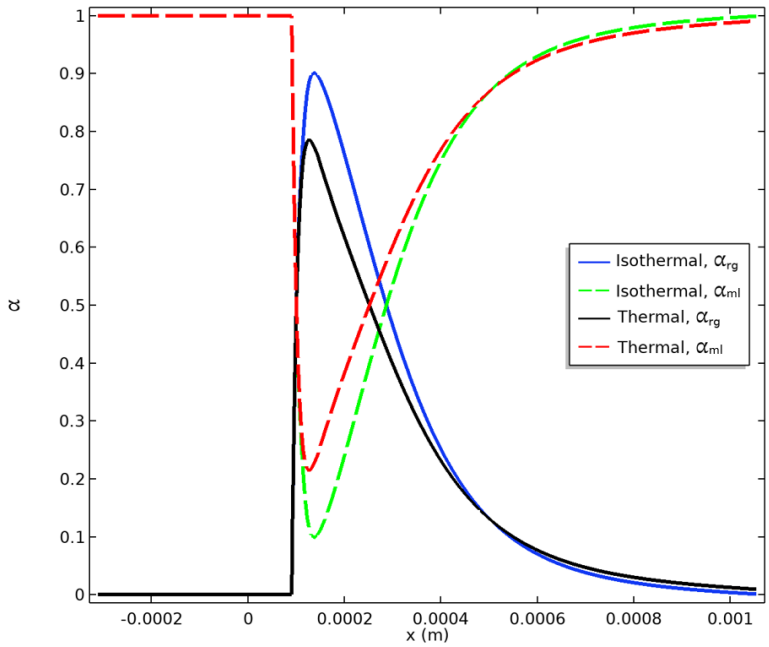

(a)

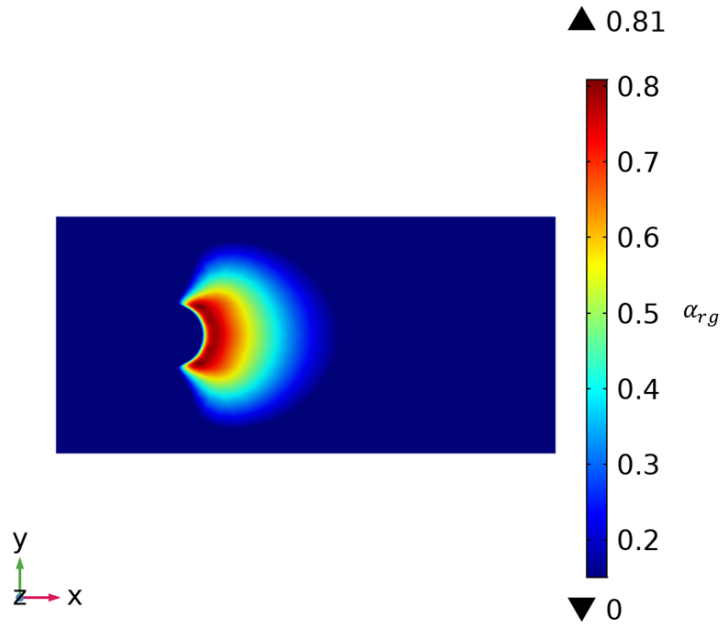

(b)

Figure 6: (a) Fraction volumique de gaz réfrigérant et fraction volumique d'huile/réfrigérant liquide dans le mélange total, α_{rg} et α_{ml}, respectivement, le long x à $y = 0$ (ligne centrale) et $z = h$ (surface supérieure) en résolvant le problème EHD et Thermo-EHD avec la présente modélisation de la cavitation basée sur la solubilité. (b) Fraction volumique du gaz réfrigérant dans le mélange total α_{rg} au niveau du plan défini par $z = h$ (surface supérieure) obtenue en résolvant le problème Thermo-EHD avec la présente modélisation de la cavitation basée sur la solubilité. Voir Figure 1 pour le système de coordonnées.

La comparaison entre les modélisations Thermo-EHD et EHD a été effectuée. Il est intéressant de mentionner que la Figure 6 (a) révèle la fraction volumique de l'espace de contact occupée par le gaz réfrigérant α_{rg} et l'huile liquide/réfrigérant α_{ml}, où α_{ml} est égal à 1-α_{rg}. Comme on peut le voir sur les figures ci-dessus, la prise en compte des effets thermiques produit une chute de pression plus faible dans la zone de cavitation (voir la figure 4), car une plus grande quantité de réfrigérant dissous reste dans la solution huile/réfrigérant (voir la figure 5) et moins de gaz réfrigérant est libéré par rapport au cas isotherme (voir la figure 6 (a)). Ce résultat est cohérent avec celui rapporté par Gasche [21], qui a affirmé que la fraction massique du gaz réfrigérant prédite par le modèle thermique est plus petite que celle du modèle isotherme. Cela s'explique par le fait que la diminution de la température due au changement de phase, comme nous l'avons vu précédemment, crée un effet de concurrence qui décourage la libération du gaz réfrigérant. En conséquence, la chute de pression est modérée, et la composition de la solution huile/réfrigérant pour le problème Thermo-EHD est obtenue sous les effets concurrents de la pression et de la température.

e Contamination par des gouttelettes d'eau à l'entrée des contacts EHD

Des observations directes des gouttelettes d'eau dans l'émulsion d'huile à l'entrée des contacts EHD en condition de roulement pur sont réalisées.

Pour valider la stratégie de modélisation, les mêmes conditions opératoires que celles utilisées dans l'expérience précédente sont appliquées dans la modélisation numérique. Les calculs numériques sont effectués à différentes vitesses de roulement, comme dans les expériences. Le diamètre des gouttelettes d'eau est fixé à 8 µm sur la base des résultats des expériences précédentes. La figure 7 (b) montre un exemple de trajectoires de gouttelettes d'eau dans l'huile à 0,015 m/s obtenues par modélisation numérique. Pour révéler l'influence des gouttelettes d'eau sur le contact, la position des gouttelettes d'eau les plus proches du contact sur la ligne centrale est déterminée, dans la présente étude, comme l'intersection du cercle limite et de la ligne centrale, comme le montre la figure 7. La distance entre cette position et le point central du contact est définie comme la distance d'entrée des gouttes d'eau x_w. La modélisation numérique peut reproduire les trajectoires des gouttelettes d'eau dans l'huile, et montre un bon accord qualitatif avec les résultats expérimentaux.

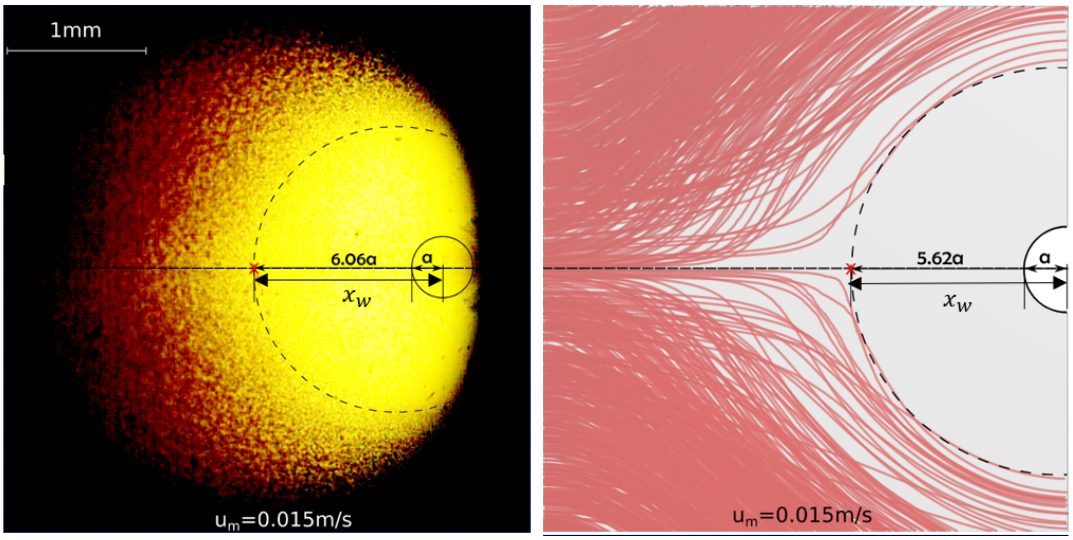

(a) (b)

Figure 7: Trajectoires des gouttelettes d'eau dans l'huile à l'entrée d'un contact EHL et estimation de la distance d'entrée avec un diamètre caractéristique des gouttelettes de 8 µm avec (a) observations expérimentales à 0,015 m/s, (b) résultats numériques à 0,015 m/s

La distance d'entrée adimensionnelle des gouttes d'eau X_w peut être définie comme suit :

$$X_w = \frac{x_w}{a} \tag{23}$$

où a est le rayon Hertzien de la zone de contact.

Afin d'étudier plus en détail l'effet des gouttelettes d'eau sur le contact, X_w est comparé à la position critique X_c qui indique l'emplacement du ménisque air-huile où le changement du régime de lubrification sur-alimenté à sous-alimenté se produit sous une lubrification à l'huile pure. X_c écrit (dans des conditions d'huile pure), selon Hamrock et Dowson [28] :

$$X_c = 1 + 3.06((\frac{R_x}{a})^2 H_c)^{0.58} \tag{24}$$

où, R_x est le rayon réduit de la bille en contact avec le plan. H_c l'épaisseur centrale adimensionnelle du film.

Figure 8 montre les résultats expérimentaux X_w comparés à X_c pour des gouttes d'eau de taille initiale de 8 µm et 60 µm à différentes vitesses de roulement u_m.

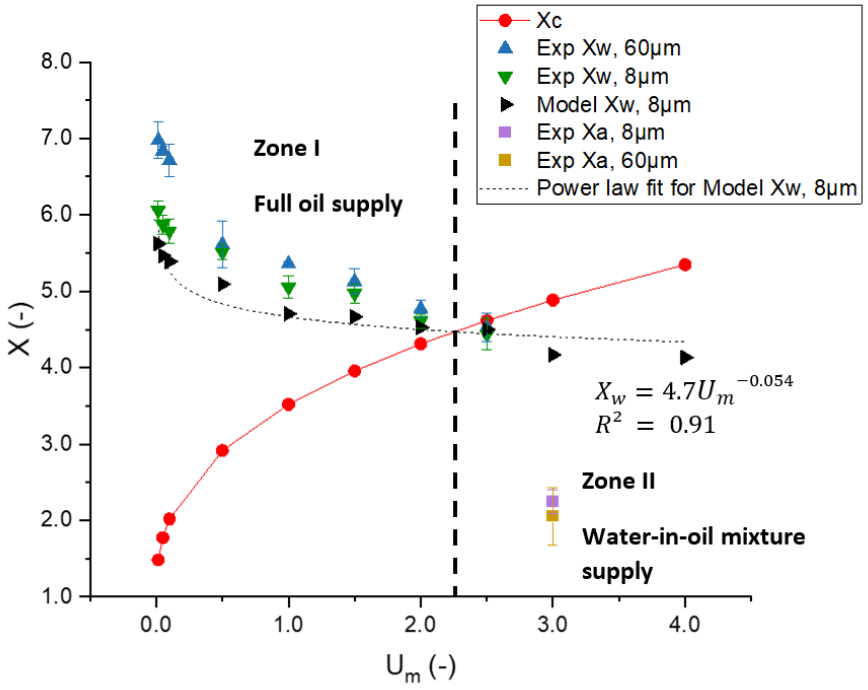

Figure 8: Comparaison entre la position X_w des gouttes d'eau obtenue expérimentalement et numériquement pour des tailles de gouttes de 8 µm et 60 µm et la position critique X_c du ménisque du contact sous-alimenté lubrifié à l'huile pure. X_a la position la plus proche de la zone de contact influencée par le ménisque air-huile

On considère que les gouttelettes d'eau n'ont pas d'influence sur la zone de contact lorsque $X_w > X_c$, puisque la zone de contact est sous un aliment intégral en huile (voir Figure 8 Zone I). Cependant, si des gouttelettes d'eau pénètrent dans la zone critique (lorsque $X_w \leq X_c$), la capacité de formation de film peut être affectée puisque la zone de contact est alimentée par un mélange eau/huile (voir Figure 8 Zone II). Même si les gouttelettes d'eau ne s'écoulent pas en fin au contact, on s'attend à ce que la quantité d'huile qui alimente la zone de contact diminue en raison de la présence de gouttelettes d'eau. Comme on peut le voir sur la figure 8, la capacité de formation de film de l'huile n'a aucune raison d'être influencée par les gouttelettes d'eau à faible vitesse de roulement. Cependant, lorsque la vitesse augmente, les gouttelettes d'eau se rapprochent et pénètrent finalement dans la zone critique, ce qui entraîne l'apport du mélange eau-huile dans la zone de contact. Il convient de noter que, dans la présente expérience, lorsque la vitesse de roulement augmente jusqu'à 3 m/s ($U_m = 3$), quelle que soit la taille des gouttelettes d'eau, un ménisque air-huile apparaît dans la zone d'observation. Il pousse la gouttelette d'eau vers le contact, dont la position est présentée comme X_a, et provoque une sévère sous-alimentation de la zone de contact.

Une étude paramétrique a été réalisée avec le modèle numérique pour étudier les impacts de divers paramètres opératoires sur l'écoulement de l'émulsion eau dans l'huile. Les gouttelettes d'eau sont plus susceptibles de s'approcher du contact lorsque la vitesse de roulement, la charge appliquée et la viscosité du lubrifiant sont grandes et que la taille des gouttelettes d'eau est petite. Une expression semi-analytique pour la position X_w des gouttelettes d'eau les plus proches est proposée, combinant les effets de la vitesse de roulement, de la charge appliquée et de la viscosité du lubrifiant : $X_w^{sa} = 4.6U_m^{-0.054}\bar{\eta}^{-0.084}W^{-0.296}$. En comparant ensuite avec les positions critiques associées, l'influence des gouttelettes d'eau sur le contact peut être déterminée.

f Conclusions

Un défi industriel est la lubrification avec des mélanges d'huile et de fluide environnant le contact. Cette étude expose les mécanismes de lubrification avec des mélanges de fluides dans et autour des contacts EHL. Deux mélanges industriels communs, le mélange huile/réfrigérant et le mélange huile/eau, qui représentent deux types d'états mixtes (des fluides miscibles et des fluides immiscibles), sont étudiés séparément. Pour le mélange huile/réfrigérant, une modélisation originale de la cavitation basée sur la solubilité est développée pour les contacts ponctuels Thermo-EHD. Pour le mélange huile/eau, une nouvelle approche expérimentale et numérique se concentrant sur les trajectoires des gouttelettes d'eau dans l'huile à l'entrée des contacts EHD est introduite.

Pour le mélange huile/réfrigérant, la solution numérique a montré une similarité globale avec les observations et les mesures expérimentales. Le modèle numérique permet de trouver la variation de la densité et de la viscosité dans la région pressurisée et dans la région de cavitation en fonction de la pression locale, de la température et de la fraction massique du réfrigérant. Il peut prédire à la fois la rupture et la reformation du film d'huile, ce qui permet d'obtenir l'emplacement et la taille de la zone de cavitation. Dans la région de cavitation, la pression est naturellement obtenue sur la base de mécanismes physiques sans hypothèse géométrique sur la forme de la zone de cavitation. De plus, comparé aux autres modèles de cavitation de la littérature, le modèle présent s'est avéré plus avantageux pour décrire l'écoulement d'une solution dans la zone cavitée et pour offrir une explication plus rationnelle des mécanismes en jeu. Plusieurs conclusions sont tirées concernant le comportement de la lubrification par une solution huile/réfrigérant :

- Les effets thermiques ont très peu d'influence sur le calcul de l'épaisseur du film lubrifiant pour la lubrification huile/réfrigérant dans le contact EHD dans des conditions de roulement pur, mais génèrent des disparités dans la zone de cavitation. L'analyse isotherme représente une condition plus

critique que l'analyse thermique, car elle prévoit une fraction volumique plus importante de gaz réfrigérants dans la zone de cavitation.

- La solubilité du réfrigérant doit être prise en compte car la concentration du réfrigérant varie en fonction de la température et de la pression locale, ce qui modifie les propriétés du mélange.

- Par rapport à l'huile pure, les solutions huile/réfrigérant peuvent potentiellement réduire la quantité d'huile liquide pour le contact suivant en raison de leurs plus grandes zones de cavitation.

D'autre part, une analyse expérimentale et numérique originale des risques de contamination par des gouttelettes d'eau dans l'émulsion d'huile à l'entrée des contacts EHD est présentée. Une observation directe originale des gouttelettes d'eau dans l'émulsion d'huile à l'entrée de la zone de contact a été réalisée. Elle a permis de suivre les trajectoires des gouttelettes d'eau colorées s'approchant de la zone de contact. En comparant les résultats numériques aux données expérimentales, il a été démontré que la modélisation numérique peut reproduire qualitativement et quantitativement les trajectoires des gouttelettes d'eau. Cela permet une étude paramétrique plus poussée des impacts de divers paramètres de fonctionnement sur l'écoulement de l'émulsion «eau-dans-huile». Les risques potentiels de contamination ont été évalués en comparant la position des gouttelettes d'eau les plus proches du contact avec la position critique du ménisque à laquelle la sous-alimentation se produit dans des conditions d'huile pure. Enfin, une expression semi-analytique incluant les effets de vitesse, charge et viscosité de l'huile pour la position des gouttelettes d'eau est proposée. Les principales conclusions de cette étude sont les suivantes :

- Lorsque les gouttelettes d'eau pénètrent dans une zone critique, le contact n'est plus alimentée complètement par une huile, mais par un mélange d'huile/eau. Par conséquent, la capacité de formation de film peut être affectée.

- Les gouttes d'eau sont plus susceptibles de s'approcher du contact avec l'augmentation de la vitesse de roulement, de la charge appliquée et de la viscosité du lubrifiant.

General Introduction

Lubrication has long been recognized as a promising solution to reduce friction by separating the contacting surfaces with a lubricant film. It is currently employed in most of modern engineering systems. Numerous efforts have been devoted to this subject over the last several decades, making significant progress in the knowledge of thin-film lubrication mechanisms involving a single fluid. Unfortunately, sealing never completely isolates the lubricant from the contact environment, and the interaction of the lubricant with other operating fluids is still largely unexplored. In many bearing applications, the fluid that separates the contacting parts is not only the lubricant (an oil or grease) but rather a mixture including the surrounding fluid (water, coolant, fuel, etc.). The consequences of lubrication with such mixtures require special attention since the lubricating ability of the lubricant mixture may differ significantly from that of the neat one. To maintain the performance of a wide range of relevant industrial applications, a thorough understanding of lubrication with mixtures is essential.

In the framework of rolling element bearing application, this work investigates the ElastoHydrodynamic Lubrication (EHL) with mixtures of oil and operating fluids. The oil/refrigerant mixture and the oil/water mixture, both of which represent two types of mixed states, miscible fluids, and immiscible fluids, are thoroughly explored as common mixtures found in the industry. Throughout this work, a dual problem is addressed, and therefore distinct research methodologies are proposed to handle the relevant challenges.

Chapter 1 begins with an overview on lubricated contacts. Literature-based research on EHL contact and its surroundings is provided. Then, the industrial challenge concerning lubrication with oil and operating fluids is presented. Two current issues, the oil/refrigerant mixture and the oil/water mixture are emphasized. This state of the art seeks to provide insight into the encountered issues, the existing solutions, and unanswered concerns about the lubrication with mixtures of oil and operating fluids, in and around the EHL contact.

The research methodologies used throughout this work are detailed in Chapter 2. The presentation of the research methodologies is divided into two sections, devoted to the miscible and immiscible fluids encountered in lubricated contacts. Using the oil/refrigerant solution as an example for miscible fluids, a numerical approach is proposed to investigate the film-forming ability in the pressurized region and the evaporation/condensation of refrigerant in the cavitation region. For the water droplets in oil emulsion, representing immiscible

fluids, numerical and experimental techniques are proposed to study the trajectories of water droplets in oil at the inlet of the lubricated contacts in order to assess the risks of contact contamination by water droplets.

A Thermal ElastoHyrodynamic Lubrication (Thermal-EHL) analysis is provided in Chapter 3 for oil/refrigerant lubricated contacts. Numerical EHL and Thermal-EHL solutions with solubility-based cavitation modeling are given first. Then, the choice of the cavitation model for oil/refrigerant solutions is discussed. Comparisons with pure oil cavitation are made under the same operating conditions. Finally, an industrial case study involving a refrigerant compressor is carried out.

Chapter 4 presents a dual experimental and numerical investigation of water droplets in oil emulsion. The experimental results of direct observations of a micro-sized water-in-oil emulsion flow at the inlet of an EHL point contact are presented first. The numerical results are then validated by comparisons with experimental data. On this basis, the effects of different operating conditions on water droplet flow, such as rolling velocity, water droplet size, applied load, and lubricant viscosity, have been analyzed. Finally, a semi-analytical expression is offered to evaluate the risks of water contamination of an EHL contact.

Chapter 1

State of the art

In this chapter, first, a general introduction to lubricated contacts is provided. Special attention is given to the ElastoHydrohynamic Lubrication regime, with studies on the areas in and around the contact being highlighted. Then, the industrial challenges concerning lubrication with a mixture of oil and operating fluids are presented, with two current issues, the oil/refrigerant mixture and the oil/water mixture emphasized. Finally, the objectives and methodologies of the thesis are summarized.

1.1 Lubricated contacts

The constant exploration of friction contributes to the advancement of human technology, from generating fire with sticks to today's development of high-speed trains and space stations. Depending on the situation, friction can be beneficial or harmful. In numerous applications, friction is a critical factor that should be limited, as it increases the system's energy consumption and causes wear and damage to the contacting surfaces. Lubrication is one of the techniques to reduce friction by separating the two surfaces with a lubricant film. The first confirmed evidence of its usage by Man dates back to ancient Egypt [1], when oil was used as a lubricant to move large and heavy objects.

Although the practice of lubrication to reduce friction has existed for a long time, the first scientific investigation on the fundamental principles of lubrication mechanisms did not come out until the nineteenth century with the works of Hirn [1], who reported the first experiments in studying lubrication with air and water. Then, with the introduction of mineral oils into the industry, two pivotal experimental investigations by Beauchamp Tower [2] and Nicoli Petrov [3] in 1883 made a significant contribution to the development of lubrication theory. Their research indicated that the contact surfaces could be fully separated by a fluid film, and friction forces in such adequately lubricated contacts are governed by the shearing of the viscous lubricant between the two surfaces. They pointed out that the most significant aspect of understanding lubrication mechanisms is to analyze the pressure generated by hydrodynamic effects. In 1886, Osborne Reynolds [4] established the well-known Reynolds' equation for the hydrodynamic lubrication theory to give a theoretical explanation to the experimental observations of Tower [2] and Petrov [3]. This theory is derived from the equations of motion, continuity equation, and Newton's shear stress-velocity gradient relation, providing a good estimation of pressure distribution with different geometries and kinematics of the moving parts. Reynold's remarkable work is the foundation of all current lubrication theories and enabled an essential understanding of thin-film lubrication mechanisms, which led to the development of various technologies.

Nowadays, the application of lubrication has extended to almost all modern engineering systems, including machinery, instruments, automobiles, etc. It is also being used on the cutting edge of science and engineering in industries like nanotechnology, aerospace, and biotechnology. A thorough understanding of the mechanics and control of lubricated contacts is essential to help the industry become more sustainable and eco-friendly.

1.1.1 Lubrication regime

Three lubrication regimes can be defined according to their range of friction coefficients as shown in the curve inspired by Stribeck curve [5] (see Figure 1.1):

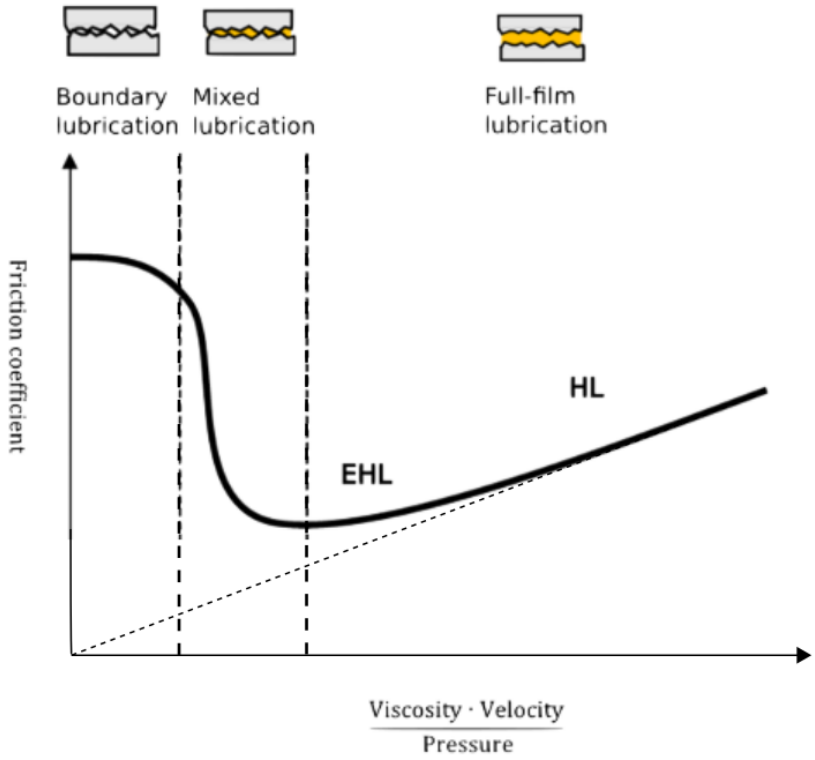

Figure 1.1: Curve inspired by Stribeck curve for the different regimes

- In the boundary lubrication regime, the asperities of the surfaces in contact sustain the load, resulting in significant friction. This type of lubrication regime, which is driven by tribo-chemical interactions, happens at low to moderate speeds and for low viscosity fluids.

- In the mixed lubrication regime, the hydrodynamic effect that generates pressure inside the film becomes progressively more important, and the load is supported by the asperities still in contact, but also by a partial

film of oil of a thickness comparable to the size of the asperities. The friction coefficient of this regime is lower than that of the former regime.

- Full-film lubrication involves a lubricant film that is bigger than the surface roughness and the load is entirely supported by the pressure generated within the lubricant film, resulting in relatively low friction coefficients.

The present study focuses only on the full-film lubrication regime, which can be further subdivided into two types of lubrication (see Figure 1.2):

- Hydrodynamic Lubrication (noted as HL in Figure 1.1 and 1.2 (a)), which is characteristic of conformal contacts with large contact surfaces (e.g., Journal bearings), generates relatively low pressure ($0.1 - 10$ MPa) that does not induce large elastic deformation of the contacting surfaces in comparison to the film thickness.

- ElastoHydrodynamic Lubrication (noted as EHL in Figure 1.1 and 1.2 (b)), in which very high pressure ($0.4 - 4$ GPa) is generated in a thin lubricant layer ($0.1 - 1$ µm) and the viscosity of lubricant can increase from the ambient condition by several orders of magnitude due to the piezo-viscosity effect. In this lubrication regime, the elastic deformation generated is significant and is generally larger than the film thickness. Non-conformal contacts with small contact areas, which can be found in gears and roller/ball bearings, are representative of this type of lubrication.

(a) (b)

Figure 1.2: Illustration of (a) Hydrodynamic Lubrication with undeformed contacts and (b) Elastohydrodyamic lubrication with deformed contacts

The current study mainly concerns ElastoHydrohynamic Lubrication (EHL), where a strong coupling between hydrodynamic and elastic deformation of surfaces is involved.

1.1.2 ElastoHydrodynamic Lubrication

The essential features of ElastoHydrodynamic Lubrication were revealed with the work of Ertel [6] and Grubin [7]. In their study, the elastic deformation of contacting surfaces was first taken into account for the estimation of film thickness by using Hertz theory [8] for elastic bodies in dry contact and Barus' piezo-viscosity law [9]. As a result of their research, the fundamental phenomena of EHL were identified: large elastic deformation and important piezo-viscosity effects.

Over the last several decades, with the advancement of both experimental technologies based on optical interferometry techniques and numerical approaches derived from more powerful computers, significant progress has been made in the knowledge of phenomena occurring in and around the EHD contacts.

As mentioned previously, Ertel [6] and Grubin [7] proposed a first expression of the film thickness as a function of different parameters with the solution of the Reynolds equation. Their work has been refined by Dowson and Higginson [10] and Hamrock and Dowson [11], who introduced dimensionless parameters and numerical treatments. However, the resolution of the EHL problems remains complex. The piezo-viscosity effects (strong dependence of the viscosity on the pressure) generate significant pressure and strong fluid-solid coupling. As a result, the resolution of this highly non-linear problem involving the coupling of the Reynolds equation, elastic deformation, and load balance equation becomes challenging. Many numerical techniques have been developed to face this problem, including the finite difference discretization [12, 13] or the finite element method [14, 15].

Another major difficulty in the numerical study of EHD contacts remains in the consideration of thermal effects. At severe operating conditions (e.g., high sliding), the thermal effects in EHD contacts can no longer be ignored as the heat generated is significant and can lead to a reduction in film thickness and friction coefficients. The variation of temperature within the film thickness induces significant viscosity gradients across the film, which contradicts the assumptions of Reynolds theory. In 1962, a Generalized Reynolds equation was proposed by Dowson [16] by modifying the classical one to allow the variation of viscosity across the film thickness. It was further developed by Cheng et al. [17, 18] with more complex pressure viscosity law. Habchi et al. [15, 19] recently proposed a full-system approach using the finite element method that can efficiently solve EHL and Thermal-EHL problems.

In parallel to these numerical investigations, many experimental works have been performed, providing qualitative and quantitative validations to theoretical findings (e.g., full-film separation and film thickness distribution). One of the

most employed methods is optical interferometry, pioneered by Gohar [20] and Foord et al. [21]. An example of the particular horseshoe shape of the film thickness distribution obtained with this technique can be found in Figure 1.3.

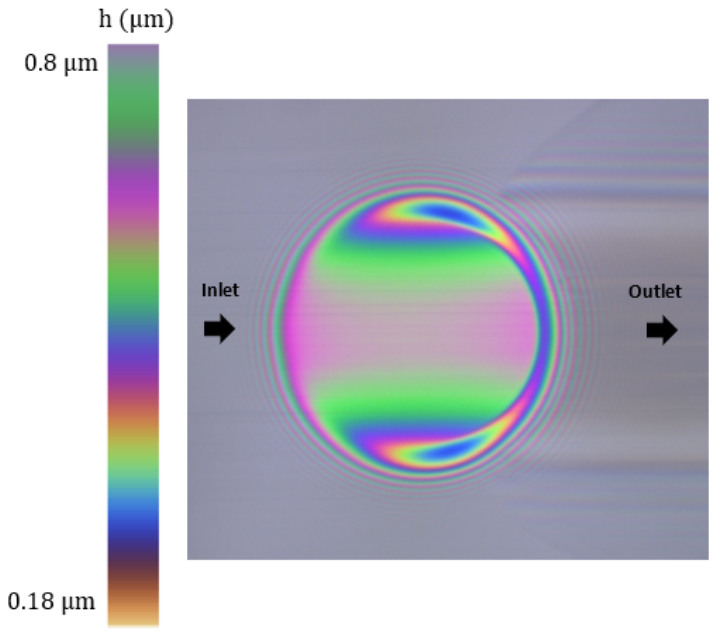

Figure 1.3: Film thickness distribution in an EHL contact using optical interferometry (obtained with LaMCoS tribometer "Jerotrib" by the current author)

A lubricated EHL circular contact is composed of different zones (see Figure 1.4), each of which plays an essential role in its performance. The investigation of physical phenomena in these different zones and their coupling will be the main focus of this thesis. Understanding the physical events that occur around the contact area, on the other hand, can be of fundamental importance since these zones can have a significant impact on lubricated contacts under real operating conditions in the industry.

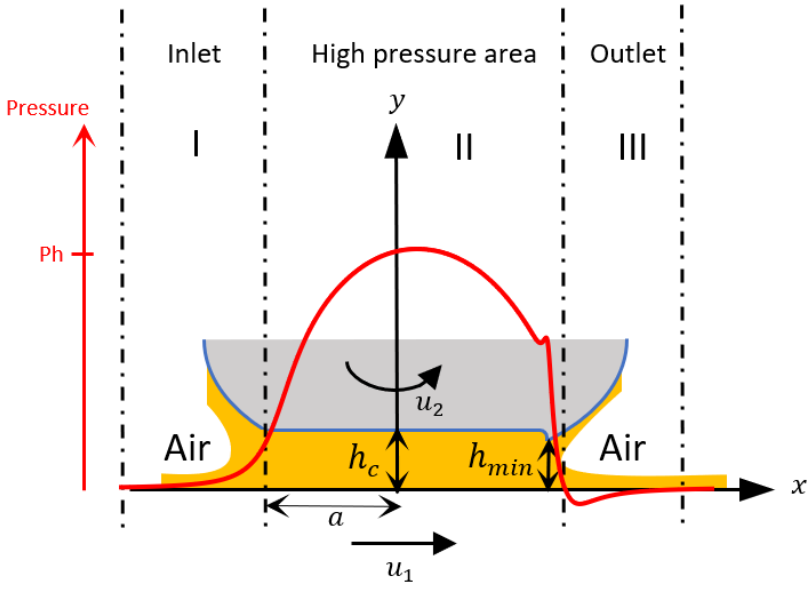

Figure 1.4: Definitions of the different zones of an ElastoHydrohynamic Lubrication (EHL) contact and schematization of resulting pressure profile. With h_c the central film thickness, h_{min} the minimum film thickness, a the Hertzian radius, p_h the maximum Hertzian pressure and u_1, u_2 the velocities of surfaces

Contact inlet

The inlet area is crucial for the film-forming in the lubricated contacts as it dominates the generation of pressure. At the inlet of the EHL contact (see zone I of Figure 1.4), due to the convergent geometry, pressure begins to be generated downstream from the air/lubricant meniscus through hydrodynamic effects, leading to a significant increase of viscosity owing to the piezo-viscosity effects. As a result, two contacting surfaces are separated with the built-up lubricant film thickness. Only a small part of lubricant passes through the contact, while the rest is ejected around or turned back as reverse flow [22].

The air/lubricant meniscus is ideally placed to be far enough from the contact area to ensure that the inlet area is filled with lubricant (fully-flooded condition). However, in many EHL cases, this condition cannot be satisfied and the problem of lubricant starvation arises. An example of the shape of the air/lubricant meniscus under a starvation condition in the case of a point EHL contact is given in Figure 1.5.

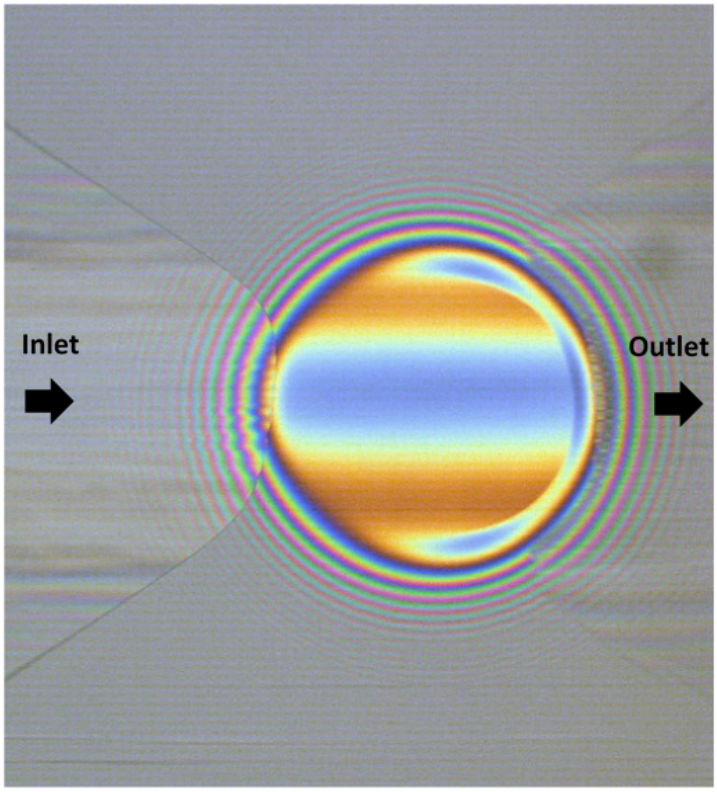

Figure 1.5: Interferogram of location of the air/oil meniscus in a severely starved circular contact obtained with the Jerotrib test rig [23]

In 1971, Wendeven et al. [24] investigated experimentally the position of inlet air/oil meniscus in point contact and observed that with inadequate lubricant, the closer the air-lubricant meniscus approached the contact region, the thinner film thickness was generated. A few years later, Chiu [25] demonstrated experimentally that the degree of EHD film starvation increases with both rolling speed and viscosity. Similar behavior has also been reported in other experimental works [26, 27]. It has been found throughout these experiments that the position and shape of the meniscus are a consequence of the supply rate which depends on many different parameters such as the kinematics, the geometry, and the rheology of the lubricant, and the surface tension between lubricant/air and lubricant/solid.

Regarding the modeling work of starvation phenomenon in EHD contacts, the initial attempts focus on the influence of the position of lubricant/air meniscus on the generation film thickness. In 1970, Wolveridge [28] proposed an expression to calculate thickness reduction with the position of lubricant/air meniscus for line contacts. Later, Hamrock and Dowson [29] extended it for point contacts and proposed a critical position determining the transition between fully flooded and starved conditions. However, since the position of the

lubricant/air meniscus is often unknown, another criterion involving the proportion of lubricant has been proposed to evaluate the starvation degree. In 1996, based on the Elrod model [30], Chevalier [31] introduced an alternative parameter θ to represent the proportion of lubricant in the gap upstream of the contact area and reported the first results for steady-state circular EHD contacts. This model has been extended by Damiens et al. [32] for elliptical contacts and completed by Van Zoelen [33] for the case of severe starvation.

High pressure area

In the high-pressure area (see zone II of Figure 1.4), velocity accommodation causes significant shear stresses at the contacting surfaces, and frictions are generated. In the EHL regime, the pressure rises dramatically and can reach several GPa. The surfaces are then elastically deformed, and the film thickness is reduced to its smallest value h_m. The central film thickness h_c is thus distinguished from the minimal film thickness h_m in the EHL regime (see zone II of Figure 1.4).

Within the high-pressure area or Hertzian area with a the radius of the contact area, the pressure distribution can be very well approximated by using the Hertz theory [8] with p_h the maximum Hertzian pressure.

Contact outlet

The EHL contact outlet (see zone III of Figure 1.4) is prone to lubricant film disruption due to its divergent geometry. After being strongly compressed and sheared in the contact area, the lubricant is subjected to a sudden pressure drop and the rupture of the continuous lubricant film may occur. It is essential to analyze this phenomenon known as cavitation because it might impact the degree of starvation or the lubrication conditions of the next contact. The 1st Leeds-Lyon Symposium, edited by Dowson et al. [34], held in 1974, was the first to devote its whole focus on the topic of the cavitation phenomenon, where the research on fundamental aspects of cavitation, classical film rupture boundary conditions theory and cavitation damage have been presented and discussed. Later, another symposium regarding the cavitating fluid film was held by NASA Lewis Research Center [35]. It included fundamental and experimental observations on cavitation, as well as improved models based on the film rupture boundary conditions theory. The physical nature of the film rupture was finally exposed with the experimental discovery of the sub-ambient pressure upstream of the outlet meniscus [36–39]. The consideration of this cavitating area in detail has been demonstrated crucial in the machine elements with divergent clearance gaps such as journal bearings, spur gears, and rolling

element bearings. The sub-cavity pressure in the divergent gap gives rise to different physical phenomena [34], which are exposed in the following.

If pressure drops below the atmospheric pressure, the gas in the surrounding environment might be sucked into the negative pressure region. When the pressure falls below the saturation pressure of one or multiple substances dissolved in the lubricant, the dissolved substance can be released from the solution in gaseous form. If the pressure in the lubricant continues to fall to its vapor pressure, boiling of liquid may occur.

Various approaches have been proposed in lubrication studies to model cavitation, these models in the literature can be roughly classified into two categories [40]. The first group of models, which included the half-Sommerfeld model [41], Reynolds or Swift-Stieber model [42], and Jakobsson–Floberg–Olsson (JFO) cavitation model [43, 44], relied on film rupture boundary conditions. The second type of model dealt with the lubricant as a homogeneous two-phase flow, where the shapes of the cavitation area were not assumed a priori and the transient phase change was considered. A detailed review of these cavitation models is presented in Chapter 2.

Despite the progress achieved in understanding the fundamental mechanism of cavitation, the outlet area received little attention from the physical viewpoint in EHL studies. Most EHL works adopt the classical Reynolds boundary conditions [4], where the sub-cavity pressure is ignored or simply set to ambient pressure or zero-gauge pressure in numerical works.

Recently, a few experimental observations on cavitation at the EHL outlet have been performed. The vaporous cavitation of oil at the outlet of an EHL contact was observed and examined qualitatively by Bruyère [45] with a ball-on-disk apparatus. Stadler et al. [46] and Emden et al. [47] measured the oil cavity length in EHL rolling point contact and studied the influence of different operating conditions on vapor bubble length. Otsu et al. [48] investigated the effects of surrounding gas on cavitation in EHL sliding point contact in a sealed chamber. Figure 1.6 shows an example of a typical cavitation bubble in an EHL contact outlet [47].

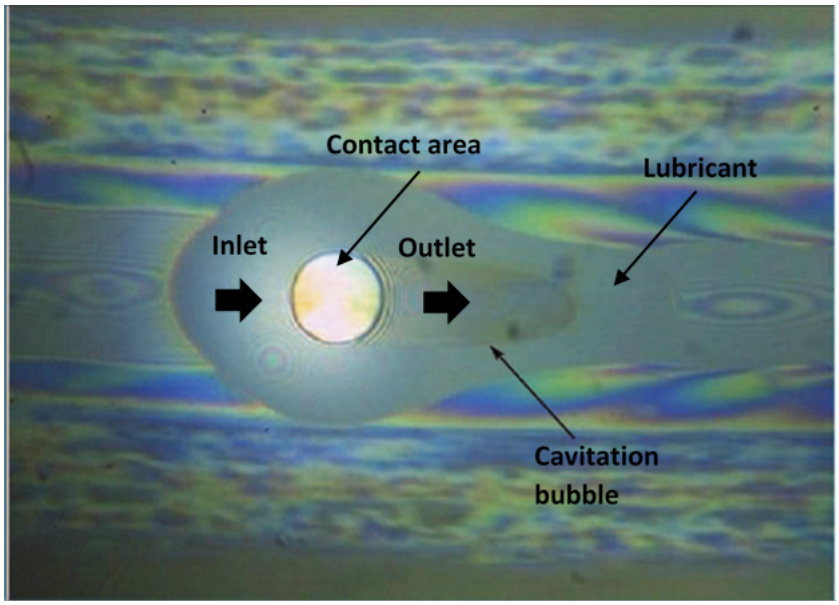

Figure 1.6: Optical interferometry of cavitation bubble in an EHL contact outlet [47]

1.1.3 Intermediate conclusion

This section highlights various numerical and experimental investigations in the literature, in and around the EHL contact. It should be emphasized that in most EHL theories presented before, idealized conditions are considered, while many practical industrial difficulties are neglected. For example, as previously stated, simplifications of the Reynolds equation are no longer justified when the fluid film is ruptured (cavitation and starvation), or when the thermal effects and non-Newtonian effects cannot be ignored.

Another specific case is when the fluids involved in the lubrication are other than neat lubricant (such as oil). It should be noted that the lubricating ability of these mixtures requires special consideration because they can differ significantly from that of neat oil. More details on this issue are provided in the following section.

1.2 Lubrication with oil and operating fluids: an industrial challenge

In the EHL approaches presented previously, a single piezo-viscous fluid is assumed to lubricate rolling contacts. However, in many industrial applications,

the fluid that separates the contacting parts is not just the lubricant (an oil or grease), but often a mixture including the surrounding fluid. For example, engine oil in the lubrication system of vehicles can be contaminated by antifreeze and fuel. Under high system temperatures, oxidation products can develop and mix with oil. Cleaners, lubricants, chemicals, greases, and detergents are all examples of liquid contaminants. These can induce a wide range of lubricant chemical composition alterations. Water is the most common source of contamination, which can be found in the lubricating oil of almost all water-cooled machines [49]. In the paper industry, for example, water contamination is an inevitable part of the manufacturing process. Despite the contaminated effects, some components are combined with oil on purpose. For example, additives are added to engine oils to improve base oil characteristics, while solvents are mixed up with heavy oils to enhance oil recovery and process [50]. In addition, machine elements are often required to operate in environments other than ambient air. Some of the surrounding gases (such as carbon dioxide, argon, and helium) may dissolve in oil [48]. Furthermore, to simplify the design, some mixing working fluids are even being examined as oil replacement lubricants. For example, together with oil, refrigerant is unavoidably involved to lubricate the bearings of refrigerant compressors. The refrigerant concentration in oil should be managed to guarantee the efficient operation of the lubrication system. However, the limiting refrigerant dilution level is difficult to determine [51]. One of the latest trends is even to employ pure refrigerant lubrication (PRL) using magnetic bearings or special hybrid bearings [52, 53].

Because contact parts are inevitably lubricated with a mixture of oil and operating fluids in some cases, and the latter may significantly alter the lubricating ability, it is now a challenge for the industry to anticipate the proper operation of bearings under non-optimal lubrication conditions. The present study mainly concerns two current industry challenges: oil/refrigerant mixtures and oil/water mixtures.

1.2.1 Oil/refrigerant mixture

The oil/refrigerant mixture is problematic for the refrigeration compressor application. In the present design of refrigeration compressors, components such as gears, bearings, and screws (see Figure 1.7) are cooled and lubricated by a dedicated lubrication circuit [54], which would ideally be operated with pure oil. However, in practical applications, the lubricant used in the compressor needs to be miscible with the system refrigerant to ensure that oil will return to the compressor after going through the refrigeration system's cycle [55]. Since oil is in contact with refrigerant and miscible with it, the bearing system in the refrigeration compressor is actually lubricated by a solution, which is a homogeneous mixture of oil and dissolved refrigerant [56].

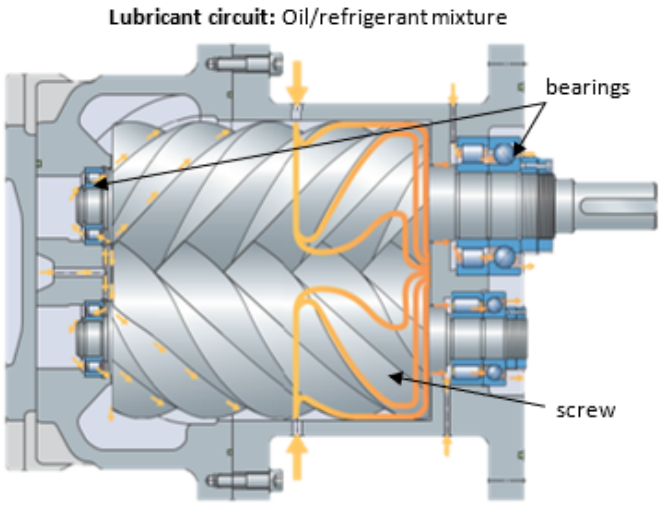

Figure 1.7: Lubricant flow paths in a screw compressor

To understand the consequences of lubricating the contact with an oil/refrigerant mixture in refrigeration compressors, considerable attention has been made to this kind of mixture since the early 1990s. It has been demonstrated experimentally that the dilution of refrigerant in oil has effects of reducing the viscosity and the piezo-viscosity of the solution, and increasing the compressibility, thus decreasing the lubricating abilities of contacts [56–58]. Many studies were performed to measure the film thickness with an oil/refrigerant solution to quantify the effect of refrigerant dilution in oil in EHD contacts [55, 59, 60]. Figure 1.8 illustrates the influence of the refrigerant dilution on the viscosity of the mixture.

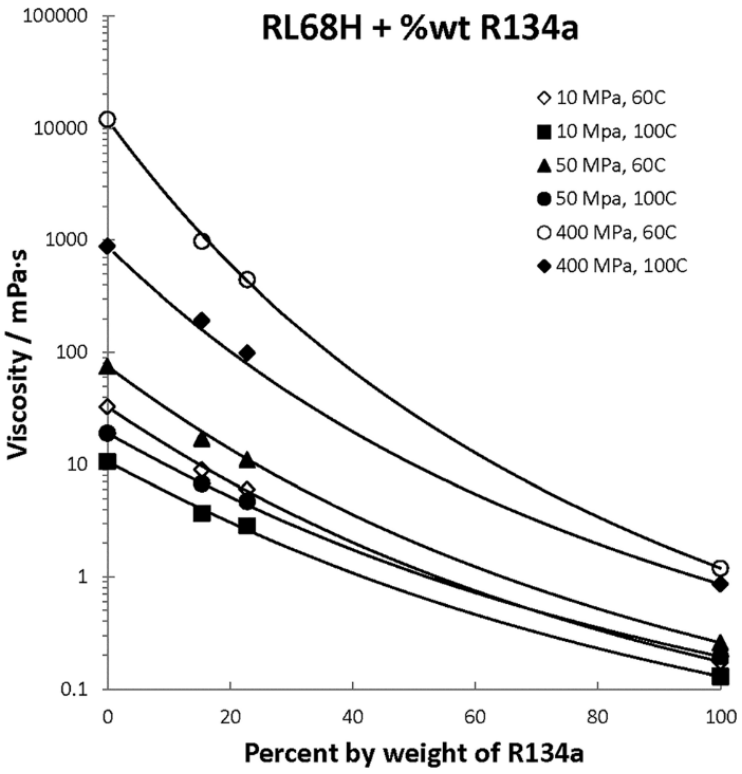

Figure 1.8: Mixing chart of viscosity for the oil/refrigerant system from Ref. [61]

It can be seen from the figure that the viscosity of the oil/refrigerant solution drops sharply as refrigerant concentration increases because the viscosity of the refrigerant is orders of magnitude smaller than that of the oil.

Another issue with oil/refrigerant mixtures is that the refrigerant is highly volatile, therefore the refrigerant concentration in oil is not always constant since the refrigerant dissolved in oil may evaporate or condense when local temperature and pressure change [62]. Because the saturation pressure of the oil is extremely low in comparison to the mixing refrigerant, the vapor phase of the mixture can be assumed to be entirely composed of gaseous refrigerant, and the phase diagram of the oil/refrigerant solution differs significantly from that of a regular mixture. As a result, the liquid-vapor equilibrium of the oil/refrigerant system can be represented by a mixture thermodynamic property known as solubility, which is defined as the mass fraction of the refrigerant in a saturated oil/refrigerant solution at a thermodynamic equilibrium state. The solubility of an oil/refrigerant system, depends on the one hand, on pressure and temperature conditions, and on the other hand, on the nature of the refrigerant and the oil. An example of the typical solubility curve for the oil/refrigerant system is given in Figure 1.9.

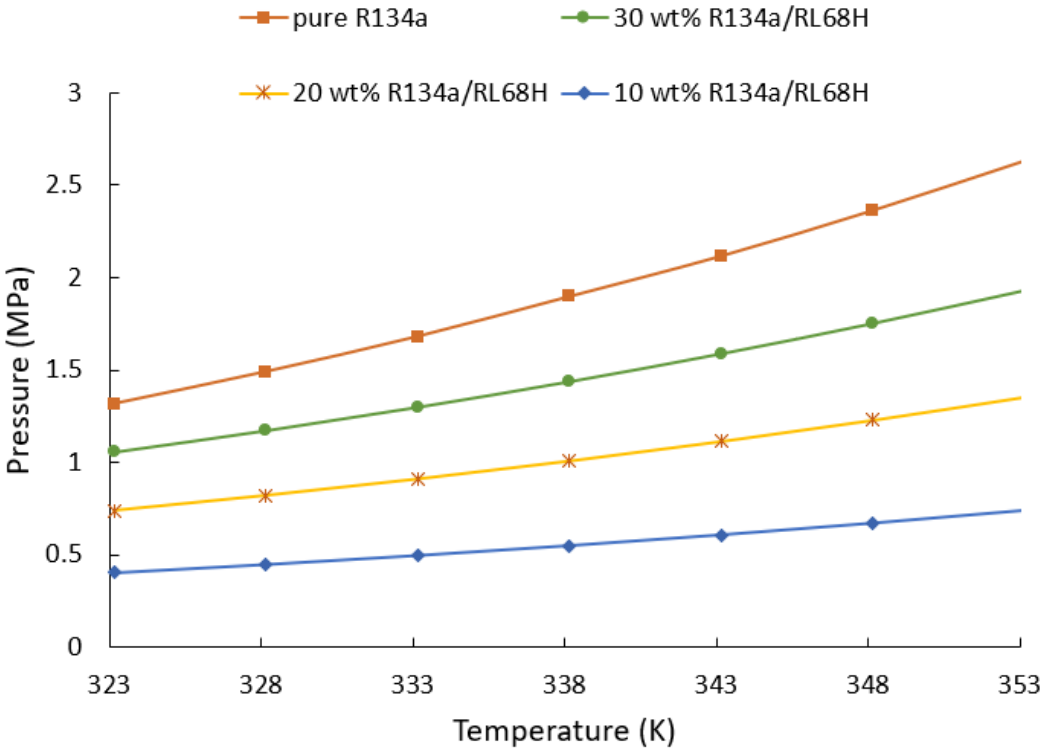

Figure 1.9: Solubility curves of an oil/refrigerant mixture [63]

As can be seen from Figure 1.9, the refrigerant concentration in the oil increases with pressure and decreases with temperature. The composition of the oil/refrigerant solution is of great significance; a slight variation in refrigerant concentration can have a significant effect on its properties, and therefore a considerable influence on film formations [64]. Bearing life can be significantly reduced owing to wear, surface distress and corrosion-enhanced fatigue caused by poor lubrication conditions of oil/refrigerant solution [51, 65]. Consequently, anticipating the appropriate operating conditions of bearings under oil/refrigerant solution lubrication is crucial.

Proper evaluation of the oil/refrigerant mixture properties is an essential stage for estimating EHL film thickness. Considerable efforts have been made to evaluate the lubricating properties, particularly the viscosity pressure dependence of oil/refrigerant solutions. As mentioned previously in Section 1.1.1, very high pressure ($0.4 - 4$ GPa) can be generated in the EHL regime. Measuring the viscosity of lubricants under high pressure is one of the most accurate ways to characterize the lubricants [66]. Many high pressure-viscosity data of neat oil are available in the literature, and the viscosity of both synthetic and mineral common lubricating oils have been investigated experimentally under high pressure and temperature range [67–69]. However, when it comes to the oil/refrigerant solution, the measurement is more difficult than for the neat ones

as the viscosity of solutions cannot be evaluated at atmospheric pressure due to the high volatility of refrigerants. In practice, a pressurized compressor sump is employed in the refrigeration compressor, therefore the EHL inlet pressure for oil/refrigerant solutions is higher than the atmospheric pressure commonly found in classical cases. Several experiments managed to measure the viscosity of some oil/refrigerant systems at saturation pressure or a little higher up to 140 MPa [58, 70–74], however still significantly less than the operating pressure in oil/refrigerant lubricating film. Recently, with the new high-pressure viscometer developed by Bair et al. [75], the viscosity of some combinations of refrigerant/oil solution was firstly measured to high-pressure [63, 76]. For example, viscosity measurements were reported in their research at pressure up to 350 MPa for the mixture of polyester oil and refrigerant R134a with different refrigerant concentrations [63, 75]. Density measurement under high pressure for this oil/refrigerant combination was also provided [77]. These primary rheological measurements permitted the first quantitative analysis for the oil/refrigerant solution lubricated point contacts [61], which was validated by experimental data [74].

Although extensive studies of EHL in oil/refrigerant solutions have been carried out, it has been limited to the investigation of the contact area. Little attention has been paid to the cavitation phenomenon (see Section 1.1.2) occurring at the outlet of the EHD contacts, which is crucial for oil/refrigerant solutions. As mentioned previously, one important feature of the oil/refrigerant solution is its dynamic composition varying with pressure and temperature due to the solubility of refrigerant in oil. It has been observed in the experiments [58] that the sudden pressure drops or variations of temperature at the bearing cavity could enable some of the dissolved refrigerants to evaporate. The cavitation could invoke the disruption of the continuous lubricant film, thus considerably affecting the lubrication of the next rolling element, particularly in a bearing with multiple contacts. To the best of the author's knowledge, no experimental studies have been performed to investigate the cavitation at the outlet of EHD contacts for oil/refrigerant systems as presented in Section 1.1.2 for neat oil. Several initial attempts have been made, however, to explore refrigerant out-gassing in oil in a more simple geometry, such as a straight horizontal small diameter tube [78–81], to provide a basic methodology for the study of oil/refrigerant lubrication in refrigeration compressors. As the oil/refrigerant solution moved towards the exit of the tube, pressure decreased owing to the friction forces. It caused the dissolved refrigerant to be released from the oil in gaseous form, and even a foam pattern developed in the flashing flow at the end of the tube when the void fraction reached a very high level (see Figure 1.10 from Ref. [82]). Based on the experimental results, some numerical models have been proposed to predict the pressure drop in the tube [80, 83, 84]. In 2006, Grando et al. [85] developed a solubility-based cavitation model to analyze lubrication with oil/refrigerant solution in journal bearings based on earlier studies. This model has been applied later to the modeling of the dynamic piston in the refrigeration compressor [86] and has been further developed

under non-isothermal conditions, where the conservation equation of enthalpy was added and solved with a finite volume method [87].

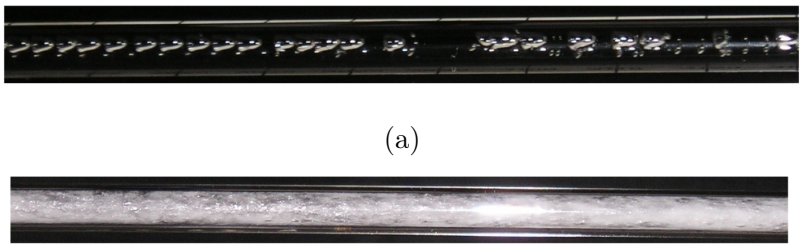

(a)

(b)

Figure 1.10: Flow patterns of the ester oil ISO VG10l-refrigerant R134a mixture flowing through a straight horizontal tube: (a) bubbly flow and (b) foam flow from Ref. [82]

1.2.2 Oil/water mixture

Undesired water has been considered as one of the most deleterious contaminants in lubricated systems [88]. The universal presence of water makes it the most widespread and common contaminant as it can enter lubricants in a variety of ways. Water can condense in oil reservoirs or be absorbed directly by the oil from humid air. The bearing system employed in the hot rolling mills is particularly vulnerable as it is inevitably exposed to large quantities of water. Besides, other sources like leaking steam joints and spraying of clean-up water could cause water contamination as well. Additionally, water is a by-product of the combustion of gasoline and diesel engines in the exhaust gases, which can sometimes enter the sump due to the leakage of joints or improper scavenging [89]. A leaky heat exchanger or oil cooler is also a common source of water contamination for applications like steam turbines and gearboxes, where thermal energy transfer is involved [90].

Oil/water mixtures differ significantly from oil/refrigerant mixtures in that water and oil are not miscible. Depending on water content amounts, the mixture of water and oil exists in different states. The first state is known as dissolved water in oil where water molecules are dispersed throughout the oil. In general, the level of holding water for most industrial oil ranges from 400 to 600 ppm depending on the type, age, and temperature of the oil [91]. If dissolved water continues to increase and exceeds the saturation point, emulsified water will appear in oil as a micro-sized suspension [92]. This form of water-in-oil emulsion is often subject to continuous churning, heating, and high pressurization, which may be engendered by varied causes in operations like high-velocity pipelines, high-shear pumps, or fine filtration mediums. With additional quantities of water in oil, the mixture tends to separate into two distinct

phases with a layer of macro-sized pockets of free water in the oil phase. This state of free water usually comes from condensation or leaks and can often be found at the bottom of sumps and tanks [90]. Among the different states of the water-in-oil mixture, dissolved water is considered to be the least concern to the lubricating quality or performance of the lubricant. It is shown that a small amount of dissolved water has almost no effect on the compressibility or viscosity of the oil [93]. Emulsified oil can be formed when mixing with larger quantities of water. Oil-in-water emulsions, on the other hand, are no longer considered contaminants but instead popular lubricants for cooling and metal cold-rolling processes, the lubricating properties of which have been widely investigated [94–100].

The effects of water on lubricated systems have been extensively studied and can be classified into long-term and short-term effects [91, 101]. Currently, the existing studies are mostly focused on the long-term effects which mainly involve the corrosion on bearing surfaces and chemical changes in the properties of lubricating oils. It has been shown that water can decrease the bearing life dramatically in the long term [88, 102, 103]. Short-term effects include the immediate impacts of water on lubricating oil, such as some changes in viscosity and piezo viscosity [49, 101, 104], both of which have a major influence on film-forming ability. The effects of water in oil as an emulsion on the instant lubricating ability of the contact area have been studied experimentally [92, 105–109], however, the published findings show some discrepancies. The results in the literature may be classified based on the ratio of the central film thickness $h_{c,mix}$ obtained in the water/oil mixture conditions over the mean water droplet diameter D_d, as summarized in Table 1.1. The effect of water droplets on film thickness can be revealed by comparing $h_{c,mix}$ to $h_{c,oil}$, which is the central film thickness obtained with pure oil.

Table 1.1: Experimental data on effects of water droplets in oil on film thickness

$\frac{h_{c,mix}}{D_d}$	Reference	Rolling velocity (m/s)	Water droplet diameter (µm)	Lubricant viscosity Pa · s	Maximum Hertzian pressure (GPa)	Water droplet effect
≥ 1	Dalmaz, 1981 [109]	0.1-3	0.5	0.143	0.12-0.19	$\frac{h_{c,mix}}{h_{c,oil}} > 1$
	Wan et al, 1984 [92]	0.1-2	0.5	0.069-0.092	0.56	
< 1	Wan et al, 1984 [92]	0.1-0.7	4-5	0.092	0.56	$\frac{h_{c,mix}}{h_{c,oil}} = 1$
	Hamaguchi et al., 1977 [105]	0.54	1.5	0.065	0.7	
	Benner et al., 2006 [107]	1-4	3.14	0.036	0.7	
	Liu et al., 1994 [106]	3.14	< 1	0.049	0.9	$\frac{h_{c,mix}}{h_{c,oil}} < 1$

It has been found that the central film thickness $h_{c,mix}$ formed by the water-in-oil emulsion is thicker than that formed by the base oil alone $h_{c,oil}$ when the emulsion's mean particle size D_d is smaller or in the same order as the central film thickness $h_{c,mix}$ [92, 109]. In the research of Wan et al. [92] and Dalmaz [109], the film thickness of oil containing 40 wt% water was measured by using the optical interferometric technique. The water particle employed in their studies was 0.5 µm in diameter, which is in the same order as EHL film thickness. For entrainment speed from 0.1 to 3 m/s, a slight increase in film thickness was observed in both of their studies. Since it is believed that these very fine droplets could enter into the contact [92], the rise in the film thickness can be explained by the fact that the presence of water droplets in oil increases the viscosity of the lubricant as it has been demonstrated in Ref. [101, 104]. Previous investigations, however, are contradictory when the mean droplet size is larger than the film thickness. Some studies [92, 105, 107] found that water-in-oil emulsions behave as pure oil in terms of film-forming ability and suggested that water droplets of large sizes were pushed out before entering the contact area. Hamaguchi et al. [105] measured the film thickness with the optical interference method for water in liquid paraffin and mineral oil emulsions. The mean particle size used was 1.5 µm and oil with up to 70 wt% water content was tested at 0.54 m/s in pure rolling point contact. They stated that the thickness of the EHL film was independent of water content and droplet size, and could be predicted from emulsion base oil. The same conclusion has been drawn by Wan et al. [92], based on their experiments on the water-in-oil mixture with

water droplets size around 4 µm, at $0.1 - 0.7$ m/s. Recently, Benner et al. [107] performed the experiments with emulsions containing up to 30 wt% water for a range of velocity from 1 to 4 m/s with the mean water particle diameter of 3.14 µm. Both film thickness and friction were investigated and no variations with different water concentrations were observed in their experiments. Liu et al. [106], on the contrary, suggested that large water patches formed in the contact region decreased the film thickness. They measured the EHD line contact film thickness with an X-ray transmission technique at 3.14 m/s with the water droplets size of about 1 µm and reported a slight decrease in film thickness for different water concentrations in oil. Another interesting feature has been reported by Ratoi-Salagean and Spikes [110]. They observed a decrease in film thickness of tested water-in-oil emulsion at high speed and supposed that starvation in the inlet might occur. However, since the experimental studies in the literature were mostly focused on measurements of film thickness or friction in the contact area, it is difficult to reach a general agreement on emulsion flows at the inlet of the contact area. Meanwhile, direct observation of emulsion flow has received little attention as a more straightforward technique. Few direct observations for oil-in-water emulsion have been performed [111–113], which demonstrated that emulsion film-forming ability was highly dependent on the rolling speeds. These experiments provided a direct evaluation of the existing theories and were considered crucial in helping to understand the lubrication mechanisms of oil-in-water emulsions. Unfortunately, in the case of water-in-oil emulsions, to the best of the author's knowledge, there exists only one direct observation (see Figure 1.11) by Liu et al. [91]. They examined the flow of macro-sized free water in oil at the contact's entry and discovered that free water could aggravate oil starvation.

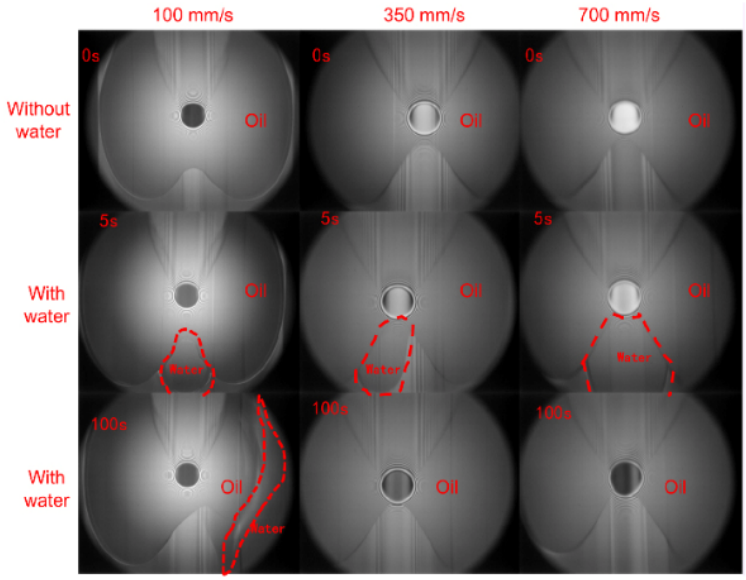

Figure 1.11: Influence of a 2 µL water droplet on the oil reservoir under different lubricating conditions from Ref. [91]

In addition to the experimental work, various theoretical models for studying water/oil emulsions have been presented. Based on continuum mechanics of mixtures, Al-Sharif et al. [114] developed an extended Reynolds equation for a binary mixture of journal bearing. Wang et al. [115] then applied this equation for lubrication with emulsion in EHL line contacts. Recently, this model has been employed by Benner et al. [107] to the EHL point contacts with water-in-oil emulsions. However, the continuum mechanics approach is considered to be appropriate only when the gap of solid surfaces is greater than the diameter of droplets, as droplet interaction with other droplets or surfaces is not considered in this approach [114–116]. For the thin film regime, where the gap is some fraction of droplet size, the concept of dynamic concentration of dispersed phase was proposed by Wilson et al. [98]. They defined a concentration region in which droplets bigger than the gap was thought to be sandwiched between the two solid surfaces. Later, this concentration model was further developed by introducing the corrections to pressure gradients caused by oil-water interactions [117]. Yan and Kuroda [116] developed a more general model by combining the work of Wilson et al. [98, 117] and that of Al-Sharif et al. [114]. They employed different effective viscosity of the mixture for the different regimes and applied it to the HL line contact studies. Recently, Lo et al. [97] found that the pressure gradient of the dispersed phase and continuous phase is not proportional to its volume fraction. They modified Yan and Kuroda's model and involved the transition from a region where the lubricant gap is larger than the diameter of droplets to a region where the lubricant film is thinner than the diameter of droplets. It is worth mentioning that the aforementioned theories focused mostly on oil-in-water emulsions. Oil droplets were supposed to be concentrated in water approaching the contact area, followed by phase inversion. The regions of oil-in-water emulsion lubrication in an EHL inlet zone described based on these theories can be found in Figure 1.12. Liu et al. [106] proposed a two-phase hydrodynamic film model, where the water is assumed to exist in the form of patches and suspended droplets. An equivalent viscosity was introduced in Reynolds equations to represent the bulk properties of emulsions. The above theoretical models focus on the calculation of concentration distribution of the dispersed phase in the continuous phase and are capable to predict the inversion between the two phases. They cannot, however, be utilized to determine the trajectories of water droplets in oil.

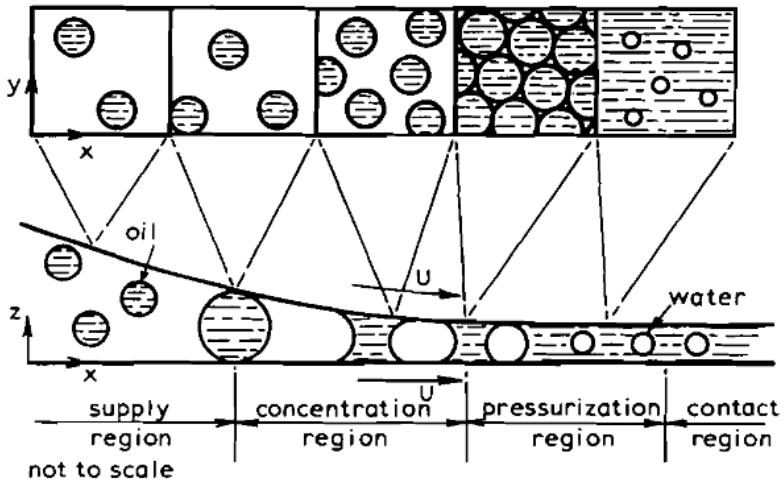

Figure 1.12: Regions of emulsion lubrication in an EHL inlet zone from Ref. [117]

1.2.3 Intermediate conclusion

General context and problems of operating fluids in lubrication systems were presented in this section, with two current industrial challenges: the oil/refrigerant mixture, and the oil/water mixture, highlighted. The studies involving oil/refrigerant mixtures and oil/water mixtures are of significant difference due to their distinct mixed states. When refrigerant mixes with oil in the refrigeration compressor, due to the miscibility, a solution is formed, containing a homogeneous mixture of oil and volatile refrigerant. Consequently, attention should be paid to the film-forming ability of oil/refrigerant solutions in the pressurized region and refrigerant evaporation/condensation in the cavitated region. Water, on the other hand, is not miscible with oil and can exist in oil as suspended water droplets. As previously stated, water droplets have been observed to be ejected under pressure and shear before entering the contact area [91, 107, 118], hence the fundamental step of investigations is the study of water droplets in oil flow at the inlet area.

1.3 Summary and objectives of the thesis

Numerous efforts have been devoted to the EHL studies in the past, providing an essential understanding of thin-film lubrication mechanisms. However, there are still many unknowns concerning the interaction of the lubricant with its surroundings, especially around the contact area. Whereas classical EHL

theory assumes that a single piezo viscous fluid lubricates rolling-sliding contacts, lubrication systems often involve fluids other than pure lubricants. Depending on the applications, the lubricating fluid can be a mixture of lubricant and surrounding fluids. Lubrication with such mixtures is a current industrial challenge. The research presented in this thesis aims to provide a better understanding of the risks for an EHL contact, which is lubricated with a mixture of oil and operating fluids.

Two common industrial mixtures are investigated: the oil/refrigerant mixture and the oil/water mixture, both of which are examples of two types of mixed states: miscible fluids and immiscible fluids, respectively. Based on the previous literature review, it can be inferred that the context of these two types of mixtures in EHD contacts differs significantly. Depending on the characteristic features of mixtures, the investigations will focus on different zones of the contact area (inlet and outlet of the contact).

Throughout this work, a dual problem is addressed, and therefore distinct research methodologies are required to handle the relevant challenges. In the next chapter, the different approaches implemented to investigate miscible and immiscible fluids are presented.

Chapter 2

Research Methodology

A dual problem is addressed in this chapter. First, the necessity of developing distinct research methodologies for different kinds of mixtures is emphasized. Using the oil/refrigerant solution as an example, a homogeneous two-phase flow approach completed with solubility-based cavitation modeling is provided for miscible fluids. For immiscible fluids such as water-in-oil emulsion, an in-situ visualization technique is proposed to observe directly the motion of water droplets. A numerical method for water droplet tracing is also developed.

2.1 A dual problem

As mentioned in Chapter 1, lubrication systems in industrial applications often involve fluids other than the neat lubricant, but a mixture of the lubricant and the surrounding fluid. When it comes to a mixture, the first step is to determine its mixed state because the behavior of different types of mixtures varies considerably. The mixed state is determined by the composition of the mixture, as well as the pressure and temperature conditions. In general, a binary mixture system has three levels of miscibility [119]: miscible, partially miscible, and immiscible. If two substances mix in any proportions or concentrations to form a solution, they are miscible. They are partially miscible when they mix in only certain proportions. Immiscible means that two substances cannot completely mix to form a solution. When they combine, they may separate into layers or produce a heterogeneous mixture.

The oil/refrigerant mixture and the oil/water mixture, both of which are representative of two types of mixed states, miscible fluids, and immiscible fluids, are investigated in this work as common mixtures found in the industry. Based on the previous literature study, it can be concluded that the context of these two types of mixtures varies considerably. The oil/refrigerant mixture involved in the refrigeration compressor application is actually a solution, which is a homogeneous mixture of oil and volatile refrigerant. The oil/water mixture studied in this work, on the other hand, is an emulsion with water droplets in oil. Because of the different characteristics of these two mixtures, the EHL investigations in oil/refrigerant solutions and water droplets in oil emulsion differ significantly. There are two major issues with the oil/refrigerant solution in EHL contacts. First, the dilution of the refrigerant in oil can reduce the lubricating capacity of oil. Second, because of its volatility, the refrigerant may evaporate dramatically at the contact outlet, thus affecting the lubricating situation for the following contact [120]. As a result, EHL studies should focus on the film-forming ability of oil/refrigerant solutions in the pressurized zone and refrigerant evaporation/condensation in the cavitated region. On the other hand, the problem of water droplets in oil emulsion is addressed at the contact inlet. Because water droplets have been reported in the literature to be

potentially expelled away from the contact under pressure and shear when approaching the contact region [91, 107, 118], the water droplet motion at the inlet area is critical in EHL studies to evaluate the risks of water droplet contamination in the oil. Since this thesis addresses a dual challenge, two distinct EHL research methodologies are proposed to handle the respective problems: miscible fluids and immiscible fluids.

2.2 Miscible fluids

2.2.1 Problem formulation

The oil/refrigerant solution in the refrigeration compressor lubrication system is explored in this work as an example of miscible fluids lubricated contacts. As previously mentioned in Chapter 1, the bearing system in the refrigeration compressor is lubricated by a solution, which is a homogeneous mixture of oil and dissolved refrigerant. The dilution of the refrigerant in oil reduces its lubricating ability by reducing the viscosity and the piezo-viscosity of the solution and increasing the compressibility [121]. Another main issue of the oil/refrigerant solution in EHL contacts is the refrigerant cavitation phenomenon at the contact outlet due to the high volatility of the refrigerant, schematically presented in Figure 2.1. As can be seen from this figure, the bearing presents a convergent-divergent geometry. After being strongly compressed and sheared in the contact area, the oil/refrigerant solution flow enters the divergent region at the contact outlet, where it suffers a sudden drop of pressure. When the pressure in the cavitated region falls below the saturation pressure of the oil/refrigerant solution at the local temperature, an amount of excessive refrigerant will evaporate and be released from the oil/refrigerant solution. As the solution flow moves further towards the contact outlet, the refrigerant gas can be re-dissolved in the solution because of the recovery of the pressure to the surrounding pressure. The mass fraction of the refrigerant in the liquid oil/refrigerant solution depends on the initial concentration of the refrigerant, the local pressure, and temperature.

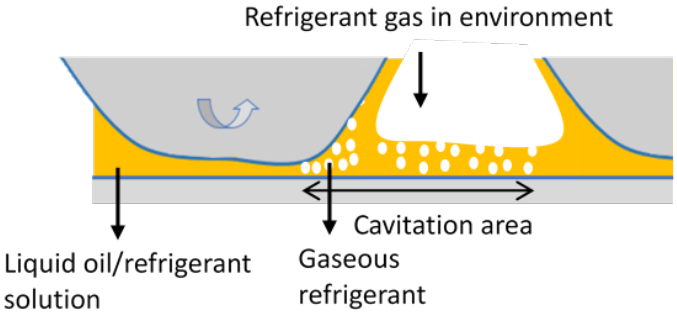

Figure 2.1: Schematic of the oil/refrigerant solution at the outlet of the first point contact, flowing towards the successive contact

Accordingly, the investigation of the oil/refrigerant solution should consider not only the pressurized region, accounting for a liquid solution of oil and dissolved refrigerant but also the cavitation region, where liquid and gas phases interact. Because a pressurized compressor sump is used in the refrigeration compressor and the pressure applied around the contact area is higher than atmospheric pressure [61], the experimental observations of the cavitation area must be performed in a pressurized environment, which is extremely difficult. As previously stated in Chapter 1, to the best of the author's knowledge, no experimental studies have successfully observed the cavitation at the outlet of EHL contacts for oil/refrigerant systems due to the limitations of the experimental approach. As a result, the current study seeks to investigate the cavitation area of oil/refrigerant systems using a numerical approach. A numerical analysis of Thermal ElastoHyrodynamic Lubrication (Thermal-EHL) has been developed for an oil/refrigerant system to predict the film-forming ability in the contact area and the potential risks of the refrigerant evaporation at the contact outlet [120].

2.2.2 Cavitation models

Literature review of cavitation models

Considerable amounts of cavitation models for pure oil have been proposed over the years, of which the evolution over time could be found in an extended review by Braun and Hannon [122]. According to Bayada and Chupin [40], these models in the literature can be roughly classified into two categories.

The first group of models, such as the classical half-Sommerfeld, the Reynolds, and the Jakobsson–Floberg –Olsson (JFO) cavitation models, used the approach based on film rupture boundary conditions [122]. Half-Sommerfeld model [41] distinguished the cavitation region and the pressurized region with a predefined

pressure condition p_{cav} and considered that pressure remained constant for the entire cavitation region. The Reynolds model also known as Swift-Stieber model [42] inherited the constant pressure assumption of the Half-Sommerfeld condition, however, a zero-pressure gradient condition was assumed instead for the start of the cavitation. Although none of these models accounted for the film reformation and the mass conservation, they have been widely used to describe the cavitation phenomena because of their simplicity [40]. Conversely, the JFO cavitation model [43, 44] was a mass conserving one and it took also the film reformation into consideration. Several algorithms have been proposed in association with this theory and one of the most famous is known as Elrod and Adam (EA) algorithm [123]. Intermediate boundary conditions were implied in this algorithm by introducing a switch function to terminate the pressure gradient in the cavitation region. Further developed versions based on the EA algorithm have been proposed by many authors, such as Vijayaraghavan and Keith [124], Brewe [125] and Sahlin et al. [126]. Kumar and Booker [127] proposed a cavitation model based on the finite element method where some notions of two-phase flow have been introduced. This model has been extended later by Boedo et al. [128] to EHL studies by coupling finite element algorithm with bearing elasticity. Attempts have also been made by Bonneau et al. [129] for EHD analysis with a new cavitation model by combining Murty's [130] algorithm with the JFO cavitation condition.

Note that these previous models were all based on the film rupture boundary conditions and the cavitation process was not modeled directly [131]. The ignorance of two-phase flow in the cavitation region led to the difficulty of considering the variation of density and viscosity in this area.

The second type of model dealt with the lubricant as a homogeneous two-phase flow, where the shapes of the cavitation area were not assumed and the transient phase change was considered [40]. A better knowledge of the characteristics of the different phases was required as the constitutive equation was solved for the mixture flow. Recently, a popular trend to deal with cavitation was to calculate the simplified properties of the mixture based on the assumption that the phase change process is isentropic. Associated models have been proposed for both Reynolds system [40] and Navier-Stokes system [45, 132]. In some other research, a simple polynomial curve fitting is used to ensure a gradual smooth phase transition [133, 134]. It must be emphasized that the above cavitation models were mostly applied to the pure lubricant where the gas-liquid mixture in the cavitation area was of the same fluid [40].

Several attempts have been made to investigate the cavitation of a lubricant solution composed of different substances. Xing et al. [135] used a 3-D Navier-Stokes equation combined with a homogeneous cavitation model for a mixture of oil and originally dissolved gas. A few other models have been developed based on solubility, which is a thermodynamic property of a mixture system.

In these models, the local mass fraction of dissolved substance was no longer constant and was calculated based on its solubility in the liquid. A cavitation model based on air solubility for oil/air mixture has been developed and applied to journal bearing by Li et al. [136]. Similarly, Grando et al. [85] performed an analysis for lubrication with oil/refrigerant solution in journal bearing by using a solubility-based cavitation model. This model has been applied later to the modeling of the dynamic piston in the refrigeration compressor [86] and has been further developed under non-isothermal conditions, where the conservation equation of enthalpy was added and solved with a finite volume method [87].

Novel cavitation model for oil/refrigerant solutions

Inspired by the previous work of the solubility-based cavitation model, a novel cavitation model proposed by the current author [120] for oil/refrigerant solutions is presented in this section.

Considering the existence of liquid-gas phase change in the cavitation area, it is essential to characterize the lubricant mixture by evaluating properly its local compositions. It should be noticed that the oil/refrigerant solution used in the refrigeration compressor is composed of a low vapor pressure oil and a volatile refrigerant [137]. As a result, the gaseous phase is assumed to be only formed by refrigerant gas and the liquid phase is a solution of oil and dissolved refrigerant. The presence of oil vapor is not considered in this work (for validation of this assumption, see Chapter 3). To couple with the generalized Reynolds equation, the density and viscosity of the mixture are calculated based on refrigerant solubility.

The liquid refrigerant mass fraction in the total oil/refrigerant solution can be expressed as:

$$w_{rl} = \frac{m_{rl}}{m_{rl} + m_{ol}} \tag{2.1}$$

where m_{rl} and m_{ol} are, respectively the mass of the liquid refrigerant and the liquid oil.

At a thermodynamic equilibrium state, the mass fraction of the refrigerant in a saturated oil/refrigerant solution is defined as solubility $w_{sat}(p, T)$. It depends on the different combinations of the oil/refrigerant solution, as well as pressure and temperature. The value of solubility increases with pressure and decreases with temperature [80].

The initial mass fraction of the refrigerant $w_{rl,in}$ at the inlet is calculated by its solubility in oil at a given pressure p_s and temperature T_s in the compressor sump [61]:

$$w_{rl,in} = w_{sat}(p_s, T_s) \tag{2.2}$$

Moreover, the liquid solution of oil/refrigerant is considered saturated or sub-saturated so that no additional refrigerant from the environment can be dissolved in the oil [61]. As there is no phase change in the pressurized region, the local mass fraction of liquid refrigerant then gives:

$$w_{rl} = w_{rl,in} \tag{2.3}$$

The cavitation phenomenon occurs when local solubility $w_{sat}(p,T)$ falls below the initial mass fraction of refrigerant $w_{rl,in}$ due to the decrease of pressure or increase of the temperature. In the configuration of the present work, the outlet of the lubricated contact is prone to this phenomenon because of its divergent geometry, where the oil/refrigerant solution suffers a sudden drop of pressure. An amount of excessive refrigerant will evaporate and be released from the oil/refrigerant solution and then be re-dissolved because of the recovery of the pressure to the outside pressure.

As a result, the local mass fraction of the liquid refrigerant in the cavitation region can be expressed as:

$$w_{rl} = w_{sat}(p,T), \quad \text{if} \quad w_{sat}(p,T) \leq w_{rl,in} \tag{2.4}$$

It should be noticed that, in the present case, the evaporation and dissolution of the gaseous refrigerant are considered to be instantaneous and the system is assumed to reach the thermodynamic equilibrium instantly [85]. For more rigorous investigation, additional information on the evaporation and dissolution rate is required. To summarize, the local composition of the oil/refrigerant solution can be expressed as follows:

Mass fraction of liquid refrigerant in the solution w_{rl}:

$$w_{rl} = \begin{cases} w_{rl,in}, & \text{if} \quad w_{sat}(p,T) > w_{rl,in} \\ w_{sat}(p,T), & \text{if} \quad w_{sat}(p,T) \leq w_{rl,in} \end{cases} \tag{2.5}$$

Mass fraction of liquid oil in the solution w_{ol}:

$$w_{ol} = 1 - w_{rl} \tag{2.6}$$

For the mixture of oil/refrigerant solution and refrigerant gas, a homogeneous compressible flow is assumed as it was observed that gas and liquid in this system moved at a very similar speed [78]. The liquid and gaseous phases can be considered to share the same pressure field since the surface tension effects can be neglected [138].

With the above assumptions, the averaged property of oil/refrigerant solution and refrigerant gas can be calculated. The mass fraction of the refrigerant

gas x_{rg}, which represents the ratio of the mass of refrigerant gas m_{rg} in the total mass of the mixture, is given by:

$$x_{rg} = \frac{m_{rg}}{m_{rg} + m_{ml}} \tag{2.7}$$

where the total mass of mixture is the sum of the mass of the liquid solution m_{ml} ($m_{ml} = m_{rl} + m_{ol}$) and the mass of the refrigerant gas m_{rg}.

By considering the mass conservation of oil and refrigerant between the inlet and an arbitrary position of lubricating flow at an equilibrium state, x_{rg} writes [85]:

$$x_{rg} = \frac{m_{rl,in} - m_{rl}}{m_{rl,in} - m_{rl} + m_{ml}} = \frac{w_{rl,in} - w_{rl}}{1 - w_{rl}} \tag{2.8}$$

The volume fraction of refrigerant gas α_{rg}, which is defined as the ratio between the refrigerant gas volume and the total volume of the mixture, can be expressed in terms of the mass fraction of the refrigerant gas x_{rg} and the liquid and gas densities, ρ_{ml} and ρ_{rg} respectively:

$$\alpha_{rg} = \frac{x_{rg}\rho_{ml}}{x_{rg}\rho_{ml} + (1 - x_{rg})\rho_{rg}} \tag{2.9}$$

Accordingly, the density of the two-phase mixture can be written as:

$$\rho_m = \alpha_{rg}\rho_{rg} + (1 - \alpha_{rg})\rho_{ml} \tag{2.10}$$

Various correlations have been proposed in the literature to estimate the viscosity of a two-phase flow mixture. Some of them are attributed to the detailed interface of liquid and gas. Llewellin [139] applied a linear Jeffreys model to consider the effects of gas volume fraction, the relaxation time, and bubble size distribution on the viscosity of the bubbly liquid. Murai and Oiwa [140] reported that when individual bubbles deform transiently, the effective viscosity of the mixture increases. Different viscosity correlations have been proposed by them according to the capillary number which is calculated from surface tension, bubble radius, and shear rate. Whereas the average viscosity is often used to describe a homogeneous two-phase mixture when surface tension is negligible [138, 141], which corresponds to the case of the present study. However, it is difficult to assign a general definition of average viscosity. Owen [142] assumed that the mixture viscosity equals the liquid viscosity. Cicchitti et al. [143] defined the viscosity based on the mass fraction of each phase. Dukler et al. [144] presented the viscosity by the volume fraction of each phase. Other forms of viscosity expressed by volume fraction also exist in the literature [145–147]. The impacts of these different correlations are evaluated by Wong et al. [141] by comparing predicted pressure drops for the liquid-gas mixture of refrigerant along the capillary tube with measured data Dukler. They reported

that the Dukler viscosity correlation gives the best prediction with an average error of 0.81 %. The Dukler viscosity correlation was then used by many authors [83, 87, 136, 148] to calculate the average viscosity of homogeneous liquid-gas mixture. Therefore, this correlation is also adopted in the present work:

$$\mu_m = \alpha_{rg}\mu_{rg} + (1 - \alpha_{rg})\mu_{ml} \tag{2.11}$$

It should be noticed that, in the present work, the evaporation of refrigerant at the exit of the contact is defined as refrigerant cavitation to distinguish from vaporous cavitation which implies the boiling of the oil when the film pressure falls below the vapor pressure of pure oil [122].

It is critical to emphasize that, for a more thorough analysis, the effects of shear stress should be considered in the cavitation criterion for the flowing fluids. According to Joseph [149] and Bair [63], cavitation occurs when the largest principal stress becomes tensile. The pressure threshold which determines the cavitation in the flowing fluid should be the sum of p_{sat} and $\mu\dot{\gamma}$ [148]. Where, μ is the viscosity, $\dot{\gamma}$ is the shear strain rate, and p_{sat} is the thermodynamic saturation pressure calculated in the conditions where the fluid is in a steady and equilibrium state. However, in the current study, considering simply saturation pressure as the pressure threshold for phase transition in cavitating flows is appropriate since a steady and equilibrium condition for fluid is assumed [148, 150]. Furthermore, the velocity of the flowing fluid is low, and the pure rolling condition is addressed. As a result, shear stress is negligible and can be ignored during fluid flow.

2.2.3 Numerical modeling of oil/refrigerant lubricated EHD contacts

When a load is applied, if the radii of curvature of the contacting bodies in the principal directions are not equal, the contact area takes the shape of an ellipse. It is known as an elliptical contact. In the case of contacts between two spheres, the contact area is in the shape of a circle, which is referred to as a circular contact. Besides, line contacts represent the contacts between the elements that can be considered infinitely long in one of the main directions. By applying a normal load, a contact zone of the form of the strip is obtained.

In the present study, a lubricated circular contact configuration is considered as shown in Fig. 2.2 (a). An adaptation of this model to line contact is described in Appendix A. According to Habchi [15], the geometry can be reduced to a contact between a plane and a sphere of radius R (see Figure 2.2 (b)). The contacting surfaces are separated by a thin film of lubricant, submitted to an external load w, and have constant surface velocities only in the

x-direction. Pure rolling condition is considered, which means the plane and the sphere surface move along the x-direction with the same velocity $u_{1x} = u_{2x}$. Smooth surfaces and a fully-flooded lubrication regime are assumed. A permanent regime is assumed since the system in the present study is considered to reach the thermodynamic equilibrium instantly.

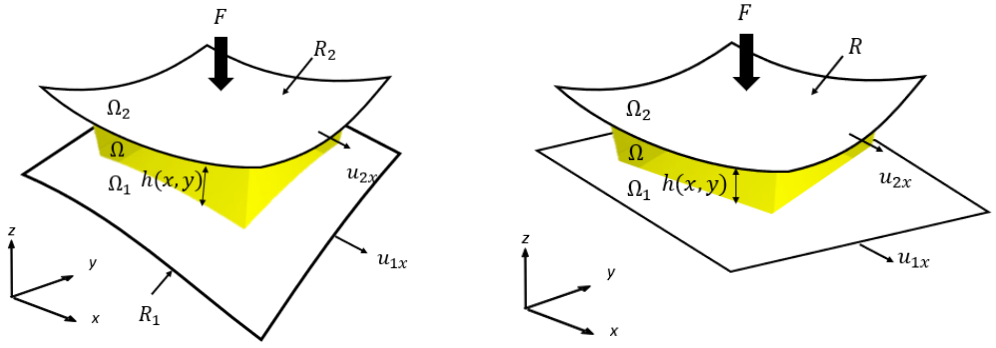

(a) (b)

Figure 2.2: (a) Typical lubricated point contact schema and (b) its equivalent contact geometry. Ω is the fluid domain. Ω_1 and Ω_2 correspond to the top and bottom solid, respectively.

The numerical procedures proposed by Habchi [19] for a single-phase fluid are here adapted for the oil/refrigerant solution. A homogeneous two-phase flow approach is developed based on finite element resolution of the different Thermal-EHL equations by considering steady-state conditions [120]. The pressure distribution within the lubricant film is described by the generalized Reynolds equation. It is completed by the novel cavitation model presented in the previous section to account for both the pressurized region and cavitation region. The elastic deformation of the contacting elements is calculated by the linear elasticity equations. The temperature variation in the lubricated contact is governed by the energy conservation equation. Note that, compared to the work of Habchi [19], the energy conservation equation is modified to consider the heat transfer caused by the liquid-gas phase change. Finally, the equality between the applied force and pressure generated by the lubricating film is ensured by the load balance equation. The above equations are discussed in detail in the following sections.

Generalized Reynolds equation

The Generalized Reynolds equation [151] adapted for a two-phase flow by introducing the mixture properties defined in the cavitation model section (see Section 2.2.2) is solved on the two-dimensional contact area Ω_R, of which the dimension is $16a \times 6a$, defined for $x \in [-4.5a, 11.5a]$ and $y \in [-3a, 3a]$, with

a the Hertzian contact radius (see Figure 2.3 (a)). It should be noticed that the outlet length of the contact has been extended to 11.5a to ensure that the domain is large enough for accurately capturing cavitation and film reformation. The Generalized Reynolds equation allows for the variations of both viscosity and density across the film:

$$-\frac{\partial}{\partial x}\left[\left(\frac{\rho_m}{\mu_m}\right)_e \frac{\partial p(x,y)}{\partial x}\right] - \frac{\partial}{\partial y}\left[\left(\frac{\rho_m}{\mu_m}\right)_e \frac{\partial p(x,y)}{\partial y}\right] + \frac{\partial \rho^*_{x,m}}{\partial x} + \frac{\partial \rho^*_{y,m}}{\partial y} = 0 \quad (2.12)$$

where the integral terms are written as follows:

$$\begin{aligned}
\left(\frac{\rho_m}{\mu_m}\right)_e &= \frac{\mu_{e,m}}{\mu^{'}_{e,m}}\rho^{'}_{e,m} - \rho^{''}_{e,m} \\
\rho^*_{x,m} &= \rho^{'}_{e,m}\mu_{e,m}(u_{2x} - u_{1x}) \\
\rho^*_{y,m} &= \rho^{'}_{e,m}\mu_{e,m}(u_{2y} - u_{1y}) \\
\rho_{e,m} &= \int_0^{h(x,y)} \rho_m(p,T,w)\, dz \\
\rho^{'}_{e,m} &= \int_0^{h(x,y)} \rho_m(p,T,w) \left(\int_0^z \frac{1}{\mu_m(p,T,w)}\, dz^{'}\right) dz \\
\rho^{'}_{e,m} &= \int_0^{h(x,y)} \rho_m(p,T,w) \left(\int_0^z \frac{z^{'}}{\mu_m(p,T,w)}\, dz^{'}\right) dz \\
\frac{1}{\mu_{e,m}} &= \int_0^{h(x,y)} \frac{1}{\mu_m(p,T,w)}\, dz \\
\frac{1}{\mu^{'}_{e,m}} &= \int_0^{h(x,y)} \frac{z}{\mu_m(p,T,w)}\, dz
\end{aligned} \quad (2.13)$$

The boundary condition for the previous equation is:

$$p = p_s \quad \text{on } \partial\Omega_R \quad (2.14)$$

It should be noticed that, in the current study, the pressure p_s applied around the contact area $\partial\Omega_R$ is higher than atmospheric pressure because a pressurized compressor sump is employed in the refrigeration compressor [61].

Since the Generalized Reynolds equation coupled with the mixture properties defined in the new cavitation model(see Section 2.2.2) is solved on the whole contact area Ω_R, which includes the exit of the contact, the free boundary problem is naturally solved.

Additionally, a symmetry condition on the $x - z$ plane at $y = 0$ is applied to reduce computational efforts.

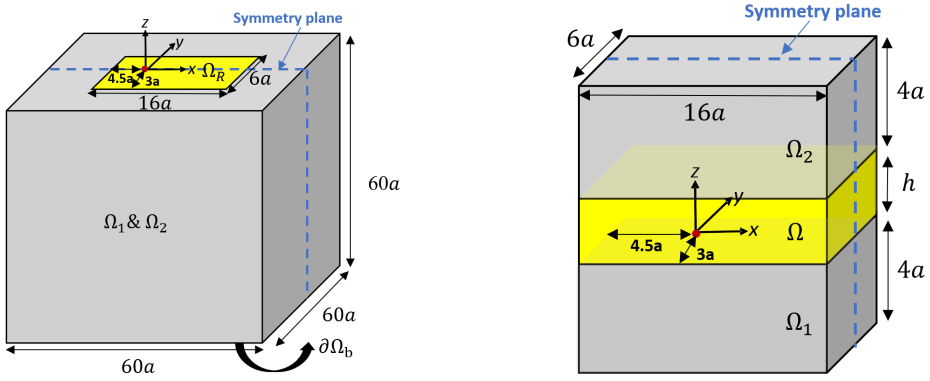

(a) (b)

Figure 2.3: Geometries used for (a) the EHL problem and (b) the Thermal problem

Linear elasticity equation and load balance equation

The film thickness includes the elastic displacement of the surface $\delta(x, y)$, the separation of the solid bodies h_0 and the original undeformed geometry of the contacting surfaces:

$$h(x, y) = h_0 + \frac{x^2 + y^2}{2R} - \delta(x, y) \tag{2.15}$$

The linear elasticity equation is solved on a three-dimensional equivalent domain $\Omega_1 \& \Omega_2$, defined for $60a \times 60a \times 60a$ (see Fig. 2.3 (a)), of which the material properties (Young's modulus E_{eq} and Poisson's ratio υ_{eq}) are obtained by applying the equivalent model proposed by Habchi et al. [15]:

$$\begin{aligned} E_{eq} &= \frac{E_1^2 E_2 (1+\upsilon_2)^2 + E_2^2 E_1 (1+\upsilon_1)^2}{[E_1(1+\upsilon_2) + E_2(1+\upsilon_1)]^2} \\ \upsilon_{eq} &= \frac{E_1 \upsilon_2 (1+\upsilon_2) + E_2 \upsilon_1 (1+\upsilon_1)}{E_1(1+\upsilon_2) + E_2(1+\upsilon_1)} \end{aligned} \tag{2.16}$$

The elastic displacement $\delta(x, y)$ in the z direction of the contacting elements results from the linear elasticity equation, which equals to the value of the z component of the displacement vector $\boldsymbol{U(x, y, z)}$. The stress tensor σ is expressed as a function of the strain tensor $\epsilon_s(\boldsymbol{U})$ and the compliance matrix C which relates to the material properties:

$$div(\sigma) = 0 \quad with \quad \sigma = C : \epsilon_s(\boldsymbol{U}) \tag{2.17}$$

Associated boundary conditions are presented as follows:

$$\begin{aligned} &\boldsymbol{U} = 0 \quad \text{at the bottom boundary } \partial\Omega_b \\ &\sigma_n = -p \quad \text{at the contact area } \Omega_R \\ &\sigma_n = 0 \quad \text{elsewhere} \end{aligned} \tag{2.18}$$

Finally, the load balance equation writes:

$$\int_{\Omega_R} p(x, y)\, d\Omega = F \tag{2.19}$$

Additionally, a symmetry condition on the $x - z$ plane at $y = 0$ is applied to reduce computational efforts.

Energy conservation equation

The geometry for the thermal problem is schematized in Fig. 2.3 (b). The global coordinates system's origin is positioned on the plane's surface of the Hertzian contact region as shown in Fig. 2.3 (b). Considering that heat transfers are accomplished mainly by conduction and convection, the energy conservation equation applied for an infinitely small volume of internal energy writes [152]:

$$\rho \frac{De}{Dt} = -\nabla \cdot \boldsymbol{q} + \boldsymbol{\tau} : \nabla \boldsymbol{u} \tag{2.20}$$

In this equation:

- ρ is the density
- $\boldsymbol{u}$ is the velocity vector
- e is the internal energy per unit mass
- $\boldsymbol{q}$ is the conductive heat flux vector
- p is the pressure
- $\boldsymbol{\tau}$ is the viscous stress tensor

The enthalpy $\mathcal{H}$ is related to the internal energy e through the following relation:

$$e = \mathcal{H} - \frac{p}{\rho} \tag{2.21}$$

Replacing the internal energy e by the enthalpy $\mathcal{H}$ and using the continuity equation, Eq. (2.20) gives the enthalpy conservation equation as follow:

$$\rho\frac{D\mathcal{H}}{Dt} = -\nabla\cdot\boldsymbol{q} + \frac{Dp}{Dt} + \boldsymbol{\tau}:\nabla\boldsymbol{u} \tag{2.22}$$

For the convenience of implementation of the finite element method, the energy equation is then expressed in terms of temperature. The enthalpy can be expanded as a function of temperature T and pressure p through the following differential expression:

$$d\mathcal{H} = C_p dT + \frac{1}{\rho}\left[1 + \frac{T}{\rho}\left.\frac{\partial\rho}{\partial T}\right|_p\right]dp = C_p dT + \frac{1}{\rho}[1 - T\beta]dp \tag{2.23}$$

where, C_p and β are, respectively, the specific heat capacity and the thermal expansion coefficient.

The energy equations are solved in both solid domain $\Omega_1\&\Omega_2$ and lubricant film domain Ω (see Fig. 2.3 (b)), which are derived as follows respectively. Within the solid bodies Ω_1 and Ω_2, considering they have zero heat source and zero velocity in the y and z direction, the energy conservation equations become:

$$\rho_1 C_{p,1} u_{1x}\left(\frac{\partial T}{\partial x}\right) = \frac{\partial}{\partial x}\left(k_1\frac{\partial T}{\partial x}\right) + \frac{\partial}{\partial x}\left(k_1\frac{\partial T}{\partial y}\right) + \frac{\partial}{\partial z}\left(k_1\frac{\partial T}{\partial z}\right) \tag{2.24}$$

$$\rho_2 C_{p,2} u_{2x}\left(\frac{\partial T}{\partial x}\right) = \frac{\partial}{\partial x}\left(k_2\frac{\partial T}{\partial x}\right) + \frac{\partial}{\partial x}\left(k_2\frac{\partial T}{\partial y}\right) + \frac{\partial}{\partial z}\left(k_2\frac{\partial T}{\partial z}\right) \tag{2.25}$$

An equivalent single homogeneous domain Ω (see Fig. 2.3 (b)) formed by the liquid oil/refrigerant solution and the gaseous refrigerant is considered in the present work. The average thermodynamic properties for this homogeneous mixture are derived based on the volume fraction of each phase to couple with the novel cavitation model mentioned in the previous section.

Considering the compressible liquid phase as an ideal binary solution, the enthalpy can be expressed as a function of pressure p, temperature T, and mass fraction w of refrigerant in the total solution. Eq. (2.23) for the oil/refrigerant solution leads to:

$$d\mathcal{H}_{ml} = C_{p,ml}dT + \frac{1}{\rho_{ml}}\left[1 + \frac{T}{\rho_{ml}}\left.\frac{\partial\rho_{ml}}{\partial T}\right|_p\right]dp \tag{2.26}$$

where $C_{p,ml}$ is the heat capacity of the oil/refrigerant solution. As the variation of refrigerant concentration in oil is limited, $C_{p,ml}$ can be simplified as a function of the heat capacity of pure oil $C_{p,o}$ and refrigerant $C_{p,rl}$ and initial mass fraction of liquid refrigerant in total solution w_{in}:

$$C_{p,ml} = (1 - w_{in})C_{p,o} + w_{in}C_{p,rl} \tag{2.27}$$

Using Eq. (2.26) in Eq. (2.22), then invoking the Fourier's law of conduction, $q = -k_{ml}\nabla T$, where k_{ml} is the thermal conductivity of the oil/refrigerant solution, and neglecting the heat transport by the mass diffusion of refrigerant in oil, the energy conservation equation for the oil/refrigerant solution under steady-state condition gives:

$$\rho_{ml} C_{p,ml} \boldsymbol{u} \nabla T = \nabla \cdot (k_{ml} \nabla T) - \frac{T}{\rho_{ml}} \frac{\partial \rho_{ml}}{\partial T} \boldsymbol{u} \cdot \nabla p + \boldsymbol{\tau} : \nabla \boldsymbol{u} \tag{2.28}$$

where the shear term $\boldsymbol{\tau} : \nabla \boldsymbol{u}$, in our study, stands for viscous dissipation of fluid and can be expressed as:

$$\boldsymbol{\tau} : \nabla \boldsymbol{u} = \mu_{ml} \left(\nabla \cdot \boldsymbol{u}\right)^2 \tag{2.29}$$

The heat transfer between the liquid solution and the gas phase is revealed by calculating the formation/dissolution of the refrigerant gas phase. Assuming the refrigerant gas as an ideal gas($T\beta \cong 1$), Eq. (2.23) for the gas phase reads:

$$d\mathcal{H}_{rg} = C_{p,rg} dT \tag{2.30}$$

Following the same procedure for the gas phase, substitution of Eq. (2.30) in (2.22) results in:

$$\rho_{rg} C_{p,rg} \boldsymbol{u} \nabla T = \nabla \cdot (k_{rg} \nabla T) + \boldsymbol{u} \cdot \nabla p + \mu_{rg} \left(\nabla \cdot \boldsymbol{u}\right)^2 \tag{2.31}$$

Equation (2.28) and Eq. (2.31) are rewritten by multiplying respectively, the volume fraction of liquid $(1 - \alpha_{rg})$ and gas (α_{rg}) in the equivalent homogeneous domain on both sides of the equation:

$$\begin{aligned} &(1-\alpha_{rg})\rho_{ml} C_{p,ml} \boldsymbol{u} \nabla T = \\ &\nabla \cdot ((1-\alpha_{rg}) k_{ml} \nabla T) - (1-\alpha_{rg}) \frac{T}{\rho_{ml}} \frac{\partial \rho_{ml}}{\partial T} \boldsymbol{u} \cdot \nabla p + (1-\alpha_{rg}) \mu_{ml} \left(\nabla \cdot \boldsymbol{u}\right)^2 \end{aligned} \tag{2.32}$$

$$\alpha_{rg} \rho_{rg} C_{p,rg} \boldsymbol{u} \nabla T = \nabla \cdot (\alpha_{rg} k_{rg} \nabla T) + \alpha_{rg} \boldsymbol{u} \cdot \nabla p + \alpha_{rg} \mu_{rg} \left(\nabla \cdot \boldsymbol{u}\right)^2 \tag{2.33}$$

Adding Eq. (2.32) and Eq. (2.33), the energy equation, after some algebraic manipulation becomes:

$$\begin{aligned} &[(1-\alpha_{rg})\rho_{ml} C_{p,ml} + \alpha_{rg} \rho_{rg} C_{p,rg}] \boldsymbol{u} \nabla T = \\ &\nabla \cdot ((1-\alpha_{rg}) k_{ml} + \alpha_{rg} k_{rg}) \nabla T) + [\alpha_{rg} - (1-\alpha_{rg}) \frac{T}{\rho_{ml}} \frac{\partial \rho_{ml}}{\partial T}] \boldsymbol{u} \cdot \nabla p + \mu_m \left(\nabla \cdot \boldsymbol{u}\right)^2 \end{aligned} \tag{2.34}$$

Equation (2.34) can be further simplified by assuming a mean value $C_{p,m}$ of specific heat for oil/refrigerant solution and refrigerant gas:

$$\rho_m C_{p,m} \boldsymbol{u} \nabla T = \nabla \cdot (k_m \nabla T) + Q_{comp} + Q_{shear} \tag{2.35}$$

Equation (2.35) has the form of classical convection/diffusion equation as a function of temperature and reveals two heat source terms, the compression, and the shearing of the oil/refrigerant solution and refrigerant gas.

Finally, considering that the dimension of lubricant film in the z direction is much smaller than the x and y directions, the heat conduction in the film plane and the heat convection across the film thickness can be neglected [19]. Hence, Eq. (2.35) for the energy balance of the lubricant film reduces to:

$$\rho_m C_{p,m} \left(u_x \frac{\partial T}{\partial x} + u_y \frac{\partial T}{\partial y} \right) = \frac{\partial}{\partial z} \left(k_m \frac{\partial T}{\partial z} \right) + Q_{comp} + Q_{shear} \tag{2.36}$$

with

$$Q_{comp} = [\alpha_{rg} - (1 - \alpha_{rg}) \frac{T}{\rho_{ml}} \frac{\partial \rho_{ml}}{\partial T}] \left(u_x \frac{\partial p}{\partial x} + u_y \frac{\partial p}{\partial y} \right) \tag{2.37}$$

$$Q_{shear} = \mu_m \left(\left(\frac{\partial u_x}{\partial z} \right)^2 + \left(\frac{\partial u_y}{\partial z} \right)^2 \right) \tag{2.38}$$

and

$$\rho_m = \alpha_{rg} \rho_{rg} + (1 - \alpha_{rg}) \rho_{ml} \tag{2.39}$$

$$\mu_m = \alpha_{rg} \mu_{rg} + (1 - \alpha_{rg}) \mu_{ml} \tag{2.40}$$

$$k_m = \alpha_{rg} k_{rg} + (1 - \alpha_{rg}) k_{ml} \tag{2.41}$$

Heat flux continuity boundary conditions are imposed at the solid/lubricant interfaces to ensure an energetic equilibrium of the system:

$$\begin{aligned} k_m \left. \frac{\partial T}{\partial z} \right|_{z=0^+} &= k_1 \left. \frac{\partial T}{\partial z} \right|_{z=0^-} \\ k_m \left. \frac{\partial T}{\partial z} \right|_{z=h^-} &= k_2 \left. \frac{\partial T}{\partial z} \right|_{z=h^+} \end{aligned} \tag{2.42}$$

The thickness of the two bodies Ω_1 and Ω_2 of 4a (see Fig. 2.3 (b)) is considered to be thick enough that a zero-temperature gradient in the z-direction is reached for the upper and lower solid boundaries. The temperature is set to the temperature in the compressor sump T_s on these surfaces, as well as the inlet boundaries of solids. Free flux is considered for the outlet boundaries.

The boundary condition for the fluid domain in the inlet, with the velocity vector oriented towards the contact is [19]:

$$T(x_{in}, y, z) = T_s \quad \text{if} \quad u_f(x_{in}, y, z) \geq 0 \tag{2.43}$$

Again, free flux is considered otherwise.

In Eq. (2.36), u_x and u_y are the velocities field components of the lubricant along x and y, respectively. They are written as follows:

$$u_x = \frac{\partial p}{\partial x}\left(\int_0^z \frac{z^{'}}{\mu_m}\,dz^{'} - \frac{\mu_{e,m}}{\mu_{e,m}^{'}}\int_0^z \frac{1}{\mu_m}\,dz^{'}\right) + \mu_{e,m}(u_{2x} - u_{1x})\int_0^z \frac{1}{\mu_m}\,dz^{'} + u_{1x} \tag{2.44}$$

$$u_y = \frac{\partial p}{\partial y}\left(\int_0^z \frac{z^{'}}{\mu_m}\,dz^{'} - \frac{\mu_{e,m}}{\mu_{e,m}^{'}}\int_0^z \frac{1}{\mu_m}\,dz^{'}\right) + \mu_{e,m}(u_{2y} - u_{1y})\int_0^z \frac{1}{\mu_m}\,dz^{'} + u_{1y} \tag{2.45}$$

Additionally, a symmetry condition on the $x - z$ plane at $y = 0$ is applied to reduce computational efforts.

Numerical procedure

The resolution of the steady-state Thermal-EHL problem for circular point contacts with pure rolling condition is achieved based on the numerical procedure proposed by Habchi [19]. According to Habchi [153], for pure rolling cases, weak coupling strategies can provide faster convergence rates than full coupling strategies, hence they were used in this investigation. The numerical procedure is illustrated in the flow chart of Fig. 2.4. In the first step, the Generalized Reynolds equation with cross-film integral terms fully coupled with the linear elasticity and the load balance equation is solved using a Newton-Raphson procedure. Then the energy equations are solved for a given pressure profile p to give the temperature distribution. An iterative procedure is repeated between the two steps until the maximum relative difference in either solution between two consecutive iterations drops below 10^{-3} [19] with the L2 norm error.

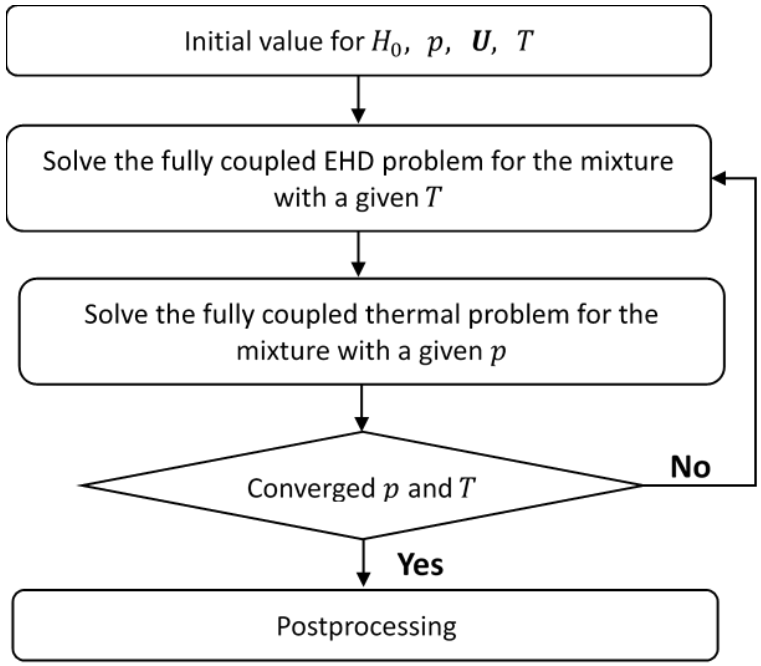

Figure 2.4: Flow diagram of the Thermal ElastoHydrodynamic Lubrication (Thermal-EHL) modeling for the oil/refrigerant solution.

Intermediate conclusion

The oil/refrigerant solution in the refrigeration compressor was explored as an illustrative case for the research methodology for miscible fluids in EHL contacts. An original Thermal-EHL computation with solubility-based cavitation modeling for point contacts has been developed in this work. Considering the mixture of oil/refrigerant solution and refrigerant gas as a two-phase homogeneous compressible flow in the cavitation area, the behavior of the lubricant can be described with the Generalized Reynolds equation coupled with the elasticity equation and the energy conservation equation, for both pressurized region and cavitation region, by introducing physical properties of the lubricant mixture.

However, as mentioned earlier in Section 2.1, a different approach is required when the lubricating fluids are not miscible. The next section is dedicated to the research methodology for immiscible fluids.

2.3 Immiscible fluids

2.3.1 Problem formulation

The lubrication of contacts with a water-in-oil emulsion is investigated in this study as an example of immiscible fluids. Unlike the homogeneous mixture generated by oil and refrigerant described in the previous section, water and oil form a two-phase flow that may behave differently. As a result, the flow of water in oil flow at the inlet area must be studied first and foremost, because the main concern is whether water penetrates the contact area. According to some studies [91, 107, 118], water droplets may be expelled before reaching the contact area under certain operating conditions. However, as presented in Section 1.2.2, few investigations in the literature focus on the trajectories of water droplets. This study aims to contribute to a better understanding of this problem by using both experimental and numerical approaches to explore under which conditions a water-in-oil emulsion at the contact inlet may produce a risk for full-film lubrication.

2.3.2 Experimental techniques

Characterization of water in oil emulsion

In order to mimic a water/oil mixture found in the hot rolling bearing system from the industrial plant (information provided by the SKF reference group). Water-in-oil emulsion was prepared from oil Morlina S1 B 320 (dynamic viscosity at 25°C = 0.781 Pa · s), 10 % by weight distilled water, containing 5 % diluted coolant (Quakerol TWN) in Heating Magnetic Stirrer FB15001 at 855 rev/min at 25°C for 1.5 h. The coolant involved is an oil-containing surfactant, which consists of 1 % surfactant, 0.5-3 % of oil (Morlina S1 B 320), and the rest of the water.

With the development of fluorescence microscopes, the fluorescent technique is becoming popular to trace the particle motions [154]. However, it is not suitable in the current case since the air bubbles formed in the mixture interfere with the detection of water droplets (see Appendix C). As a result, a water dye composed of colorants E124 and E133 was chosen for the characterization and direct observation of water droplets in oil (1 % by weight in water) [155]. Furthermore, a Raman-spectrum analysis for different compositions of the mixture was performed to confirm that the selected water dye can distinguish water droplets from air bubbles and oil. As shown in Figure 2.5, water can be identified with its characteristic O-H stretching bands at 3430 cm^{-1}.

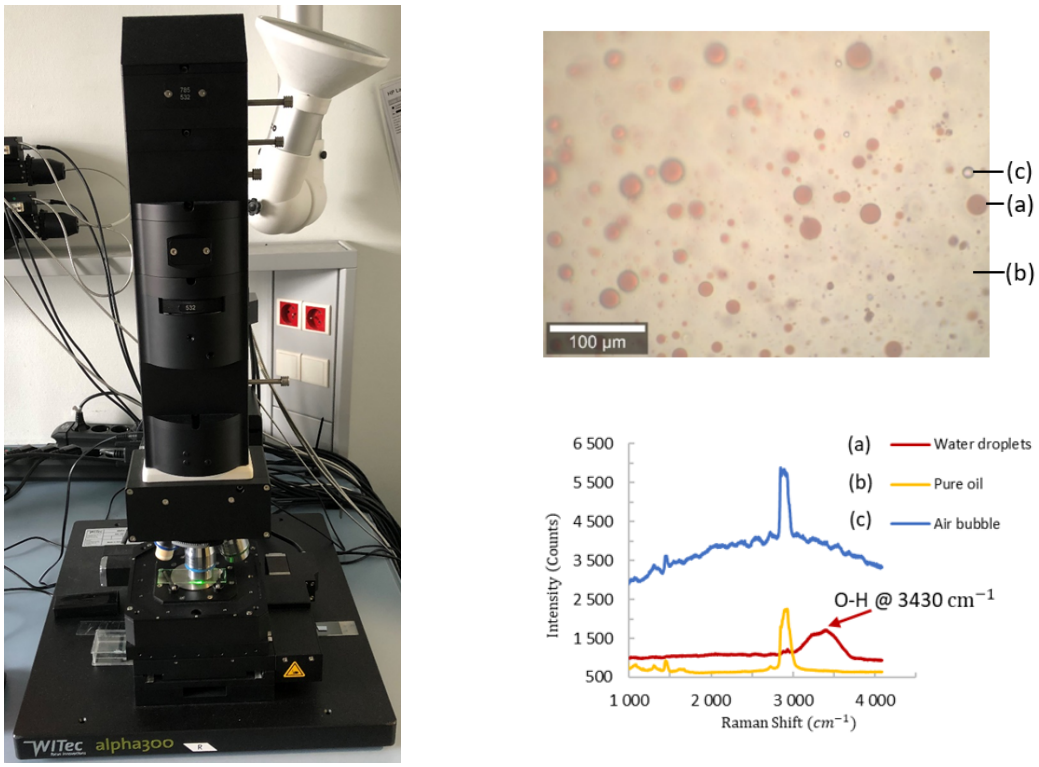

(a) (b)

Figure 2.5: (a) Confocal Raman microscope for Raman imaging and 3D depth scans and (b) raman spectrum of different compositions of the mixture

The water-in-oil emulsion was observed under an optical microscope as shown in Figure 2.6 (a). Figure 2.6 (b) is the microscope image of the emulsion after 3 hours of resting time. As can be seen from the figures, the size of water droplets increases after resting for 3 hours. The size of the droplets was analyzed with the help of the software ImageJ and the corresponding size distribution charts are presented in Figure 2.6 (c) and Figure 2.6 (d), which yield characteristic droplet diameters of 8 µm and 60 µm for the emulsion with no resting time and that with 3 hours resting time, respectively.

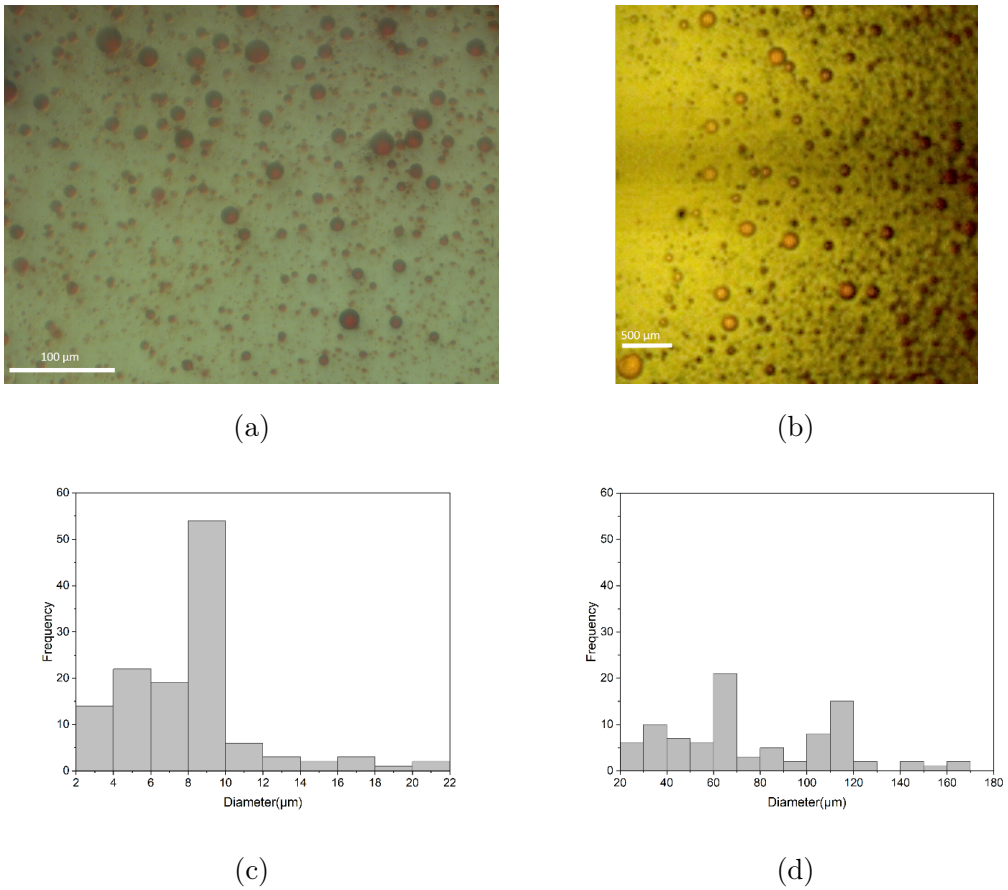

Figure 2.6: Water droplet in oil colored by water dye (colorants E124 and E133), observation with an optical microscope with (a) no resting time and (b) 3 hours resting time and size distribution with (c) no resting time and (d) 3 hours resting time. Scale is different between (a) and (b)

Direct observation at the inlet of an EHD contact

The ball-on-disc tribometer "Jerotrib" [156] is used for the experimental study. This equipment was initially intended for friction measurements and interferometric film thickness measurements from a few nanometers to 800 nm (see Figure 1.5). It can simulate pure rolling or rolling-sliding contacts with varying rolling speeds (0.01-7 m/s), geometries (spherical or barrel), and materials (e.g. balls in steel and disc in glass or sapphire). The Hertzian zone, where the lubricant film is very thin, is generally the investigation region for the interferometric technique. As a result, this approach is not used in the present work for direct observation at the inlet contact, which is located farther upstream of the contact region. However, because the microscope can be moved upstream from the contact, the test rig remains a useful tool for performing in-situ observation of the contact inlet as presented in Figure 2.7.

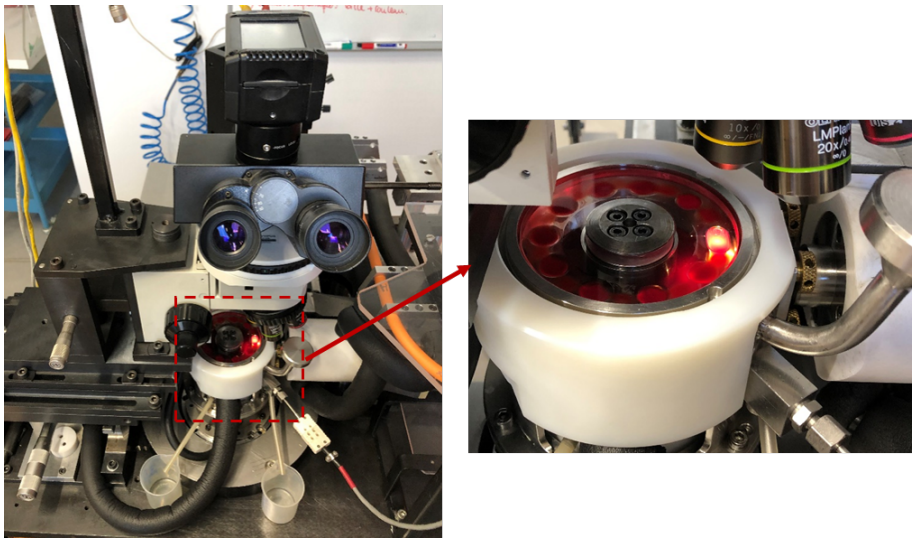

Figure 2.7: Ball-on-disc tribometer "Jerotrib" test rig.

The experimental device for direct observation can be schematized as in Figure 2.8. In the experiment, a lubricant reservoir composed of 20 ml of the water-in-oil emulsion was used, and the temperature was maintained at 25°C with a thermostat. A 25.4 mm steel ball was immersed in the reservoir and was set in contact with the glass disk by a load of 40 N, which yielded a maximum Hertzian pressure of 0.57 GPa and a Hertz contact radius a of 0.18 mm.

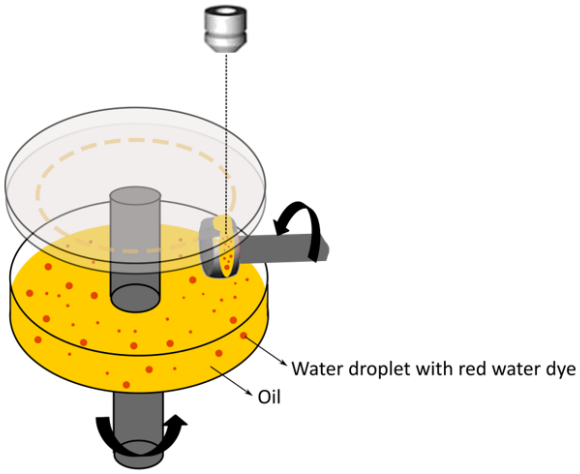

Figure 2.8: Schematic diagram of the ball-on-disc test rig.

The pure rolling condition was applied. The direct observation was made at the entrance of the contact by white light microscopy. The complete process of water droplets approaching the contact area was filmed by the high-speed camera Micro Ex4 through a transparent glass disk. The image acquisition frequency was set to 2980 fps. Direct observations in the tribometer were made for

water-in-oil emulsion shortly after the stirring, of which the initial characteristic size of water droplets was around 8 µm. The experiments were carried out by increasing the rolling speed from 0.015 m/s to 3 m/s and each speed was maintained for 15 s for filming. At 0.015m/s, it is possible to follow the individual motion of each droplets as the droplet displaced roughly by 1 diameter (for the smallest droplets) at each frame. On the contrary, at higher speed, only the region where the droplets are presented is of interest.

2.3.3 Numerical models

A numerical approach is developed based on the experimental investigation presented in Section 2.3.2. It should be noted that the objective of the numerical investigation in the present study focuses on modeling the flow of oil and trajectories of water droplets in oil at the inlet of the contact as observed in the previous experiments. Consequently, the computational domain needs to contain a large zone upstream of the contact, where thin-film theory may lose its validity. Strubel et al. [157] proposed a numerical approach to investigate the behavior of solid contaminated lubricant and particle trajectories in the upstream area. In their work, fluid flow and particle motion are evaluated with the resolutions of the Navier-Stokes equation to evaluate the pressure and velocity of oil and Newton's second law in the three-dimensional geometry of the contact inlet to calculate the trajectories of the contamination. This modeling strategy was chosen and adapted for the present study.

The configuration of the numerical model reproduced the experiments performed in the current work. A lubricated point contact is investigated, and the pure rolling condition is considered, which indicates that the plane and surface move along the x-direction with the same velocity $u_1 = u_2$ (see figure 2.9).

Definition of the computational domain

The computational domain in this work is a lubricant layer with a large area upstream of the contact area where water droplets enter and flow towards the EHD contact zone. First, the film thickness distribution $h(x, y)$ and pressure distribution $p(x, y)$ are obtained by using the finite element full system approach developed by Habchi et al. [15]. The Reynolds equation (2.12), the elasticity equation (2.17) and the load balance equation (2.19) are solved in a fully coupled way for pure oil (see Section 2.2.3). However, it should be noticed that, since the isothermal and Newtonian condition is assumed in the current oil/water mixture study, the generalized Newtonian viscosity μ_m in the equation (2.12) is replaced by the Newtonian one μ_{oil}. As a result, Equation (2.12) reduces to the Classical Reynolds equation.

The calculated film thickness $h(x, y)$ is used to build a three-dimensional geometry at the inlet zone of the contact by constructing the surface defined for $z = h(x, y)$ as shown in Figure 2.9.

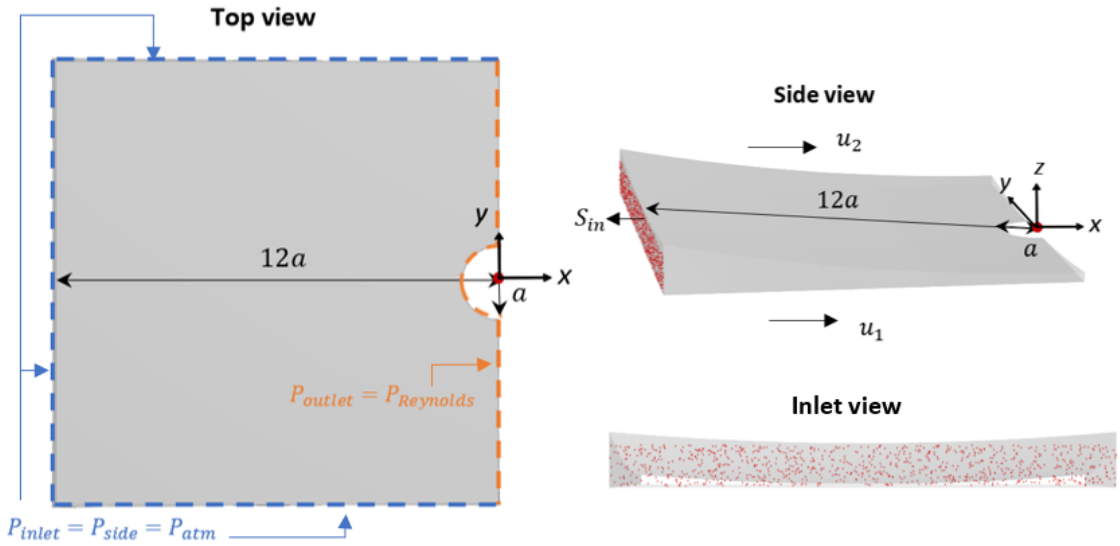

Figure 2.9: Geometries used for fluid flow and water droplets tracing computation and boundary conditions

The inlet boundary is placed at $12a$ upstream from the contact center, roughly the same position as the limit edge of the observation area in the experiments (see Section 2.3.2). The experimental results indicate that the circular Hertzian contact area is not essential to be considered in the current investigation. Furthermore, because the formed oil film at the contact inlet and the examined water droplet size are on the order of micrometers, roughly 10 times larger than the film thickness in the contact region, this area is not estimated in this work to save costs on computation. Because the concentration of water contamination in oil in the present study is small (10 wt%), a one-way coupling between water droplets and fields is assumed, which means that only the effects of the oil on water droplet motion are considered. The effects of water droplets on oil, as well as the interactions between water droplets, are neglected. By using this approach, the continuous phase (oil) and dispersed phase (water droplets) can be evaluated one after another [157].

Oil flow computation

The Navier-Stokes equation is firstly solved for fluid flow in the laminar regime (with $Re < 1$) on the generated 3D computational domain (see Figure

2.9):

$$\rho_{oil}\frac{\partial \boldsymbol{u_{oil}}}{\partial t} + \rho_{oil}(\boldsymbol{u_{oil}}\cdot\nabla)\boldsymbol{u_{oil}} = \nabla\cdot[-p\boldsymbol{I} + \mu_{oil}(\nabla\boldsymbol{u_{oil}} + (\nabla\boldsymbol{u_{oil}})^T)] + \rho_{oil}\boldsymbol{g}$$
$$\nabla\cdot(\rho_{oil}\boldsymbol{u_{oil}}) = 0 \tag{2.46}$$

Where ρ_{oil} is the density of oil, given by the Dowson and Higginson relation [10]:

$$\rho_{oil}(p) = \rho_0\frac{5.9\times10^8 + 1.34p}{5.9\times10^8 + p} \tag{2.47}$$

With $\rho_0 = 850$ kg/m^3, the atmospheric density of oil.

The viscosity of oil, μ_{oil}, is calculated by Roelands viscosity-pressure law [158]:

$$\mu_{oil}(p) = \mu_0\exp[\frac{1.98\times10^8\alpha}{0.6}(-1+(1+\frac{p}{1.98\times10^8})^{0.6})] \tag{2.48}$$

With $\mu_0 = 0.781$ Pa$\cdot$s and $\alpha = 15\times10^{-9}$ Pa^{-1}, the viscosity of oil at ambient conditions and the piezo-viscosity coefficient, respectively.

Pressure boundary conditions are imposed as in Figure 2.9: the pressure at the inlet and side boundaries are set to atmospheric pressure; the pressure at the outlet boundary is generated from the pressure distribution $p(x, y)$ calculated using the full-system approach (resolution of Reynolds equation in the contact region).

Water droplet motion computation

Since the detailed interface between water droplets and oil could not be observed in the previous experiments, water droplets are assumed to be spherical and undeformable in the present modeling. The motion of water droplets in the fluid was described by Newton's second law as follows [157]:

$$\frac{d}{dt}(m_d\boldsymbol{v_d}) = \boldsymbol{F_D} + \boldsymbol{F_G} + \boldsymbol{F_B} \tag{2.49}$$

Where $\boldsymbol{v_d}$ is the velocity of the droplet, $\boldsymbol{F_D}$ is the drag force, $\boldsymbol{F_G}$ and $\boldsymbol{F_B}$ is the gravitational force and buoyancy force. m_d is the droplet mass:

$$m_d = \frac{4\pi}{3}\rho_d(\frac{D_d}{2})^3 \tag{2.50}$$

With $\rho_d = 1000$ kg/m^3 and D_d the diameter of water droplets.

The drag force $\boldsymbol{F_D}$ describes the effects of oil on water droplet motion and is directly related to the flow regime [159], which can be determined by evaluating the value of the relative Reynolds number Re_r:

$$Re_r = \frac{\rho_{oil} D_d \boldsymbol{v_r}}{\mu_{oil}} \tag{2.51}$$

Where ρ_{oil} and μ_{oil} are the density and viscosity of the fluid, respectively. $\boldsymbol{v_r} = \boldsymbol{u_{oil}} - \boldsymbol{v_d}$ is the relative droplet velocity, and $\boldsymbol{u_{oil}}$ is the velocity of the oil. The maximum value of Re_r is 0.2, which is smaller than 1. As a result, for such a laminar flow, Stokes drag law applies [160]:

$$\boldsymbol{F_D} = \frac{18 \mu_{oil} m_d \boldsymbol{v_r}}{\rho_d D_d^2} \tag{2.52}$$

The sum of the gravity force and the buoyancy force of droplets in the fluid is given by [157]:

$$\boldsymbol{F_G} + \boldsymbol{F_B} = \frac{m_d \boldsymbol{g} (\rho_d - \rho_{oil})}{\rho_d} \tag{2.53}$$

with $\boldsymbol{g}$ the gravity vector.

In the present approach, the interaction between water droplets and the wall is simplified as the water droplets are assumed to be spherical and undeformable. A typical wall condition for tracing microscopic particles in a fluid is considered here [157], in which friction forces between water droplets and walls are ignored, and water droplets specularly reflect from the wall with no energy loss. If the water droplet comes into contact with both walls, it will freeze, which implies the water droplet location will no longer move. For more rigorous investigation, the deformation of water droplets and interfacial tension may be considered [45, 161, 162] (see Appendix D). However, because the droplet size is much smaller than the scale of the computational domain, the solid/liquid and liquid/liquid interfaces are simplified in the present work, as described above.

The original position of water droplets at the inlet plane is random (see Figure 2.9), though without any contact with walls. Assuming that water droplets are evenly distributed in the oil upstream of the inlet, the initial velocity of water droplets was set equal to that of the oil. The mass flow rate $\dot{m}_d$ and the number of water droplets N_d at the inlet can be calculated with the expression below:

$$\begin{aligned} \dot{m}_d &= S_{in} w_d \boldsymbol{u_{oil}} \rho_d \\ N_d &= \frac{S_{in} w_d}{S_d} \end{aligned} \tag{2.54}$$

With w_d the mass fraction of water in oil, S_{in} the surface of inlet area (see Figure 2.9) and S_d the surface of the cross section of water droplets at the inlet.

Intermediate conclusion

The emulsion of water droplets in oil is presented as an example of miscible lubricant in EHL contacts. The current study investigates the water-in-oil flow in EHL contacts both experimentally and numerically. In the experimental work, it is proposed for the first time to observe directly micro-sized water droplets-in-oil at the inlet of an EHL point contact with a high-speed camera and a microscope at different rolling speeds. Based on the experimental observation, a water droplet tracing numerical approach is developed to explore the impacts of different operating parameters on the flow of water-in-oil emulsion.

2.4 Conclusion

This chapter presented two distinct research methodologies to study miscible and immiscible fluids in EHL contacts, respectively. As typical examples of these two types of mixed states, oil/refrigerant solution and water droplets in oil emulsion are being investigated in detail.

For the oil/refrigerant solution, the EHL studies focus on the lubricating ability of oil/refrigerant solutions at the contact area and the refrigerant cavitation at the contact outlet. The numerical approach established in this study using a solubility-based cavitation model allows for the description of oil/refrigerant solution flow in both the pressurized and cavitated regions. A Thermal ElastoHyrodynamic Lubrication (Thermal-EHL) analysis for an oil/refrigerant system is described and will be used in the next chapter (Chapter 3), to anticipate the film-forming ability of the oil/refrigerant solution and the potential risks on the following contact induced by the refrigerant cavitation.

The investigations on emulsified water droplets in oil concentrate on the trajectories of the water droplets at the contact inlet to evaluate the risks for film thickness breakdown. Various investigating tools were demonstrated. An experimental facility allows for in-situ visualizations of the whole process of water droplets moving towards the EHD contact region at different rolling speeds. In addition, based on the experimental findings, a water droplet tracing numerical approach was proposed to reproduce the experimental observations and bringing additional information. This investigation will be presented and discussed in Chapter 4.

Chapter 3

Oil/refrigerant solution at the outlet area of EHD contacts

This chapter deals with a Thermal ElastoHyrodynamic Lubricated (Thermal-EHL) contact using an oil/refrigerant mixture. First, numerical EHL and Thermal-EHL solutions for oil/refrigerant lubricated contacts are presented. A discussion of the choice of the cavitation model for oil/refrigerant solutions is provided. Then, comparisons with pure oil cavitation are conducted. Finally, a case study representing refrigerant compressor applications is performed.

This chapter reflects the article of F.Zhang et al., entitled "Thermal-Elastohydrodynamic Contacts Lubricated With Oil/Refrigerant Solutions: A New Cavitation Modeling Approach Based on Refrigerant Solubility.", published in 2022 in the Journal of Tribology.

3.1 Introduction

As presented in Chapter 1, lubrication with a mixture of oil and the operating fluids is a current industrial challenge. This chapter aims to perform an analysis for an oil/refrigerant lubricated contact in the refrigeration compressor application. The two-phase methodology proposed in Chapter 2 for miscible fluids is adopted, and for the first time, applied to the study of Thermal-EHL point contacts in the refrigeration compressor [120]. The solubility of the oil/refrigerant system is introduced into the Generalized Reynolds equation coupled with the elasticity equation and the energy conservation equation.

First, the solutions of the EHL and Thermal-EHL contact with solubility-based cavitation modeling are analyzed to investigate the thermal effects on refrigerant cavitation. Then comparisons are made with several cavitation models in the literature. The different behaviors of pure oil and oil/refrigerant solutions in the cavitation area are also studied under the same operating conditions. Finally, the research methodology is applied to an industrial refrigerant compressor application.

3.2 Numerical results for oil/refrigerant in EHL/TEHL contacts

A common combination of the oil/refrigerant solution in refrigerant compressor, polyol ester oil RL68H and HFC-R134a, is selected in the present work, due to its full characterization [77, 85, 163]. As presented in the previous chapters, the proper evaluation of the lubricant properties is essential for EHL studies. The property correlations for all related compositions, including the pure oil

and liquid refrigerant, the oil/refrigerant solution, and the refrigerant gas, are shown below.

3.2.1 Properties of oil/refrigerant solution and refrigerant gas

Solubility

A Daniel plot provided by the oil manufacturer is used here as the solubility law for the solution of refrigerant R134a and oil RL68H [61] for temperatures above 323.15 K:

$$w_{sat}(p,T) = \left(\frac{T}{274.7(\frac{p}{1e6})^{0.1471}}\right)^{-\frac{1}{0.1284}} \tag{3.1}$$

Density and viscosity of the oil/refrigerant solution

The density and viscosity of the RL68H/R134a solution is calculated using the property relations proposed by Bair [61]. Tait Equation of State(EoS) is written for the mixture density:

$$\begin{aligned}\frac{\rho_R}{\rho_{ml}} &= \left(1 + a_v\left(T - T_R\right)\right) \cdot \left(1 - \frac{1}{1+K_0^{'}} \cdot \ln\left(1 + \frac{p}{K^{'}}\left(1 + K_0^{'}\right)\right)\right) \\ \text{with } K^{'} &= \left(K_{ol}\left(1 - w_{rl}\right)^{Q_K} + K_{rl}\right) \exp\left(-\left(\beta_{K,ol}\left(1 - w_{rl}\right)^{Q_\beta} + \beta_{K,rl}\right) T\right)\end{aligned} \tag{3.2}$$

The parameters for Eq. (3.2) are listed in Table 3.1.

Table 3.1: Values of parameters used in Tait Equation of State [61]

$K_0^{'}$	10.232
a_v	7.323×10^{-4} K^{-1}
K_{ol}	9.162×10^{9} Pa
K_{rl}	0.126×10^{9} Pa
Q_K	9.627
Q_β	6.815
$\beta_{K,ol}$	0.005723 K^{-1}
$\beta_{K,rl}$	5.8×10^{-4} K^{-1}
ρ_R	977 kg/m^3
T_R	293.15 K

The Grunberg-Nissan mixing law is used for calculating the viscosity of the RL68H/R134a solution [7] [63]:

$$\mu_{ml} = \exp\left(X_{rl} \ln \mu_{rl} + X_{ol} \ln \mu_{ol} + 1.51 X_{rl} X_{ol}\right) \tag{3.3}$$

with $X_{ol} = 1 - X_{rl}$ where the mole fraction of refrigerant X_{rl} can be expressed by its mass fraction w_{rl} as [61]:

$$X_{rl} = \frac{1}{1 + 0.444(\frac{1}{w_{rl}} - 1)} \tag{3.4}$$

The refrigerant viscosity μ_{rl} is correlated by applying Andrade equation [164] and modified McEwen model [165]:

$$\mu_{rl} = \mu_{\infty} \exp\left(\frac{E_a}{R_g T}\right)\left(1 + \frac{a_0 + \frac{a_1}{T}}{d_0 + \frac{d_1}{T}} p\right)^{(d_0 + \frac{d_1}{T})} \tag{3.5}$$

The parameters used in above equation are given in Table 3.2.

Table 3.2: Values of parameters used for the viscosity correlation of the refrigerant [61]

μ_{∞}	1.0796×10^{-5} Pa · s
E_a	7.47×10^{3} J/mol
a_0	1.229×10^{-8} Pa^{-1}
a_1	-2.129×10^{-8} K/Pa
d_0	0.9673
d_1	110.11 K
R_g	8.314 J/mol/K

Improved Yasutomi correlation is used for oil viscosity:

$$\mu_{ol} = \mu_g \exp\left[\frac{-2.303 C_1((T - 273.15) - (T_{g0} + A_1 \ln(1 + A_2 p)))(1 + b_1 p)^{b_2}}{C_2 + ((T - 273.15) - (T_{g0} + A_1 \ln(1 + A_2 p)))(1 + b_1 p)^{b_2}}\right] \tag{3.6}$$

Where the parameters used are summarized in Table 3.3.

Thermal conductivity and heat capacity of the oil/refrigerant solution

The thermal conductivity of the oil/refrigerant solution is calculated with the Flilippov equation recommended by Conde [166] and Mermond [167]:

$$k_{ml} = w_{rl} k_{rl} + (1 - w_{rl}) k_{ol} - 0.72 w_{rl}(1 - w_{rl})(k_{ol} - k_{rl}) \tag{3.7}$$

Table 3.3: Values of parameters used for the viscosity correlation of the oil [61]

μ_g	10^{12} Pa · s
T_{g0}	−82.15°C
A_1	1467.2°C
A_2	7.4×10^{-11} Pa^{-1}
b_1	9.44×10^{-9} Pa^{-1}
b_2	−0.3377
C_1	16.24
C_2	28.55°C

According to Mermond [167], the mixture specific heat of the oil/refrigerant solution gives:

$$C_{p,ml} = w_{rl}C_{p,rl} + (1 - w_{rl})C_{p,ol} \tag{3.8}$$

As the variation of temperature in this work is small, the values of the thermal conductivity and specific heat of the pure substance are obtained at studied temperature $T_s = 65$°C and summarized as in Table 3.4.

Table 3.4: Values of the thermal conductivity and the specific heat of oil and refrigerant

$C_{p,ol}$ [168]	2302.74 J/kg/K
$C_{p,rl}$ [169]	1446.5 J/kg/K
k_{ol} [168]	0.15 W/m/K
k_{rl} [170]	0.063 W/m/K

Density and viscosity of the refrigerant gas

The density ρ_{rg} (kg/m^3) and viscosity μ_{rg} (Pa · s) of gaseous refrigerant R134a is given by Grando [85] by using software REFPROP [171]:

$$\rho_{rg} = \frac{c_1 + c_2 p + c_3 T + c_4 p^2 + c_5 T^2 + c_6 Tp}{c_7 + c_8 p + c_9 T + c_{10} p^2 + c_{11} T^2 + c_{12} Tp} \tag{3.9}$$

$$\mu_{rg} = \frac{c_1^{'} + c_2^{'} p + c_3^{'} T + c_4^{'} T^2 + c_5^{'} p^3}{c_6^{'} + c_7^{'} p + c_8^{'} P^2 + c_9^{'} T} \times 10^{-6} \tag{3.10}$$

The parameters are listed in Table 3.5 and Table 3.6.

Table 3.5: Values of parameters used for the gaseous refrigerant density correlation

c_1	4.2473×10^{-3}
c_2	-1.9077×10^{-4}
c_3	0.0448
c_4	3.4605×10^{-5}
c_5	-2.4624×10^{-5}
c_6	5.383×10^{-4}
c_7	1
c_8	0.0155
c_9	-8.25×10^{-4}
c_{10}	4.568×10^{-5}
c_{11}	6.9326×10^{-8}
c_{12}	-2.1388×10^{-6}

Table 3.6: Values of parameters used for the gaseous refrigerant viscosity correlation

$c_1{}'$	10.8186
$c_2{}'$	-2.6052×10^{-3}
$c_3{}'$	0.1451
$c_4{}'$	3.7658×10^{-4}
$c_5{}'$	-2.017×10^{-7}
$c_6{}'$	1
$c_7{}'$	-2.1278×10^{-4}
$c_8{}'$	-7.752×10^{-9}
$c_9{}'$	9.6695×10^{-3}

Thermal conductivity and heat capacity of the refrigerant gas

Accoding to Laesecke et al. [170], the thermal conductivity of the saturated refrigerant gas k_{rg} (W/m/K) can be expressed with T in K as:

$$k_{rg} = -9.7578 \times 10^{-2} + 1.0504 \times 10^{-3}T - 3.6079 \times 10^{-6}T^2 + 4.4965 \times 10^{-9}T^3 \tag{3.11}$$

And the heat capacity of the refrigerant gas $C_{p,rg}$ (J/kg/K) can be calculated from the following formula with T in K [172]:

$$C_{p,rg} = \frac{19.4006 + 0.258531T - 1.29665 \times 10^{-4}T^2}{102 \times 10^{-3}} \tag{3.12}$$

3.2.2 Validation with experiments on the pressurized region

First, validations of EHL and Thermal-EHL computations were performed by comparing with the experimental film thickness measurements of Gunsel and Pozebanchuk [74], where the same oil/refrigerant solution, polyol ester oil RL68H, and HFC-R134a was used. The central film thickness was measured by using the interferometric technique in a steel ball-glass disc contact. It should be emphasized that the experiments were carried out under a pressurized refrigerant atmosphere, to simulate the environment in the compressor sump. The pure rolling condition was employed with the rolling velocity varying from 0.1 to 3 m/s, and a load w of 20 N was applied on a 19.05 mm steel ball, yielding maximum Hertzian pressure of 0.55 GPa. The pressure and temperature in the test chamber were $p_s = 1.171$ MPa and $T_s = 65°C$, which resulted in an initial mass fraction of refrigerant $w_{in} = 23.7$ % in the oil/refrigerant solution. In order to compare with the above experimental data, the same operating conditions are used in the present numerical calculations. The material properties of the glass disc used in calculations are presented in Table 3.7.

Table 3.7: Mechanical and thermophysical properties of the glass disc (from Ref. [45])

E_g	81×10^9 Pa
v_g	0.21
ρ_g	2510 kg/m^3
c_{p_g}	840 J/kg/K
k_g	1.11 W/m/K

And the material chosen for the ball bearing is grade steel(100Cr6), of which the properties are summarized in Table 3.8.

Table 3.8: Mechanical and thermophysical properties of steel 100Cr6 (from Ref. [173])

E_s	210E9 Pa
v_s	0.3
ρ_s	7850 kg/m^3
c_{p_s}	470 J/kg/K
k_s [174]	21 W/m/K

Central film thickness comparisons between numerical and experimental results are plotted in Figure 3.1.

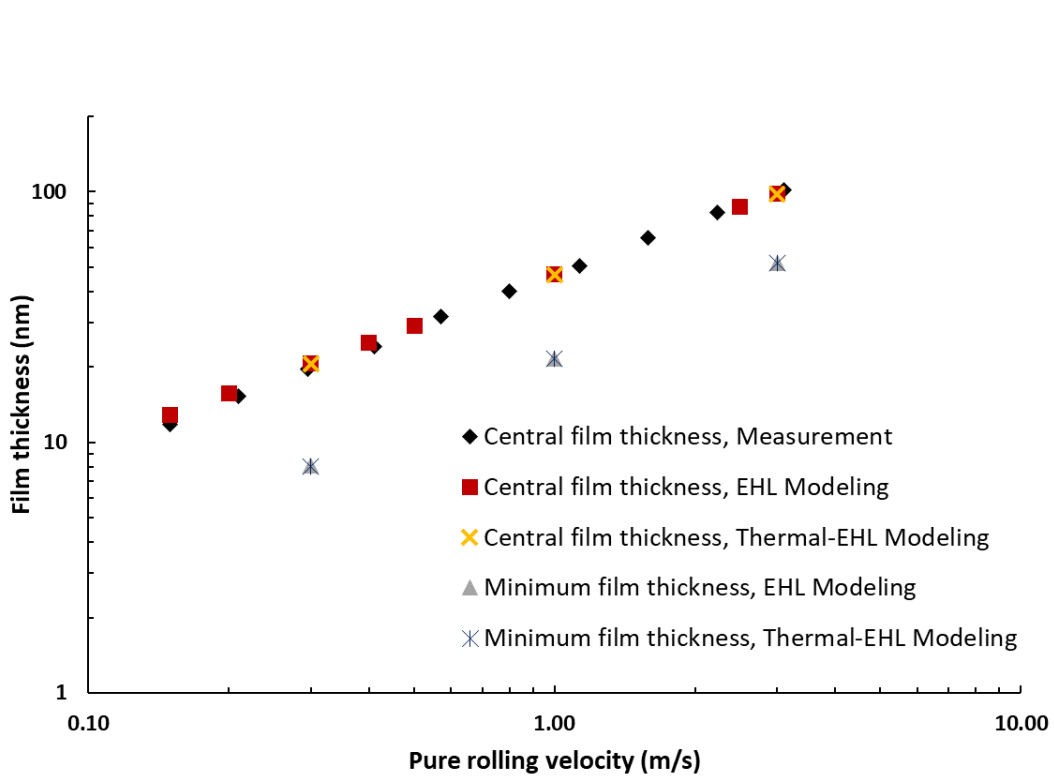

Figure 3.1: Film thickness obtained from experiments [74] and from EHL and Thermal-EHL calculations with the present solubility-based cavitation modeling for RL68H/R134a solution.

As can be seen from the figure, an excellent agreement is achieved which indicates that both the EHL model and the Thermal-EHL model developed in this work can predict film thickness appropriately. It is shown that, in the current investigation, consideration of thermal effects has no significant influence on the calculation of the lubricant film thickness as pure rolling condition is assumed. However, thermal effects must be included when characterizing the cavitation region at the outlet of the contact, as shown by the disparities in the EHL model and Thermal model results presented below. Unfortunately, to the best of the authors' knowledge, no experimental data for the cavitation area (such as pressure, mass fraction, and volume fraction) exist in the literature.

3.2.3 Numerical results for the cavitation region

It should be noticed that, in the real application of refrigeration compressor, instead of steel-glass contact, steel-steel contact is employed [51]. The mechanical and thermophysical properties of these materials are distinct from each other (see Table 3.7 and 3.8). As the purpose of this study is to investigate the oil/refrigerant solution in the refrigeration compressor, a steel-steel circular

point contact is considered for the following analysis to obtain a more similar configuration. The material properties can be found in Table 3.8.

A load $F = 10.95$ N is applied, giving a maximum Hertzian pressure of 0.7 GPa. The other parameters used in the following calculations remain the same as previously stated in the experiments of Gunsel and Pozebanchuk [74]. Temperature, pressure, mass fraction and volume fraction profile are plotted in Figure 3.2, 3.3, 3.4 and 3.5 for a rolling velocity of 1 m/s.

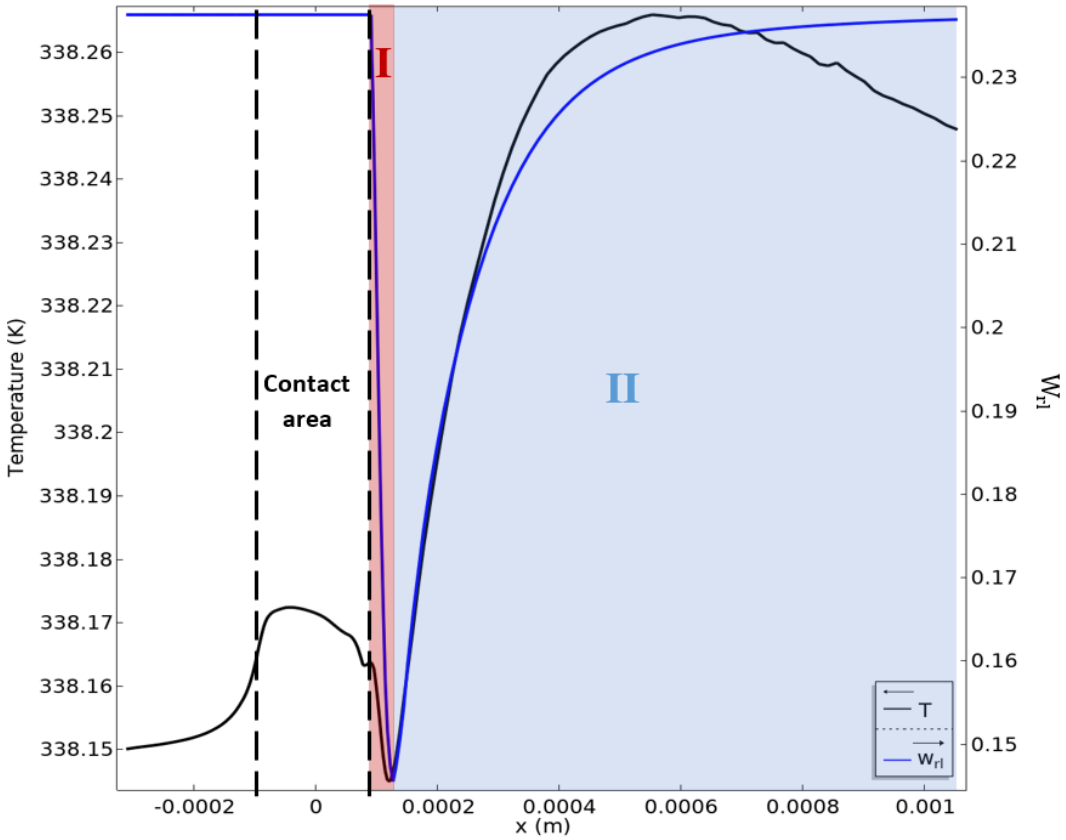

Figure 3.2: Temperature of oil/refrigerant mixture along x at $y = 0$ (central line) and $z = h$ (top surface) obtained by solving the Thermal-EHL problem with the present solubility-based cavitation modeling (see Figure 2.3 for the coordinate system). w_{rl} at the right side, stands for the mass fraction of liquid refrigerant in the oil/refrigerant solution.

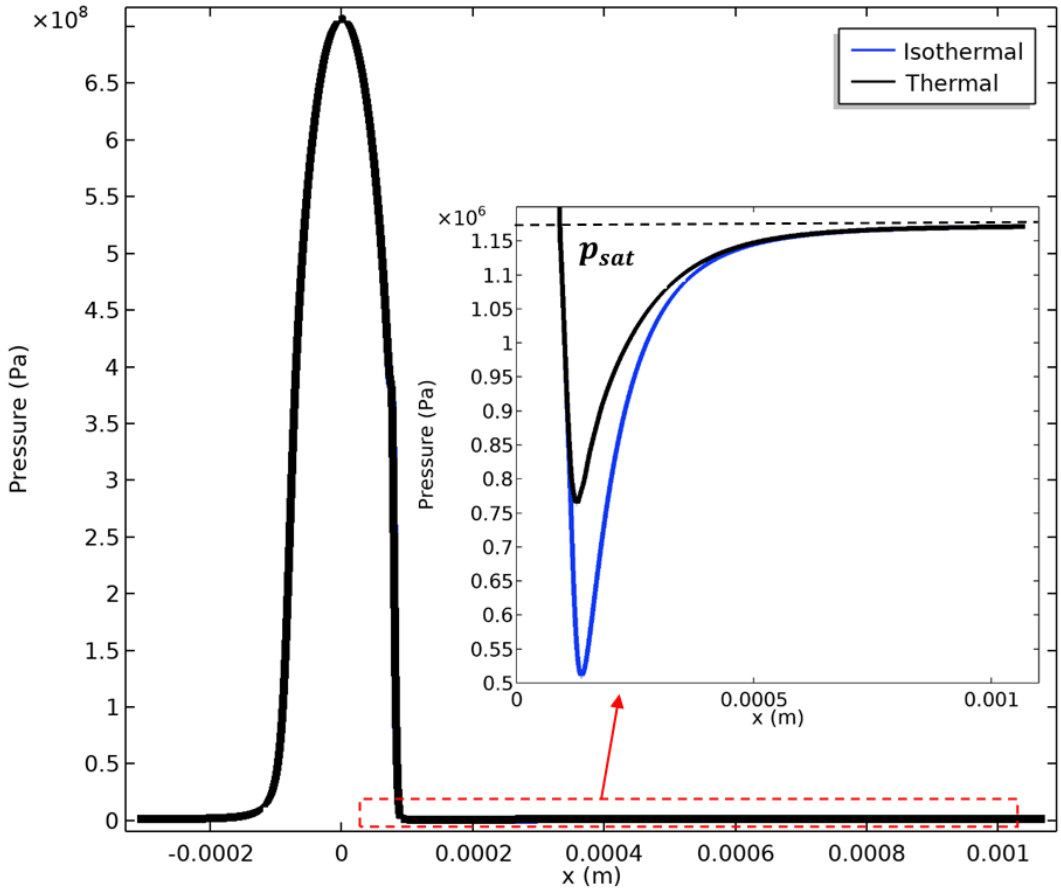

Figure 3.3: Pressure of oil/refrigerant mixture along x at $y = 0$ (central line) and $z = h$ (top surface) obtained by solving the EHL and Thermal-EHL problem with the present solubility-based cavitation modeling (see Figure 2.3 for the coordinate system).

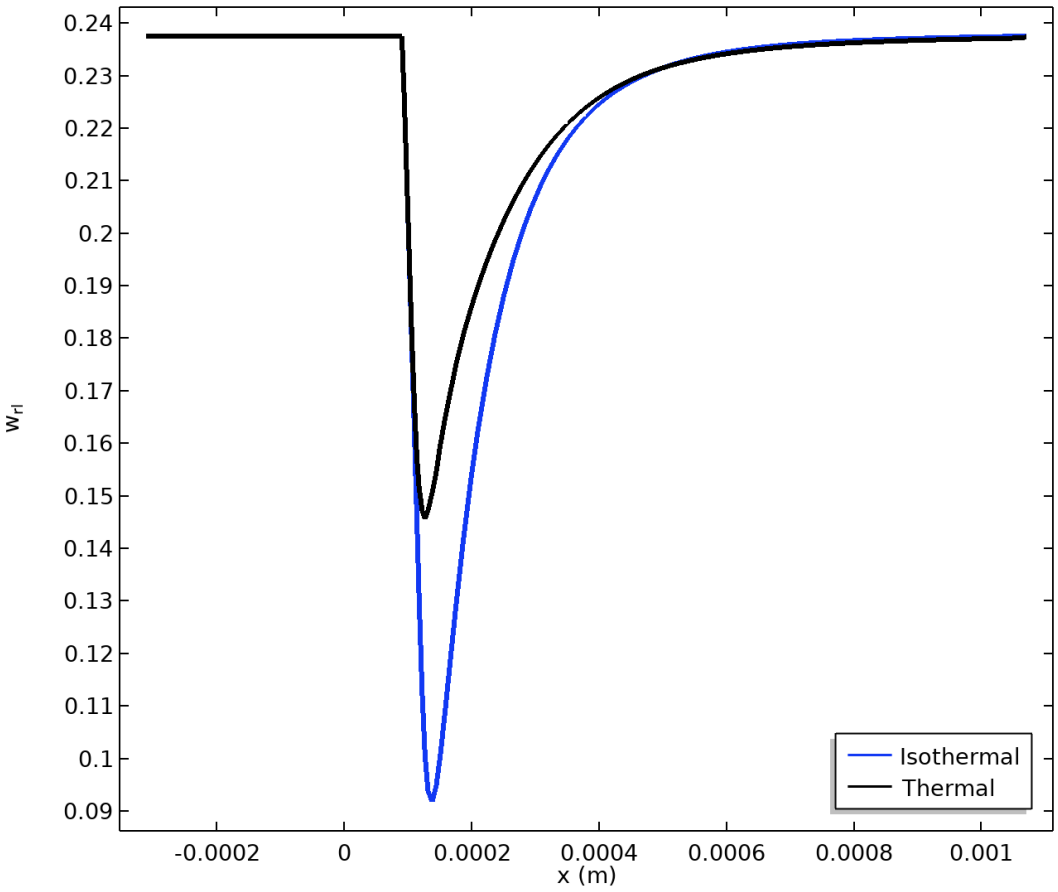

Figure 3.4: Mass fraction of liquid refrigerant in oil/refrigerant solution along x at $y = 0$ (central line) and $z = h$ (top surface) obtained by solving the EHL and Thermal-EHL problem with the present solubility-based cavitation modeling (see Figure 2.3 for the coordinate system).

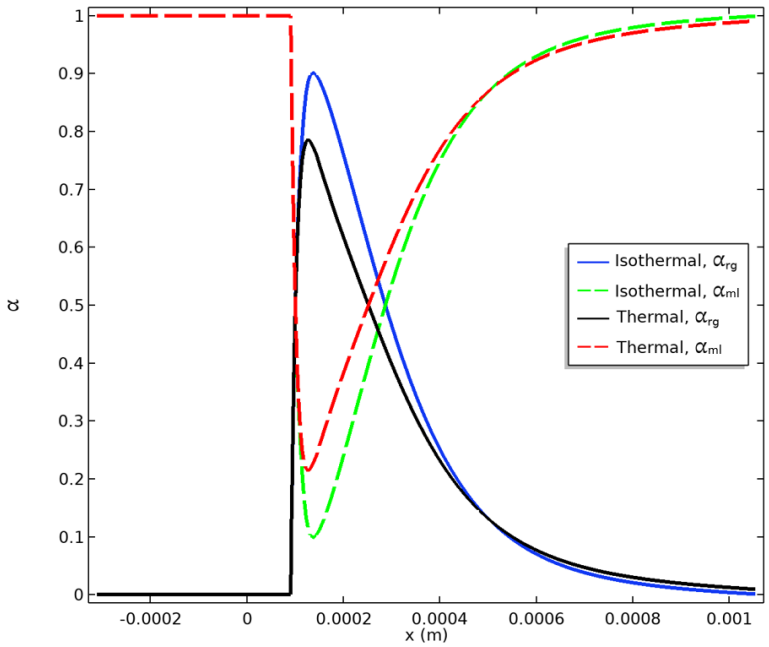

(a)

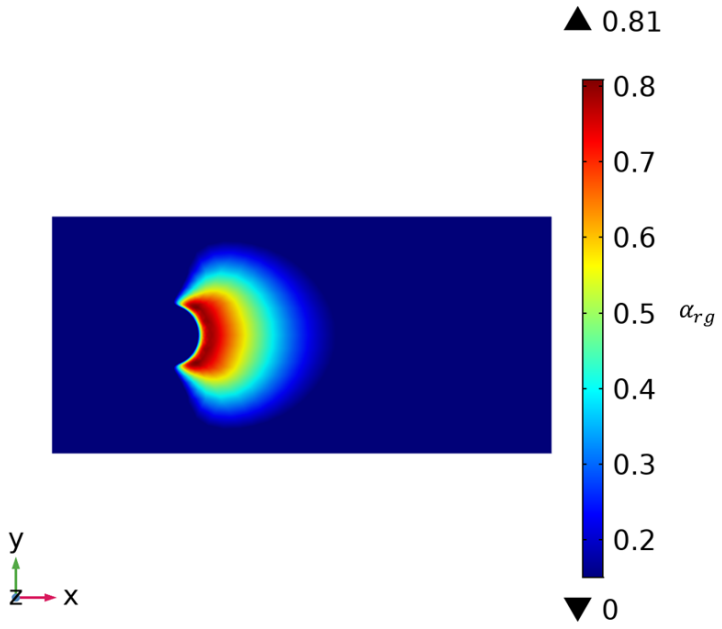

(b)

Figure 3.5: (a) Volume fraction of refrigerant gas and volume fraction of liquid oil/refrigerant in the total mixture, α_{rg} and α_{ml}, respectively, along x at $y = 0$ (central line) and $z = h$ (top surface) by solving the EHL and Thermal-EHL problem with the present solubility-based cavitation modeling. (b) Volume fraction of refrigerant gas in the total mixture α_{rg} at the plane defined by $z = h$ (top surface) obtained by solving the Thermal-EHL problem with the present solubility-based cavitation modeling. See Figure 2.3 for the coordinate system.

As shown in Figure 3.2, the temperature of the oil/refrigerant mixture is obtained with the Thermal-EHL with solubility-based cavitation modeling. Overall, temperature change in the present case is very small (-0.006 K to $+0.1$ K) compared to that obtained by Gasche [87] for a rolling piston compressor, although the general trend is consistent. It can be explained by the fact that heat transfers between the lubricant film and the solid bodies are considered in the present study but not in Ref. [87] . It is interesting to investigate the temperature profile along with the evolution of the mass fraction of the liquid refrigerant in the solution w_{rl}. The figure can be divided into two zones after the contact area. In zone I (see red zone in Figure 3.2), the evaporation of refrigerant consumes heat and induces a decrease in the temperature. In zone II (see the blue zone in Figure 3.2), the temperature increases while the refrigerant dissolves once again in the liquid solution. The decrease of the temperature at the end of zone II is because when w_{rl} approaches its maximum value $w_{rl,in}$, the heat produced by the refrigerant dissolving becomes progressively smaller, while it is constantly dissipated by the solids. It is interesting to note that the increase in the temperature due to the dissolution of the refrigerant gas is slightly higher than the decrease caused by evaporation. This difference can be explained by the fact that the conductivity of gas is lower than that of liquid, and the generated heat remains accumulated rather than being absorbed and evacuated by the solids.

The pressure distributions are presented in Figure 3.3 and the cavitation region is zoomed in. As is shown in the figure, after being strongly compressed and sheared in the contact area, the oil/refrigerant solution is at first subjected to a sudden pressure drop and falls below the cavitation pressure p_{sat}, which leads to the evaporation of refrigerant. The release of the refrigerant gas leads to a significant reduction of the mixture density, which in turn moderates the pressure drop.

The comparison between Thermal-EHL and EHL modeling has been carried out in terms of pressure (see Figure 3.3), mass fraction of liquid refrigerant in oil/refrigerant solution (see Figure 3.4) and volume fraction of the different components in total mixture (see Figure 3.5 (a)). It is worth mentioning that Figure 3.5 (a) reveals the volume fraction of the contact gap occupied by refrigerant gas α_{rg} and liquid oil/refrigerant α_{ml}, where α_{ml} equals 1-α_{rg}. As can be seen from the above figures, the consideration of thermal effects produces a smaller pressure drop in the cavitation area (see Figure 3.3), because more dissolved refrigerant remains in the oil/refrigerant solution (see Figure 3.4) and less refrigerant gas is released compared to the isothermal case (see Figure 3.5 (a)). This finding is coherent with the one reported by Gasche [87], who claimed that the mass fraction of the refrigerant gas predicted by the thermal model is smaller than the isothermal model. An explanation for this is that the decrease in temperature due to the phase change, as discussed previously, creates a competing effect that discourages the release of the refrigerant gas. As a consequence, the pressure drop is moderated, and the composition of the oil/refrigerant solution

for the Thermal-EHL problem is obtained under the competing effects of the pressure and the temperature.

Additionally, a map of the volume fraction of gas refrigerant in total mixture α_{rg} for the Thermal-EHL problem is obtained in Figure 3.5 (b), which indicates the location and the size of the cavitation region.

3.3 Discussion on the choice of cavitation models for oil/refrigerant solutions

In this section, a discussion between the novel cavitation model developed in this work and other cavitation models from the literature presented in Section 2.2.2 of the Chapter 2 is proposed. It puts into light the necessity of taking into account the solubility of the refrigerant in oil for such problems.

3.3.1 Comparisons of density-pressure relation obtained with different cavitation models

For the selected oil/refrigerant solution, a comparison of the density-pressure behavior of the present cavitation model with classical cavitation models from the literature (JFO [43],van Odyck and Venner [132], and Bayada [40]), is shown in Figure 3.6.

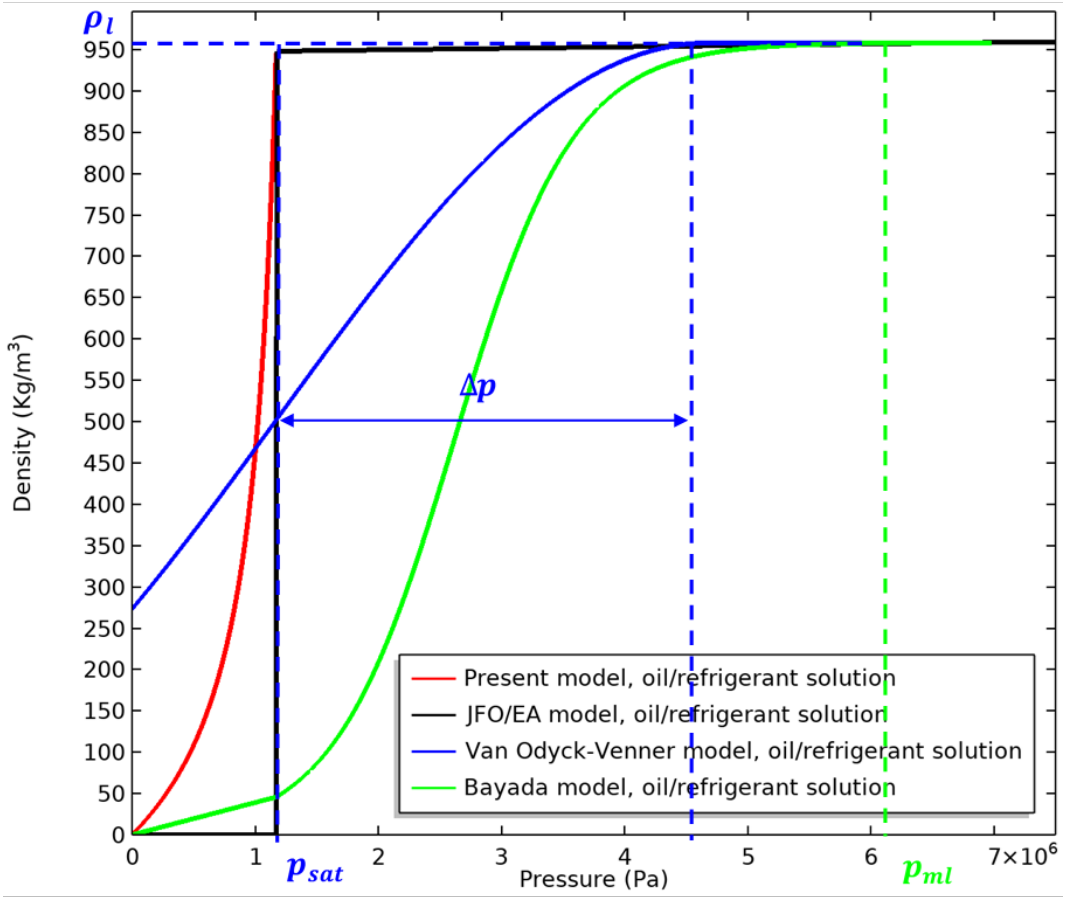

Figure 3.6: The density-pressure relations for the RL68H/R134a solution obtained with different cavitaion models (JFO [43],van Odyck and Venner [132], and Bayada [40]).

For the cavitation model of Bayada [40], the wet point p_{vm} was fixed at the saturation pressure $p_{sat} = 1.171$ MPa of oil/refrigerant solution. The densities of the liquid oil/refrigerant and gaseous refrigerant were obtained at $p = p_{sat}$: $\rho_l = 958.74$ kg/m^3 and $\rho_g = 45.87$ kg/m^3, respectively. The velocity of sound in the pure refrigerant gas c_g was given by the following expression:

$$c_g = (\frac{p_{vm}}{\rho_g})^{0.5} = 160 \text{ m/s}$$

Additionally, the bubble point p_{ml} was calculated according to:

$$p_{ml} = \rho_g c_g^2 - N \log(\frac{\rho_g^2 c_g^2}{\rho_l^2 c_l^2}) = 6.2 \times 10^6 \text{ Pa}$$

$$with \quad N = \frac{\rho_g c_g^2 \rho_l c_l^2 (\rho_g - \rho_l)}{\rho_g^2 c_g^2 - \rho_l^2 c_l^2}$$

For more details of implementation, see Appendix B.

As for the cavitation model of van Odyck and Venner [132], as the choice of the cavitation pressure p_{cav} is not specified, it was here arbitrary fixed at saturation pressure of oil/refrigerant solution p_{sat} = 1.171 MPa. The values of densities and velocity of the sound used for the model of van Odyck and Venner were the same as those used for the model of Bayada in the present work. Accordingly, the parameters required for the model of van Odyck and Venner were obtained for the RL68H/R134a system as bellows [132]:

$$c_{min} = 2c_g(\frac{\rho_g}{\rho_l})^{0.5} = 64 \text{ m/s}$$
$$\Delta\rho = \frac{1}{2}(\rho_l - \rho_g) = 456 \text{ kg/m}^3$$
$$\Delta p = \frac{1}{2}(\pi c_{min}^2 \Delta\rho) = 2964670 \text{ Pa}$$

It is worth mentioning that the cavitation model of Bayada and that of van Odyck and Venner are both based on isentropic assumptions for the phase change process, which are believed to be well adapted to the vaporous cavitation for pure oil [40]. However, as can be seen from Figure 3.6, these cavitation models based on isentropic assumptions are unable to describe properly the densities for the phase transition of the RL68H/R134a solution. The main issue consists in a much higher value of saturation pressure of the refrigerant (1.171 MPa in the present case), compared to that of the pure oil, which is commonly less than 0.1 MPa at the same temperature. This discrepancy resulted in a much higher gas density obtained at the saturation pressure, thus a larger size of phase transition area compared to that calculated for pure oil case by using these models. Therefore, the present model with the correct representations of the density-pressure relations is more adequate for describing the cavitating flow of a solution that involves a volatile fluid.

The cavitation model developed in the present work shows a good qualitative agreement with the JFO/EA model. The main improvements of the present cavitation model consist of two aspects. First, cavitation is described as a narrow transition area with a physical mechanism rather than a discontinuous jump as in the JFO/EA model. Second, the present model takes the thermal effects into account rather than assuming isothermal conditions. The compressibility law is thus a function of both pressure and temperature. As a result, the present cavitation model can be seen as an improved and more rational version of the JFO/EA model.

3.3.2 Comparisons of pressure profile obtained with different cavitation models

Additionally, the steady-state Thermal-EHL solutions obtained in Section 3.2.3 allow comparisons with those obtained by using other cavitation models. Figure 3.7 shows that pressure distributions calculated with different approaches for oil/refrigerant solution are in good agreement in the pressurized region. The discrepancies appear only in the cavitation region. Compared to the Reynolds model and the JFO/EA model, the present model allows the existence of pressure below the cavitation pressure, as observed experimentally by Etsion and Ludwig [175] and Braun and Hendricks [176]. Meanwhile, unlike the Sommerfeld and van Odyck and Venner models, the current model avoids the absolute negative pressure, which is not expected in the current investigation since the fluid involved is a mixture of oil and refrigerant rather than a pure substance [148]. Finally, in comparison with the Bayada model, about the same minimum pressure is attained due to the similarity in the mixture density in the low-pressure area (see Figure 3.6). However, the cavitation area predicted by the Bayada model begins much later than that of the present model, because of the inappropriate size of the phase transition area mentioned before. Hence, for the sake of detailed information in the cavitation region, the present model is more advantageous. Furthermore, the minimum pressure obtained in the current case 0.76 MPa, is much higher than the vapor pressure of mixing lubricating oil 3.5 Pa provided by the oil manufacturer, which validates our assumption that no vaporous cavitation takes place (no evaporation of liquid oil).

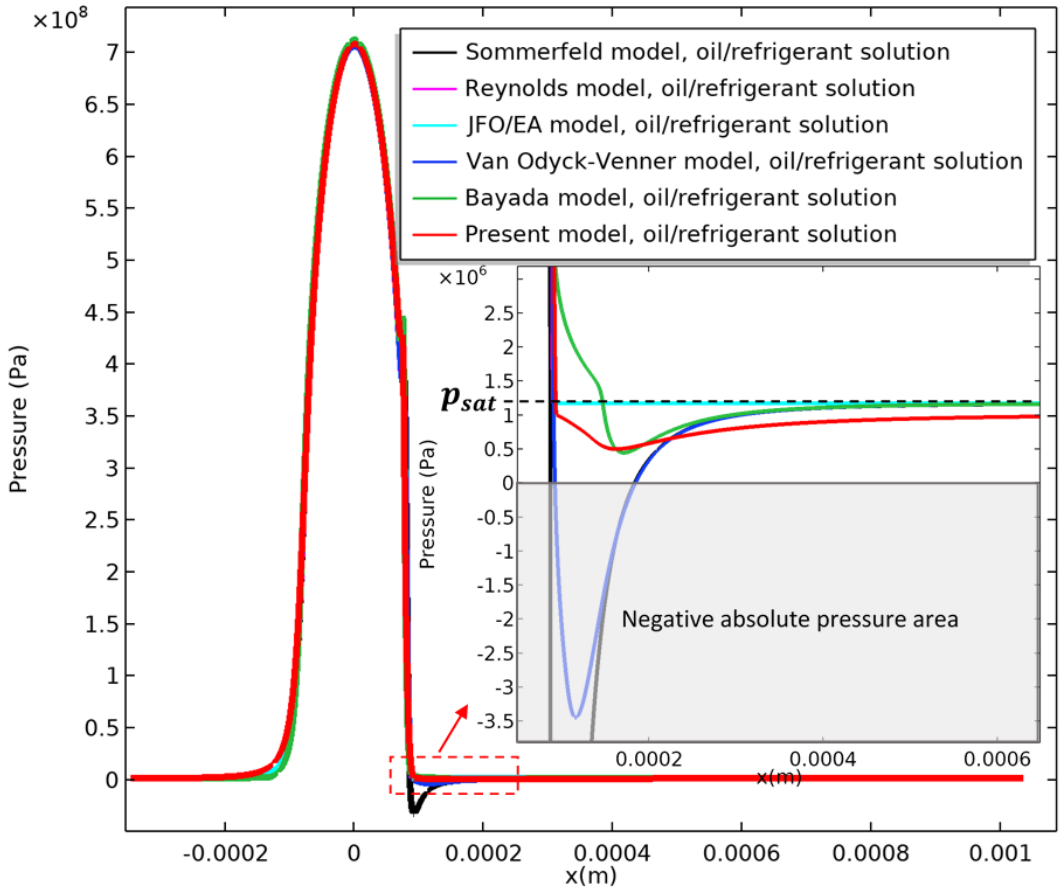

Figure 3.7: Pressure of oil/refrigerant mixture along x at $y = 0$ (central line) obtained for different approaches of cavitation modeling. See Figure 2.3 for the coordinate system.

3.4 Comparison with pure oil in the cavitation region

As mentioned earlier, the lubrication circuit in the refrigeration compressor would be ideally operated with pure oil. However, there is always some dilution of refrigerant in the lubricating oil due to miscibility. It was demonstrated in [51] that the oil/refrigerant solution had a quite different behavior compared to the pure oil when lubricating the contacts in the pressurized region. It is interesting to investigate if the oil/refrigerant solution and pure oil also perform differently in the cavitation region. For this purpose, a case study was performed to compare the cavitation phenomena in the refrigeration compressor with pure oil and with the oil/refrigerant solution. As was demonstrated in Figure 3.7, the solubility-based cavitation model developed in the present study is more adequate for describing the cavitating flow of a solution, it was

therefore adopted for cavitation modeling of oil/refrigerant solutions. However, because the evaporation of oil is not taken into account in the current study due to its extremely low vapor pressure(validation in Section 3.3.2), the current model is incapable of simulating the vaporous cavitation of oil. As a result, the cavitation model proposed by van Odyck and Venner [132] was used for modeling pure oil cavitation. The same operating conditions described in Section 3.2.3 were used for this case study. The data used for the properties of pure oil are as bellow:

$$\rho_v = 1 \text{ kg/m}^3 \quad \rho_l = 977 \text{ kg/m}^3 \quad c_g = 343 \text{ m/s} \quad p_{sat} = 3.5 \text{ Pa}$$

The profile of volume fraction of gas α_g, which represents oil vapor for the case of pure oil and refrigerant gas for the oil/refrigerant solution, is presented in Figure 3.8.

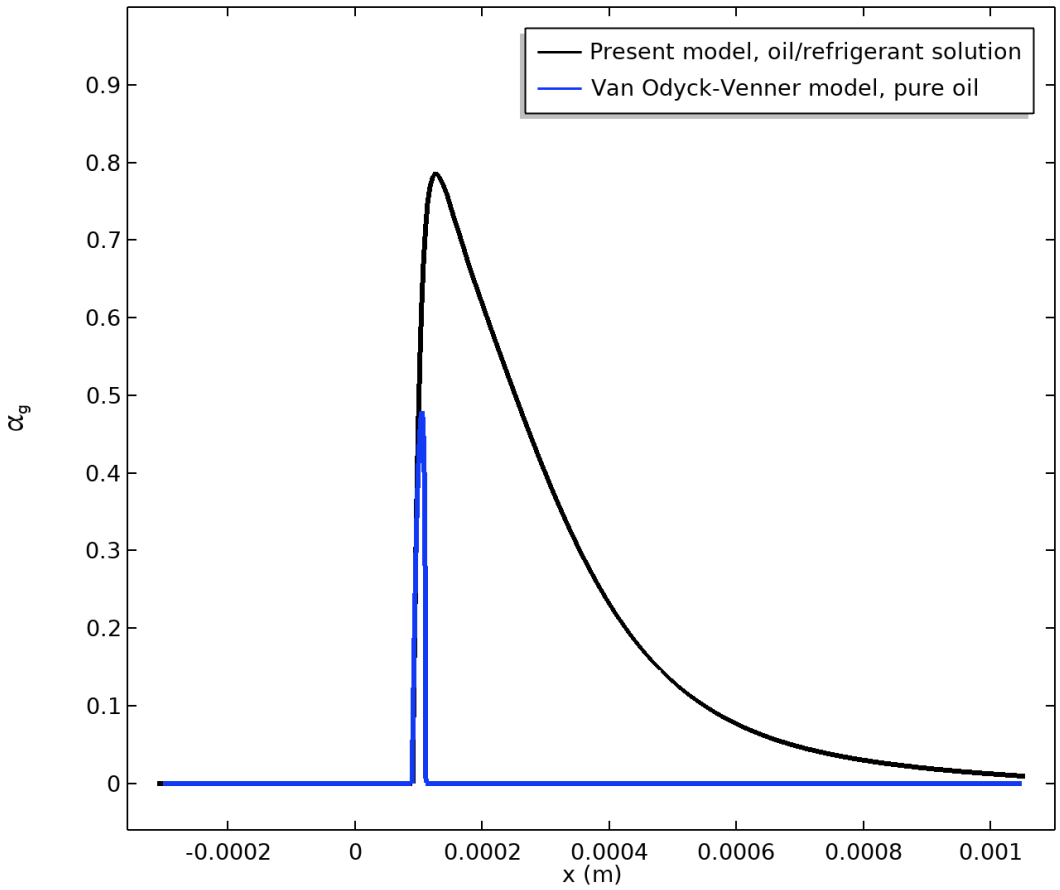

Figure 3.8: Volume fraction of gas α_g along x at $y = 0$ (central line) and $z = h$ (top surface) obtained for pure oil and oil/refrigerant solution. See Figure 2.3 for the coordinate system.

It is important to recall that a pressurized lubricant reservoir is used in the refrigeration compressor. Therefore, the surrounding pressure was set at $p = 1.171$ MPa. Consequently, the volume fraction profile of oil vapor in the

cavitation area presented in the present study can be quite different from those obtained experimentally or numerically at ambient pressure. As can be seen in Figure 3.8, the length of cavitation with pure oil is much smaller than that with the oil/refrigerant solution. This result indicates that oil cavitation has less influence than the oil/refrigerant solution cavitation on the inflow of the following contact. Additionally, oil cavitation produces a maximum volume fraction of gas of about 50 %, which is lower than that of oil/refrigerant cavitation, where the void fraction reaches up to 80 %. It was reported that, for the gas volume fraction larger than 70 %, 'flashing' phenomenon could occur in the straight tubes [80, 81, 177]. It has been observed that the liquid phase would become discontinuous and a part of the contact gap would be entirely occupied by the gaseous phase. In addition, this 'flashing' phenomenon could lead to some of the liquid phases being rejected out of contact. As the present study concerns mainly conventional two-phase flow, this 'flashing' phenomenon was not modeled. However, the present model shows its capacity of predicting the location where the potential risks would exist.

3.5 Industrial case study

A case study of a refrigerant compressor in the industry is carried out. The purpose of this case study is to assess the effect of refrigerant cavitation on the lubrication of the subsequent contact. Same oil/refrigerant solution, polyol ester oil RL68H, and refrigerant HFC-R134a, is involved, of which the detailed characterizations can be found in Section 3.2.1. A 100Cr6 steel - 100Cr6 steel elliptic contact is investigated with the material properties presented in Table 3.8. The geometry parameters for the contact can be found in Figure 3.9 and Table 3.9.

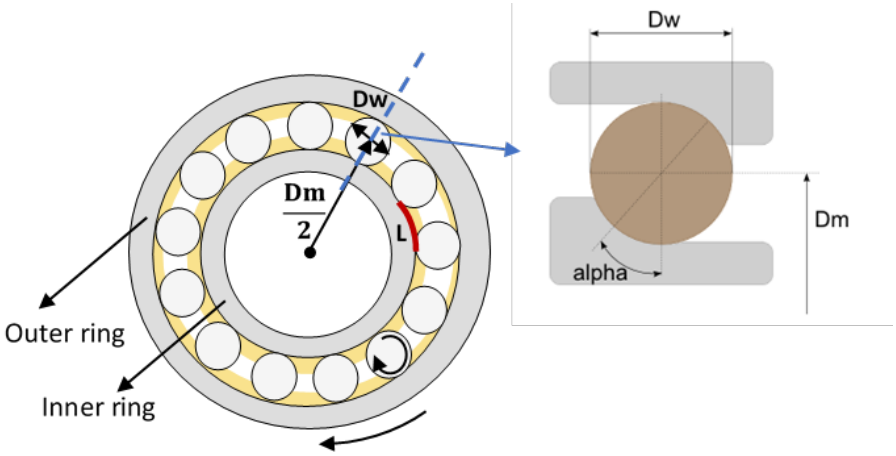

Figure 3.9: Geometry of the rolling bearings in the refrigeration compressor, with an example of a cross section via the blue, dashed line

Table 3.9: Contact parameters for the refrigeration compressor case study

Nb.balls	13
Transverse radius	6.57 mm
Inner ring radius	23.9 mm
D_m	60.4 mm
D_w	12.7 mm
$alpha$	40°

Based on the contact geometry, the distance between the centers of two successive rolling balls L gives:

$$L = 2\pi \frac{\frac{D_m}{2} - \frac{D_w}{2}}{\text{Nb.balls}} = 11.5 \text{ mm} \tag{3.13}$$

The operating conditions on a single contact used in the industrial application can be found in Table 3.10.

Table 3.10: Operating conditions on a single contact for the refrigeration compressor case study

Load w	560 N
Entrainment speed u_m	5.545 m/s
Operating temperature T_s	80°C
Operating pressure P_s	0.5 MPa

Accordingly, the Hertzian parameters for this elliptic contact are obtained as presented in Table 3.11:

Table 3.11: Hertzian parameters for the refrigeration compressor case study

$R_{x,ell}$	5.017 mm
$R_{y,ell}$	189.63 mm
a	0.13152 mm
b	1.3473 mm
p_h	1.5089×10^9 Pa
D	$0,026$

According to Nijenbanning et al. [178], the ellipsoid-on-plane contact can be simplified to an equivalent cylinder-on-plane contact for rolling EHD contacts when the ratio of ellipticity $D = \frac{R_{x,ell}}{R_{y,ell}}$ is smaller than 0.1. As a result, equivalent line contact is defined in this study for the simplification of computations. The equivalent radius of curvature R_{ell}^{eq} and corresponding normal load w^{eq} [179] can

be calculated as follows keeping the same Hertz pressure p_h and contact length a:

$$\begin{aligned} R_{ell}^{eq} &= \frac{E_{eq} a}{4 p_h} \\ w^{eq} &= \frac{\pi p_h a}{2} \end{aligned} \tag{3.14}$$

where the equivalent Young's modulus E_{eq} can be obtained with Eq. (2.16).

The numerical model proposed in Chapter 2 to describe the miscible fluids for EHL point contacts is adapted here for line contacts (detailed equations see Appendix A). As previously demonstrated, the isothermal analysis represents a more critical condition, since it predicts a larger volume fraction of gases in the cavitation area than the thermal one. Thus, an isothermal analysis is performed. The classical Reynolds equation completed with the novel cavitation model is solved on the one-dimensional contact area Ω_R defined for $x \in [-4.5a, 11.5a]$. The linear elasticity equation is solved on a two-dimensional equivalent domain $x \in [-60a, 60a] \times z \in [-60a, 0]$ (see Figure A.1). The pure rolling condition and steady-state condition are considered. The risks of the refrigerant cavitation on the subsequent contact can be evaluated by comparing the distance between the center of two successive rolling contacts L to the calculated cavitating length. The volume fraction of the refrigerant gas α_g is presented in Figure 3.10.

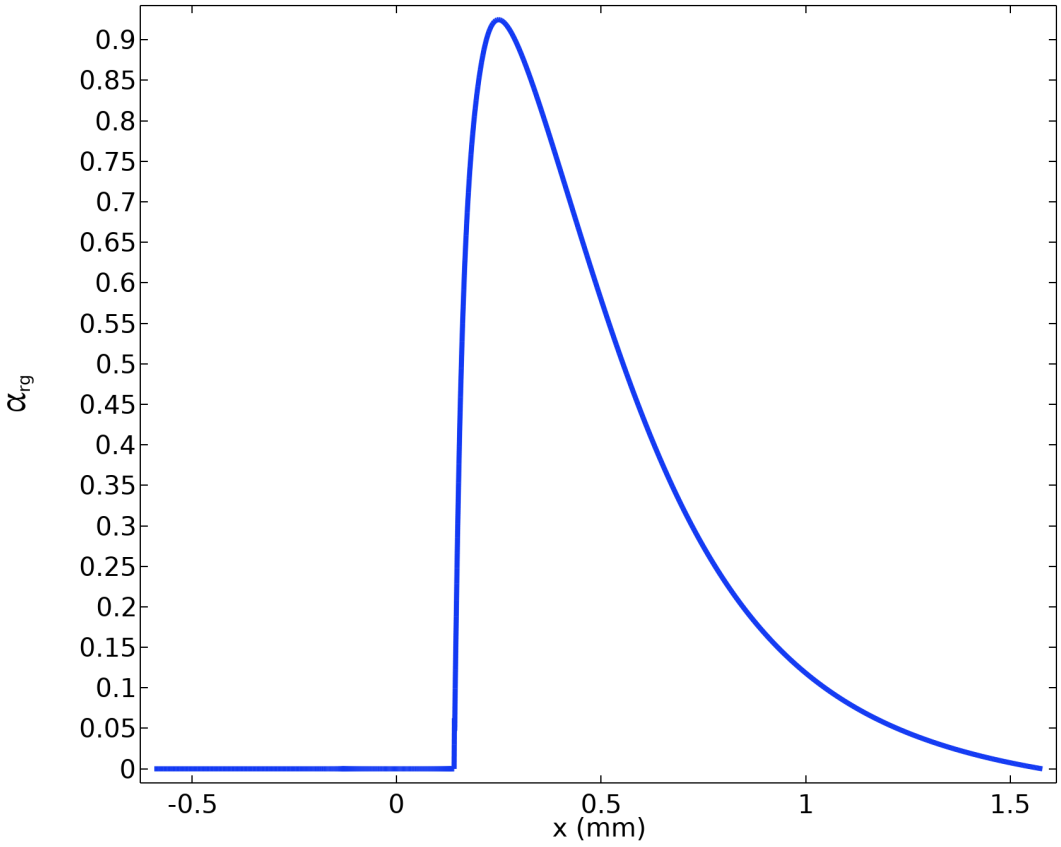

Figure 3.10: Volume fraction of gas α_g along x obtained for the oil/refrigerant solution in the case study. See Figure A.1 for coordinate system

Figure 3.10 shows that the distance L (11.5 mm) between the centers of two successive rolling contacts is significantly greater than the cavity length (about 1.5 mm presented in Figure 3.10), indicating that the refrigerant cavitation phenomena has been completed in the oil/refrigerant solution before arriving at the succeeding contact.

Without considering the rate of refrigerant dissolving in oil and the "flashing" phenomenon, which may cause liquid rejection risks, this first approach allows for evaluating the cavitation area in the framework of a ball bearing.

3.6 Conclusion

An original solubility-based cavitation modeling for Thermal-EHL point contacts has been developed in this work. The mixture of oil/refrigerant solution and refrigerant gas is considered as a two-phase homogeneous compressible fluid in the cavitation area. The behavior of the lubricant can be described with the

Generalized Reynolds equation coupled with the elasticity equation and the energy conservation equation, for both the pressurized region and the cavitation region, by introducing the physical properties of the lubricant mixture. No geometric assumption about the shape of the cavitation area is required, and no constraint on pressure (for example, assuming the pressure is constant across the cavitation area) is introduced. The sub-cavitation pressure is naturally obtained based on physical mechanisms. In addition, the density and viscosity can vary both in the pressurized region and the cavitation region as a function of local pressure, temperature, and mass fraction of the refrigerant. The model can predict both the oil-film rupture and reformation, which allows obtaining the location and the size of the cavitation area. The numerical results showed an overall similarity to the experimental observations and measurements. Comparisons have been made with several cavitation models in the literature. The present model shows a general trend consistent with the JFO condition. It is advantageous for describing the cavitating flow of a solution and for offering a more rational explanation of the mechanism of the cavitation area. Moreover, the thermal effects were considered in the present model and its influence on the cavitation region has been discussed by comparing to the isothermal solution. Finally, the different behavior of pure oil and oil/refrigerant solution in the cavitation region has been discussed. It is shown that the oil/refrigerant cavitation presents more potential risks for the performance of the lubrication system. The cavitation model in the present work was originally developed to investigate the cavitation area of the oil/refrigerant solution in the refrigeration compressor. However, it provides a general numerical procedure for modeling other solutions of lubricant and volatile liquid or non-condensable gas.

Chapter 4

Water droplets in oil emulsion at the inlet of EHD contacts

This chapter mirrors a study entitled "Water droplets in oil at the inlet of an EHD contact: a dual experimental and numerical investigation" by F.Zhang et al. submitted for publication in Tribology international. A dual experimental and numerical analysis of water droplets in oil emulsion at the inlet of EHD contacts is given in this chapter. First, the experimental findings are displayed. Then, comparisons of experimental data and numerical results are provided. Additionally, a parametric analysis is carried out.

4.1 Introduction

The effects of water in oil on the lubricated contact have been intensively researched both experimentally and numerically, as previously mentioned in Chapter 1. However, the published findings indicate some inconsistencies when the mean droplet size is bigger than the film thickness. Furthermore, most attempts concentrated on investigating the film thickness and friction in the contact area, which is incapable of understanding upstream phenomena such as water droplets expelling away from the contact, as observed in some experiments [91, 107, 118].

The goal of this work is to confront the contradictory findings in the literature from a fresh angle and to expose the influence of water-in-oil emulsion on EHL contacts under various conditions. For this purpose, an original dual experimental and numerical approach focusing on water droplet trajectories in oil at the inlet of EHD contacts was introduced in Chapter 2.

This methodology is used in the current chapter. At various rolling speeds, the first direct observations of a micro-sized water-in-oil emulsion flow at the inlet of an EHL point contact using a high-speed camera and a microscope are given. The numerical strategy will be validated by comparing numerically traced water droplet motions in oil to experimental data. The impacts of various operating parameters on the flow of water-in-oil emulsion will then be investigated.

4.2 Analyze of water droplets trajectories at inlet

Many experimental studies propose to use an interferometric approach on a ball-on-disc system to explore the impact of water droplets in oil [92, 105–109]. However, as discussed in Chapter 2, this experimental technique does not allow

for a focus on the contact inlet and hence does not achieve the study's purpose. As a result, a direct visualization technique using the water dye described in Chapter 2 is adopted. With the ball-on-disc tribometer and the experimental protocol presented in Chapter 2, direct observations of water droplets in oil emulsion at the inlet of EHD contacts under the pure rolling condition are performed. A 100Cr6 steel-glass configuration is used in the experimental study. The properties of the material can be found in Table 3.7 and 3.8. Table 4.1 presents the experimental operating conditions.

Table 4.1: Operating conditions for direct observations of water in oil emulsion at the inlet of EHD contacts

Reduced radius R_x	1.27×10^{-2} m
Load w	40 N
Entrainment speed $u_1 = u_2 = u_m$	$0.015, 0.05, 0.1, 0.5, 1, 1.5, 2, 2.5, 3$ m/s
Operating temperature T_s	25°C

The testing fluid is a water in oil emulsion with an initial water droplet size of 8 µm and 60 µm prepared as previously described in Chapter 2 from oil Morlina S1 B 320 with 10 % by weight distilled water, containing 5 % diluted coolant (Quakerol TWN). The detailed characterizations of the emulsion can be found in Section 2.3.2.

4.2.1 Definition of the inlet distance of water droplets

Results of direct observations on water droplets (with initial size of 8 µm) in oil at the contact inlet under rolling speed u_m (see Table 4.1) can be found in Figure 4.1. Water droplets can be identified with red color thanks to the water dye. As can be seen in this figure, the observation area is large compared to the size of water droplets. It is difficult to identify the trajectories of water droplet individually, especially at high velocity. However, a circle-shaped area with no or few presences of water droplets was observed in the experiments. Besides, the form and size of this area barely changed throughout time. The general motion of emulsified water in oil can be derived from the figure by tracing the limits of this area where no water droplets are present in the form of a circle (see dashed boundary line in Figure 4.1). Three colored points closest to the contact center define the circle.

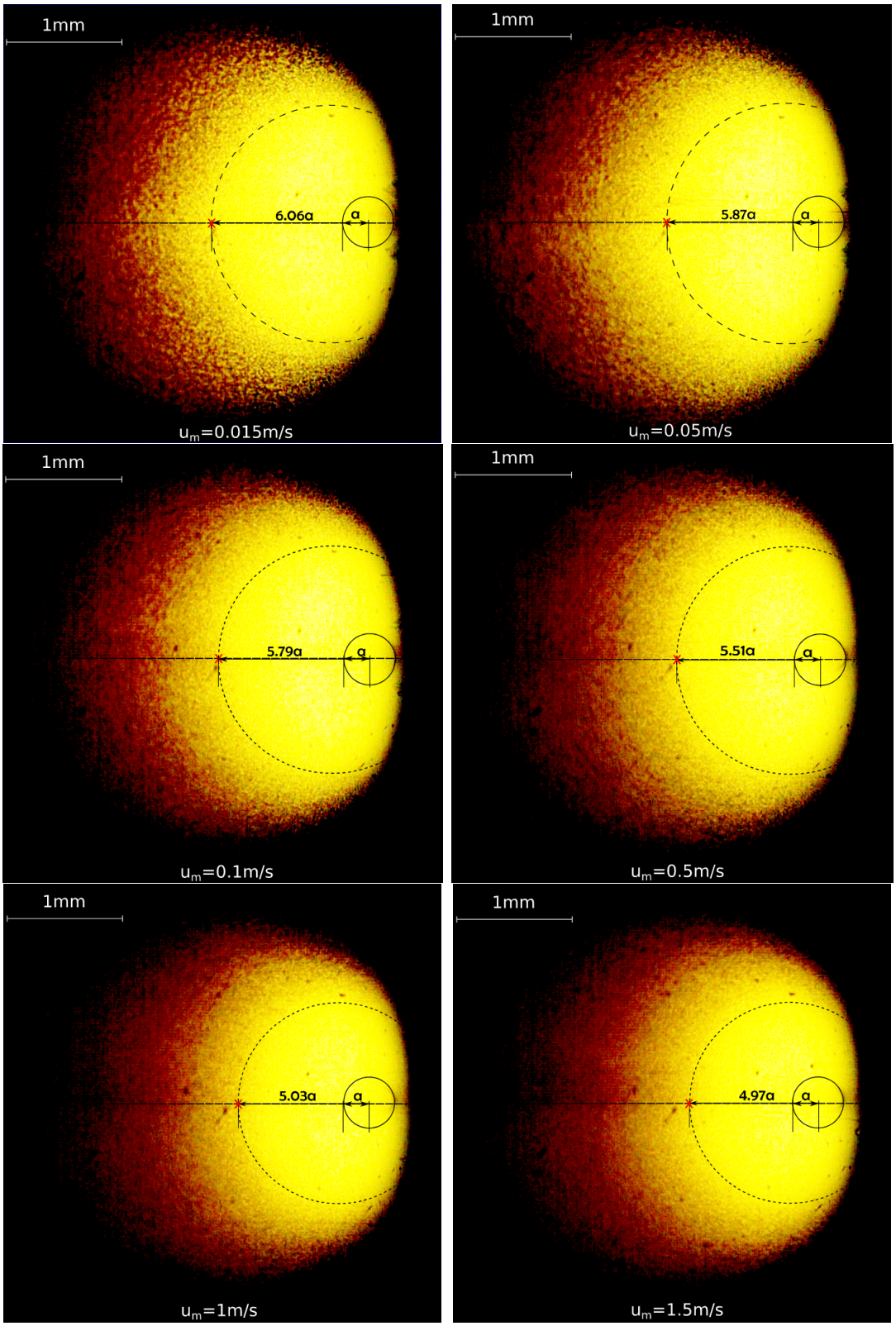
1mm
6.06a
a
u_m=0.015m/s
1mm
5.87a
a
u_m=0.05m/s
1mm
5.79a
a
u_m=0.1m/s
1mm
5.51a
a
u_m=0.5m/s
1mm
5.03a
a
u_m=1m/s
1mm
4.97a
a
u_m=1.5m/s

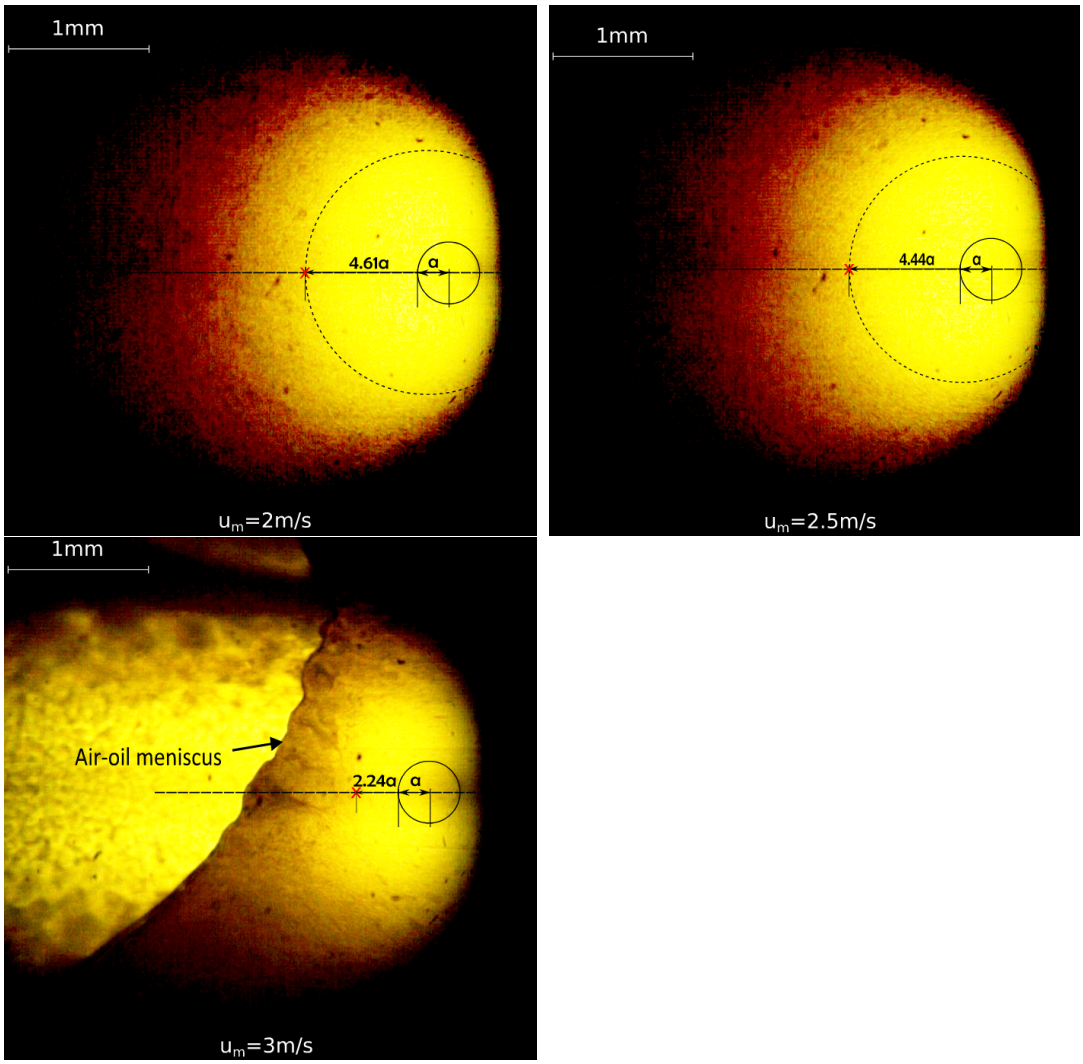

Figure 4.1: Distributions of water droplets in oil at the inlet of an EHL contact and estimation of inlet distance with characteristic droplet diameter of 8 µm

As can be seen from Figure 4.1, the water droplets flow mostly around the contact area instead of entering directly. A similar observation of water droplets being expelled away from the contact under pressure and shear has been reported in other experimental investigations [91, 107, 118]. In the present case, contact angles of 73° and 27° were obtained (see Appendix E for measurements), respectively, for water/steel and oil/steel interfaces, indicating that the wettability of water on the testing surface is much worse than that of oil. Besides, it has been verified that the water dye used in the present study does not influence the surface tension of water (see Appendix E). As a consequence, the contact surfaces have a very low influence on water entrainment (contrary to oil).

It is worth mentioning that as the rolling velocity increases, the water droplets move closer to the contact on the central line. When the velocity

increases up to 3 m/s, the oil/air meniscus appears within the observation area and pushes water droplets towards the contact.

Similar behavior on the trajectory of water droplets was observed for the water-in-oil emulsion with a larger initial water droplet size (60 µm), approaching closer to the contact area with a higher rolling velocity (see Appendix F).

To reveal the influence of water droplets on the contact area, the position of the closest water droplets to the contact on the central line is determined, in the present study, as the intersection of the limit circle and the central line as shown in Figure 4.1. The distance between this position and the central point of the contact is defined as the inlet distance of water droplets x_w. The maximum measurement error is 3 %. The dimensionless inlet distance of the water droplets X_w can be defined as follows:

$$X_w = \frac{x_w}{a} \tag{4.1}$$

with a is the Hertzian radius of the contact area (see Table 4.2).

To further investigate the effect of water droplets on the contact area, X_w is compared to the critical position X_c which indicates the location of the air-oil meniscus where the change of the lubrication regime from the fully flooded to starved condition happens under pure oil lubrication. X_c writes (in pure oil conditions), according to Hamrock and Dowson [29]:

$$X_c = 1 + 3.06((\frac{R_x}{a})^2 H_c)^{0.58} \tag{4.2}$$

Where, R_x is the reduced radius of the ball in contact with the plane (see Table 4.1). H_c, the dimensionless central film thickness, gives [11] (in pure oil conditions):

$$H_c = 1.2G^{0.53}U^{0.67}W_2^{-0.067} \tag{4.3}$$

Where U, W_2 and G are given by:

$$\begin{aligned} U &= \frac{\mu_0(u_1+u_2)}{E' R_x} \\ W_2 &= \frac{w}{E' R_x^2} \\ G &= \alpha E^{'} \end{aligned} \tag{4.4}$$

The values of the load w, the reduced elastic modulus $E^{'}$, the Hertzian pressure p_h and fluid properties can be found in Table 4.1 and 4.2.

Table 4.2: Hertzian parameters and properties of material and fluid

μ_0 (25°C)	0.781 Pa · s
ρ_0 (25°C)	850 kg/m^3
α	15×10^{-9} Pa^{-1}
E'	1.23×10^{11} Pa
a	1.84×10^{-4} m
p_h	5.65×10^{8} Pa

4.2.2 Comparison between numerical and experimental results on water droplet distributions

To validate the modeling strategy, the same operating conditions used in the previous experiments (see Section 2.3.2) are applied in the numerical modeling. Numerical calculations are performed under different rolling velocities as in the experiments. The diameter of water droplets is set to 8 µm based on the previous experimental finding. Figure 4.2 (b) shows an example of water droplet trajectories in oil at 0.015 m/s obtained by numerical modeling. The water droplet inlet distance x_w is estimated using the same method presented previously in Section 2.1 for analyzing the experimental data (the trajectories closest to the contact center define the limit circle). Thus, a comparison of water droplet distribution obtained by experimental observation and numerical modeling can be achieved. As shown in Figure 4.2 (b), numerical modeling can reproduce the circle-shaped area with no presences of water droplets in oil, demonstrating a good agreement with the experimental results.

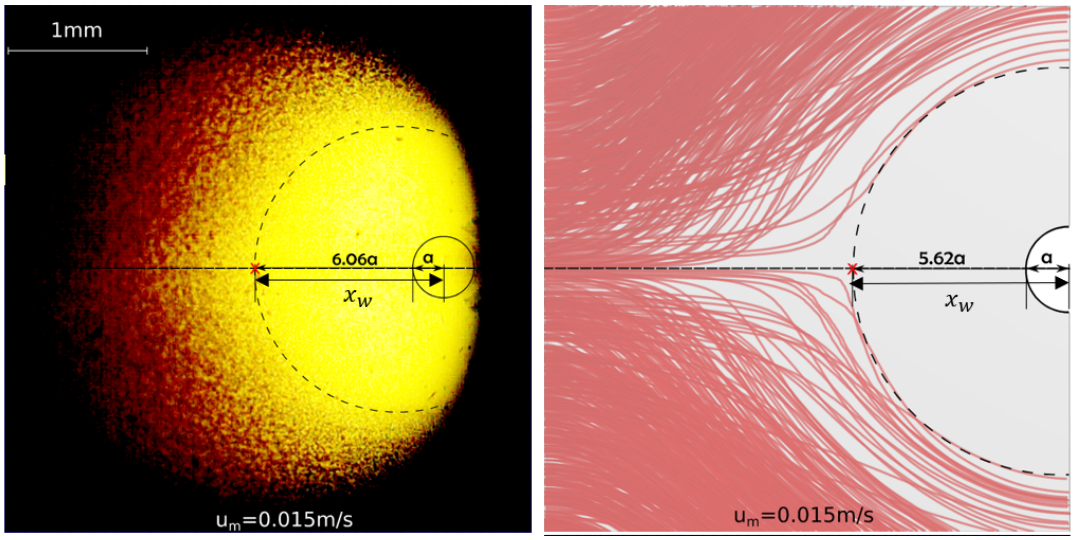

(a) (b)

Figure 4.2: Distributions of water droplets in oil at the inlet of an EHL contact and estimation of inlet distance with characteristic droplet diameter of 8 µm with (a) experimental observations at 0.015 m/s, (b) numerical results at 0.015 m/s

4.3 Parametric study

4.3.1 Velocity influence

Figure 4.3 shows the experimental results X_w compared to X_c for initial water droplet size of 8 µm and 60 µm at different rolling velocities u_m (see Table 4.1).

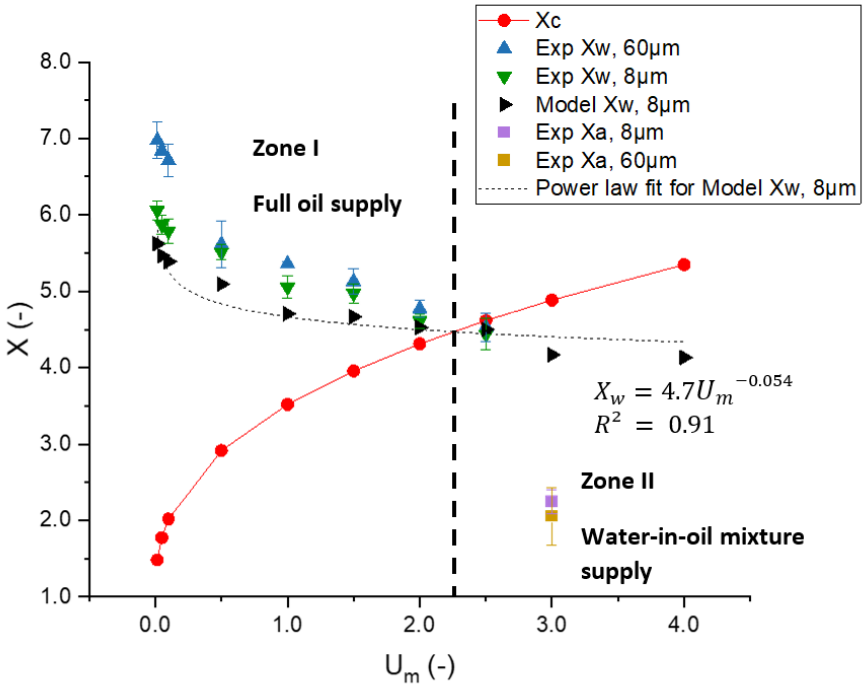

Figure 4.3: Comparison between water droplets position obtained experimentally and numerically for droplet size of 8 µm and 60 µm and critical position of starved condition on the central line. With X_c the critical position of starved condition, X_w the closest position of water droplets and X_a the closest position influenced by air-oil meniscus to the contact area.

The inlet distance influenced by air-oil meniscus is presented as X_a to be distinguished from X_w, where no air-oil meniscus was detected. For consistency, the mean rolling velocity u_m is also presented in its dimensionless form U_m:

$$U_m = \frac{u_m}{u_{ref}} \tag{4.5}$$

With $u_{ref} = 1$ m/s in the current study.

The influence of water droplets on the contact area can be derived by comparing X_w with the critical position X_c. Water droplets are considered to not influence the contact area when $X_w > X_c$, since the contact area is under full oil supply (see Figure 4.3 Zone I). However, if water droplets penetrate the critical area (when $X_w \leq X_c$), then the film-forming ability may be affected since the contact area is under a water-in-oil mixture supply (see Figure 4.3 Zone II). Even if water droplets do not ultimately flow into the contact, the quantity of the oil that feeds into the contact area is excepted to reduce due to the presence of water droplets.

As can be seen from Figure 4.3, the film-forming ability of the oil has no reason to be influenced by water droplets at low rolling velocity. However, when the velocity increases, water droplets approach closer and finally enter the critical area, resulting in the water-in-oil mixture supply of the contact area. In the current case, the film thickness may begin to decrease because of water droplets when rolling velocity increases to 2.5 m/s ($U_m = 2.5$). It should be noted that, in the present experiment, as the rolling velocity increases up to 3 m/s ($U_m = 3$), regardless of the size of the water droplets, an air-oil meniscus appears in the observation region. It pushes the water droplet towards the contact, of which the position is presented as X_a, and provokes starvation of the contact area (see Figure 4.1). The above findings confirm the assumptions of Salagean and Spikes [110], who reported the sudden reduction of the film thickness of water-in-oil emulsion at high rolling velocity and supposed that starvation might occur at the inlet.

Besides, it is interesting to note that water droplets with a larger initial size show a slightly higher value of X_w at low rolling velocity. However, X_w becomes almost the same for water droplets with different initial sizes when rolling velocity increases. It is attributed to the fact that as the rolling velocity increases, the initial big water droplets are gradually sheared into smaller water droplets, the size of which depends on the type of water-in-oil emulsion and involved surfactant [180, 181]. Indeed, it was found that the size of water droplets was smaller after the experiment.

The same procedure for estimating the inlet distance of water droplets X_w is performed for numerical results obtained with varied rolling velocities. The diameter of water droplets is set to 8 µm for the numerical calculations because the experimental results show that smaller droplets are more likely to approach the contact area. Besides, the deformation and breakup of water droplets and the presence of air-oil meniscus are not considered in the present numerical model. As can be seen from Figure 4.3, the numerical results predict the same behavior: water droplets approach closer to the contact area with the increase of the rolling velocity. A good quantitative accuracy is found since the maximum relative error with experimental data is 8 %. Furthermore, by removing the impact of the presence of an air-oil meniscus, the numerical model can extend findings at high velocity, which was not possible with the experimental tool.

In Figure 4.3, based on the numerical model, a power law fit is given as a guide to the eye: $X_w = 4.7U_m^{-0.054}$.

Results obtained for the water droplet trajectories in oil under different rolling velocities can be discussed based on the velocity profile at the contact inlet. Considering the classical assumptions of thin-film theory, the velocity components along the x and y directions can be expressed as follow [4] (see Figure 2.9 for the coordinate system):

$$\boldsymbol{u(z)} = \underbrace{\frac{1}{2\mu_f}\nabla p \frac{z}{h}(\frac{z}{h} - 1)h^2}_{\text{Poiseuille flow}} + \underbrace{\frac{z}{h}\boldsymbol{u_1} + (1 - \frac{z}{h})\boldsymbol{u_2}}_{\text{Couette flow}} \tag{4.6}$$

As can be derived from the above equation, the lubricant flow is composed of the Poiseuille flow, which is oriented upstream at the inlet as the pressure gradient is positive, and of the Couette flow, which is oriented downstream towards the contact area.

It can be deduced from Eq. 4.6 that, in the rolling direction, when the mean rolling velocity increases, the positive fluid velocity in the Couette flow increases, bringing water droplets closer to the contact region.

4.3.2 Release position and water droplet size influence

At low velocity ($u_m = 0.015$ m/s) and with a smaller observation area, trajectories of several well-identified water droplets observed in the experiments can be traced as shown in Figure 4.4.

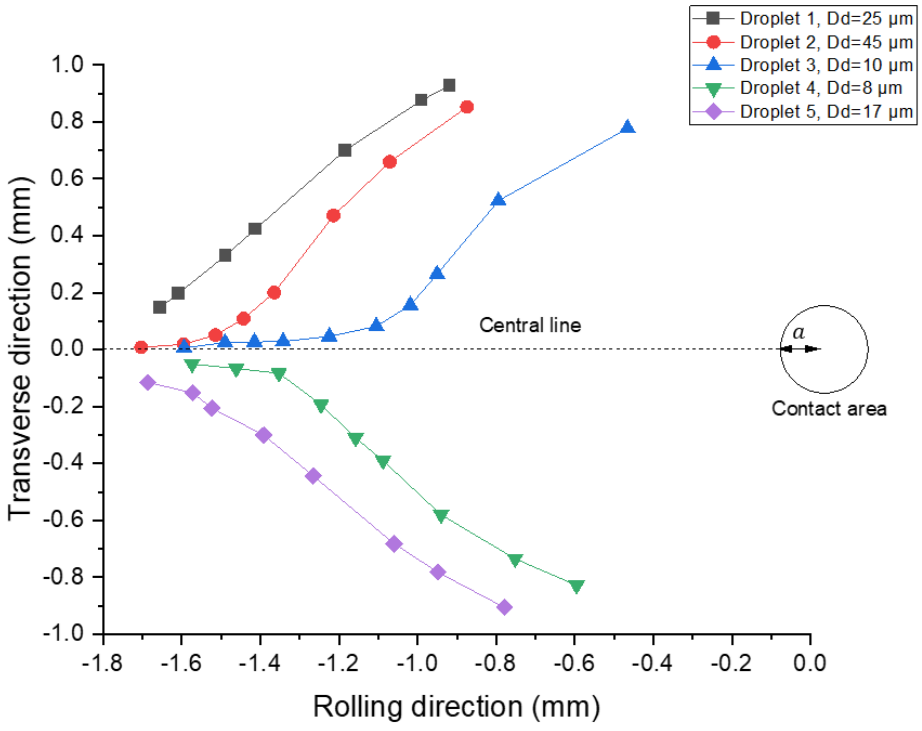

Figure 4.4: Trajectories of water droplets in oil obtained from experiments

Each curve in this figure represents the trajectory of a water droplet; 5 droplets of varying size and initial position are studied. As shown in Figure 4.4, when approaching the contact area, these droplets move in a generally similar manner. Yet, the displacement in the transverse direction along the rolling direction varies. It is mostly determined by droplet size and initial transverse position. For droplets of similar size (see Droplets 3 and 4), droplets with an initial transverse location closer to the central line have less transverse displacement while moving towards the rolling direction. Droplets of smaller sizes tend to stick to the central line when they have a similar initial transverse position (see Droplets 2 and 3). Furthermore, it seems that the influence of the initial transverse position is dominant when comparing Droplet 2 with Droplet 1 or Droplet 5. Droplet 1 (or Droplet 5) with a smaller diameter moves more greatly in the transverse direction than Droplet 2 with a larger diameter, which is due to the difference in the initial transverse position between Droplet 2 and Droplet 1 (or Droplet 5). The above findings suggest that the droplets of small size with an initial transverse position near the central line have more risks of approaching the contact area. It should be noted here that Strubel et al. [157] found similar results when studying solid particle contamination of an oil-lubricated EHL contact.

By evaluating numerous trajectories of droplets with different initial transverse positions (along the y-axis, using the coordinate system in Figure 2.9) at the inlet, it can be derived that droplets with an initial transverse position closer to the central line are more likely to approach the contact area as suggested by the experimental data. It can be explained based on Eq. 4.6, that in the transverse direction, the smallest pressure gradient generated is near the central line. As a result, the closer water droplets are to the central line, the more likely they are to go towards the contact.

The influence of the water droplet size is investigated numerically as well. Calculations for different sizes of water droplets are performed by varying the uniform diameter D_d of the inlet water droplets and the associated number N_d of droplets while keeping the water concentration constant (see Section 2.3.3 of Chapter 2). The trajectories of water droplets of different sizes at 0.015 m/s are presented in Figure 4.5. A very small reduction of x_w is noted when the size of the water droplet increases, as suggested in the experiments.

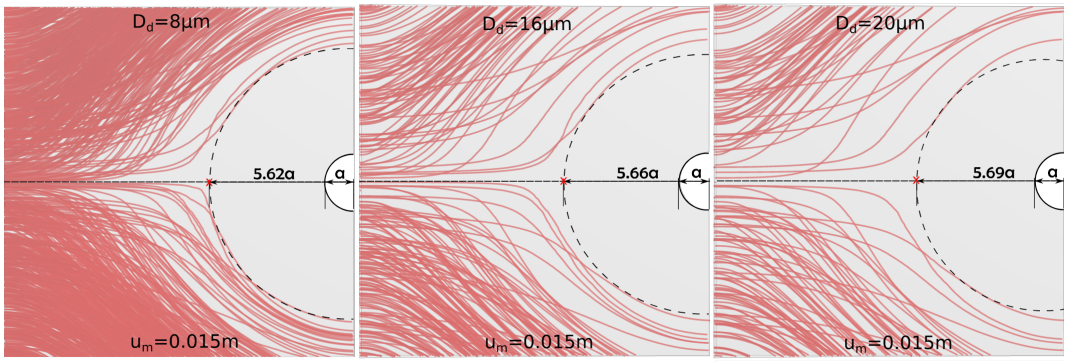

Figure 4.5: Trajectories and inlet distance of different size of water droplets in oil obtained by numerical modeling

Though the size of water droplets shows a very small influence on x_w in the present study, its influence can be discussed based on the drag force (see Eq. (2.52)). The larger the droplet, the larger the drag force, which works in the opposite direction of the relative motion of water droplets in oil [182], preventing the droplet from approaching the contact area. Furthermore, as the size of water droplets increases, for a constant water mass concentration, the number of water droplets N_d reduces. From a statistical point of view, the probability of water droplets reaching the critical position decreases as well.

4.3.3 Lubricant viscosity influence

To study the influence of dynamic viscosity of based oil on water-in-oil flow, numerical modeling is performed for water-in-oil emulsion with different oil viscosity μ_0 (see Table 4.3). The mean rolling velocity is kept constant at 1 m/s and the applied load is maintained at 40 N.

Table 4.3: Oil viscosity used for the numerical modeling

μ_0	$0.09, 0.284, 0.5, 0.781, 1.15, 1.754$ Pa · s

The modeling strategies described in Section 2.3.3 of Chapter 2 are applied. Film thickness and pressure distributions are first obtained for different oil viscosity by using the finite element full system approach developed by Habchi et al. [15]. Then, for each value of oil viscosity, a three-dimensional geometry is generated from the calculated film thickness, with calculated pressure distribution imposed at the outlet boundary. For each case, the mass flow rate ($\dot{m}_d$) and the number of water droplets N_d need to be calculated using Eq. (2.54). A dimensionless parameter $\bar{\eta} = \frac{\mu_0}{\mu_{0ref}}$ with $\mu_{0ref} = 0.781$ Pa · s is used here to represent the variation of oil viscosity.

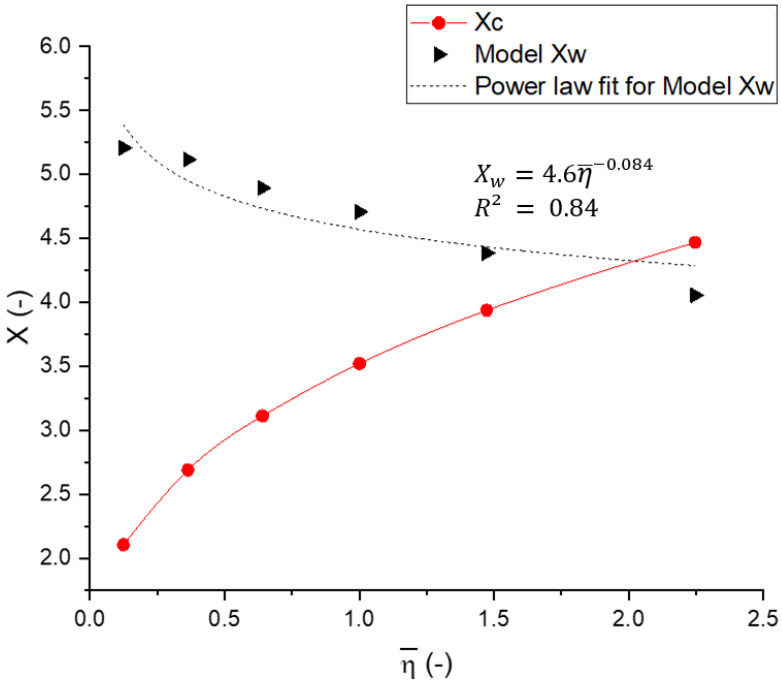

Figure 4.6: Inlet position of water droplets X_w and critical position of starved condition X_c on the central line under different oil dynamic viscosity

Figure 4.6 shows that when the dynamic viscosity of the based oil increases, the value of X_w decreases. According to Eq. 4.6, the increase of the lubricant viscosity generates lower Poiseuille effects, which allow the water droplets to get closer to the contact. Meanwhile, the critical position increases with lubricant viscosity as well. As a result, water in oil emulsion with a higher dynamic viscosity of the based oil is more likely to enter the critical area, leading to a water-in-oil mixture supply to the contact area and potentially reducing film-forming ability.

As previously, Figure 4.6 includes a power law fit: $X_w = 4.6\bar{\eta}^{-0.084}$.

4.3.4 Load influence

Finally, the load influence is investigated. Different loads considered in the present study, with the corresponding maximum Hertzian pressure p_h are summarized in Table 4.4.

Table 4.4: Applied load used for the numerical modeling

w	$20, 30, 40, 50, 60, 70$ N
p_h	$4.49, 5.13, 5.65, 6.09, 6.47, 6.81 \times 10^8$ Pa

The mean rolling velocity remains constant at 1 m/s, whereas the lubricant viscosity is set to 0.781 Pa · s.

Same modeling methodologies as previously stated for studying the influence of the lubricant viscosity are used again. A dimensionless load parameter $W = \frac{w}{w_{ref}}$ with $w_{ref} = 40$ N is used here to represent the varied loads.

The inlet distance of water droplets X_w obtained by the numerical model and the associated critical position X_c is presented in Figure 4.7.

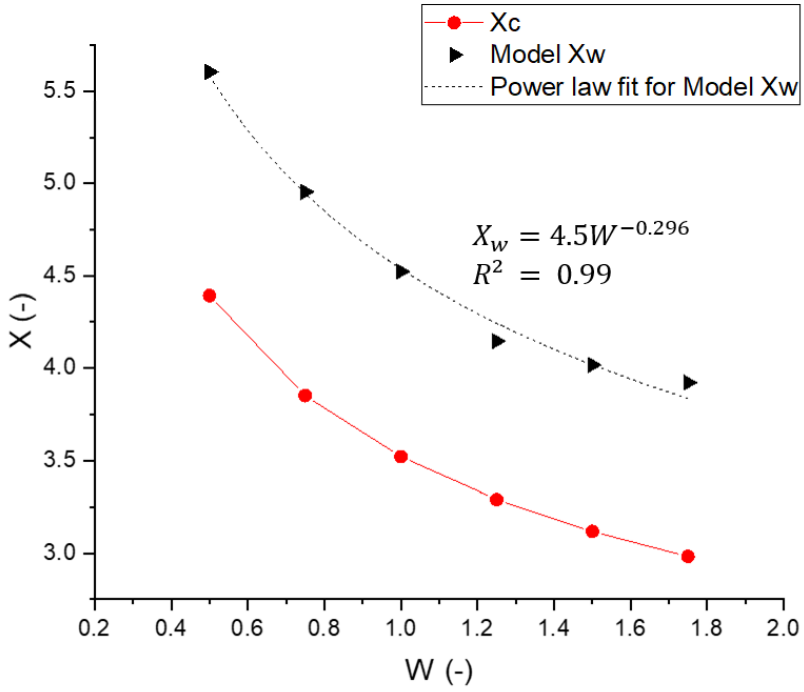

Figure 4.7: Inlet position of water droplets X_w and critical position of starved condition X_c on the central line under different load

It is shown that X_w reduces with increasing load. This can be explained as illustrated in Figure 4.8: when the load rises at a constant velocity, the pressure gradient decreases for a given dimensionless position $\frac{x_i}{a}$, resulting in reduced Poiseuille effects (see Eq. 4.6).

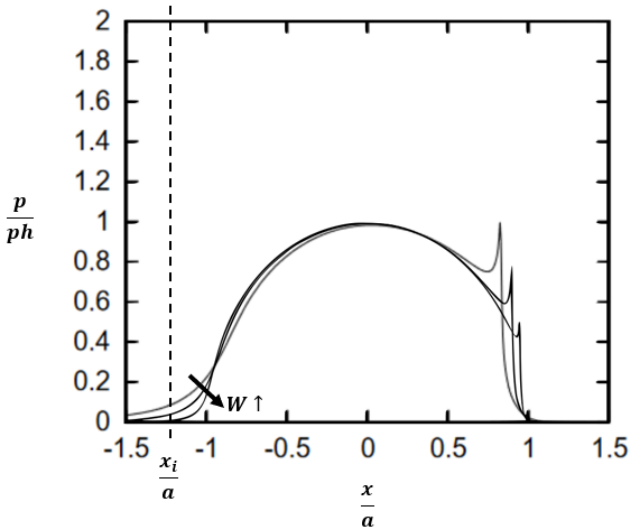

Figure 4.8: Dimensionless pressure distributions for increasing W

It is worth noting that, however, when water droplets get closer to the contact region because of heavier load, X_c decreases as well (see Figure 4.7). As a result, for a water-in-oil emulsion, the full-film forming ability may not be significantly influenced by the applied load.

Again, a power law fit describes best the variations of X_w with W is given: $X_w = 4.5W^{-0.296}$.

4.3.5 Construction of a semi-analytical model

The relations for the inlet position of water droplets X_w in terms of U_m, $\bar{\eta}$ and W are shown in Figure 4.3, 4.6 and 4.7, respectively. Three power law fits were previously derived to show the influence of these parameters. To facility the study of X_w, Figure 4.9 presents the values of X_w obtained with the numerical model as a function of U_m, $\bar{\eta}$ and W. Unsurprisingly, a linear fit is achieved that very well describes the relation of X_w with these combining parameters.

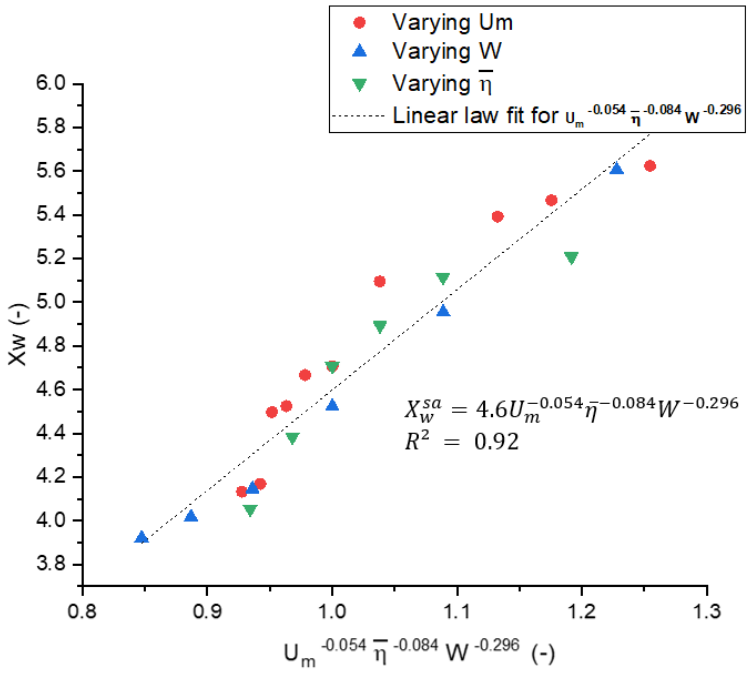

Figure 4.9: Inlet position of water droplets X_w as a function of $U_m^{-0.054}\bar{\eta}^{-0.084}W^{-0.296}$

Accordingly, a semi-analytical expression of X_w can be given:

$$X_w^{sa} = 4.6U_m^{-0.054}\bar{\eta}^{-0.084}W^{-0.296} \tag{4.7}$$

It is worth mentioning that this expression only considers the effects of rolling velocity, applied load, and lubricant viscosity. However, X_w may be affected by other factors such as water concentration, surface tension, the radius of the ball, etc.

4.4 Discussion of contradictory findings in the literature

The found influence of operating conditions on the motion of water droplets can provide a possible explanation for the contradictory findings in the literature when water droplets are larger than the film thickness. These experimental studies ($\frac{h_{c,mix}}{D_d} < 1$) are highlighted in gray in Table 4.5.

Table 4.5: Experimental data on effects of water droplets in oil on film thickness

$\frac{h_{c,mix}}{D_d}$	Reference	Rolling velocity (m/s)	Water droplet diameter (µm)	Lubricant viscosity Pa · s	Maximum Hertzian pressure (GPa)	Water droplet effect
≥ 1	Dalmaz, 1981 [109]	0.1-3	0.5	0.143	0.12-0.19	$\frac{h_{c,mix}}{h_{c,oil}} > 1$
	Wan et al, 1984 [92]	0.1-2	0.5	0.069-0.092	0.56	
< 1	Wan et al, 1984 [92]	0.1-0.7	4-5	0.092	0.56	$\frac{h_{c,mix}}{h_{c,oil}} = 1$
	Hamaguchi et al., 1977 [105]	0.54	1.5	0.065	0.7	
	Benner et al., 2006 [107]	1-4	3.14	0.036	0.7	
	Liu et al., 1994 [106]	3.14	< 1	0.049	0.9	$\frac{h_{c,mix}}{h_{c,oil}} < 1$

As can be seen from Table 4.5, the experiments of Liu et al. [106] were performed at high velocity, under heavy applied load yielding the highest maximum Hertzian pressure, and with the smallest water droplet size, which, according to the findings of the current study, is favorable to water droplets approaching the contact area. It is possible in their experiments that the inlet region, from which the central film thickness was built up, was no longer filled with pure oil but a mixture of water and oil. The contact area was thus under water-in-oil mixture supply (see Figure 4.4 Zone II) which may result in a reduction in central film thickness. Worse, severe starvation of the contact area (see Figure 4.1) could have occurred in their experiments. It should be notice that, additional film thickness measurements are necessary for rigorous validation of this film thickness decrease assumption. Unfortunately, the dedicated surface treatment of the transparent disc for film thickness measurement is not suitable for colored water droplet detection.

4.5 Conclusion

This work investigated the risks of a water-in-oil mixture at the entrance of an EHD contact using both experimental and numerical methods. Micro-sized water droplets-in-oil have been directly observed at the inlet of an EHL

contact with a high-speed camera and a microscope for the first time. The distances between the closest water droplets and the contact center have been compared with the critical meniscus position at which starvation occurs in pure oil conditions. When water droplets penetrate the critical area, the contact area is no longer under a full oil supply but rather a water-in-oil mixture supply. As a result, the film-forming ability may be affected.

Independently from the experimental results, a numerical approach was developed. Three-dimensional geometry was generated from the calculated film thickness distribution. Water droplet trajectories in oil have been traced by solving the Navier-Stokes equation (for pure oil flow) and Newton's second law (for water droplet trajectories) successively. The numerical modeling is able to reproduce water droplets distributions that are qualitatively and quantitatively similar to those observed in the experiments. A parametric study was realized with the numerical model to study the impacts of various operating parameters on the flow of water-in-oil emulsion. Water droplets are more likely to approach the contact when the rolling velocity, applied load, and lubricant viscosity is large and the size of water droplets is small. A semi-analytical expression for the inlet distance of water droplets is proposed by introducing a dimensionless parameter combining the effects of rolling velocity, applied load, and lubricant viscosity. By further comparing with the associated critical positions, the influence of water droplets on the contact area can be determined. With these results, the current work explains the contradictory findings in the literature. This significant work exposes the underlying lubrication mechanisms of water-in-oil emulsions and reveals the critical conditions in which water-in-oil emulsion affects EHL contacts.

General Conclusion

The industrial challenge of lubrication involving oil and operating fluid mixtures is investigated in this work. In the framework of Rolling Element Bearings (REBs) applications, this study exposes the underlying lubrication mechanisms of mixtures in and around the EHL contacts. Two common industrial mixtures are investigated separately: the oil/refrigerant mixture and the oil/water mixture, which represent two types of mixed states: a miscible fluid, and an immiscible fluids.

The state of the art is presented in Chapter 1, which depicts studies on EHL with neat lubricant or mixtures of lubricant and operating fluids. Numerous efforts have been made in the literature, offering a fundamental knowledge of EHD lubrication mechanisms with a single fluid. However, many unknowns remain concerning the interaction of lubricant with its surroundings, around the contact region. It is currently a challenge for the industry to predict the appropriate performance of bearings under non-optimal lubrication conditions such as lubrication with mixtures. Furthermore, the context for mixtures with different mixed states (miscible or immiscible fluids) differs greatly, necessitating separate investigations.

Based on the prior literature review, Chapter 2 presents two research methodologies developed for miscible fluids and immiscible fluids in EHL studies, respectively. Oil/refrigerant solution and water droplets in oil emulsion, as typical examples, are thoroughly investigated. For the oil/refrigerant solution, on the one hand, an original Thermal-EHL numerical approach with solubility-based cavitation modeling for point contacts has been developed. The mixture of oil/refrigerant solution and refrigerant gas is assumed as a two-phase homogeneous compressible flow in the cavitation area. Introducing physical properties of the lubricant mixture, the behavior of the miscible fluids can be described using the Generalized Reynolds equation coupled with the elasticity equation and the energy conservation equation, for both the pressurized region and the cavitation region. On the other hand, for water droplets in oil emulsion, both experimental and numerical techniques were proposed. A high-speed camera and a microscope were used in a ball-on-disc test rig to conduct original direct observations of micro-sized water droplets-in-oil at the inlet of an EHL contact. Meanwhile, a numerical approach for tracing water droplet trajectories was developed by solving the water droplet motion at the inlet zone.

In Chapter 3, a Thermal ElastoHyrodynamic Lubrication (Thermal-EHL) analysis was performed for the oil/refrigerant mixture. The newly developed

numerical model allows for the variation of the density and the viscosity in both the pressurized region and cavitation region as a function of local pressure, temperature, and mass fraction of the refrigerant. It can predict both the oil-film rupture and reformation, which allows to obtain the location and the size of the cavitation area. The sub-cavitation pressure is naturally obtained based on physical mechanisms without a geometric assumption about the shape of the cavitation area or pressure constraints. Additionally, when compared to other cavitation models in the literature, the present model proved to be more advantageous for describing the cavitation region on a physical basis. Several conclusions are reached regarding the behavior of oil/refrigerant solution in EHL contacts:

- Thermal effects have very little influence on the lubricant film thickness calculation for oil/refrigerant lubrication in the EHL contact under pure rolling conditions, but generate disparities in the cavitation zone. The isothermal analysis represents a more critical condition than the thermal analysis because it predicts a larger volume fraction of refrigerant gases in the cavitation area.

- When analyzing the oil/refrigerant solution in lubricated contacts, the solubility of the refrigerant must be taken into account since the refrigerant concentration varies with local pressure and temperature, changing the lubricating capacity of the mixture lubricant.

- Compared to pure oil, oil/refrigerant solutions can potentially reduce the amount of liquid oil for the next contact due to its larger cavitation size.

Chapter 4 investigates the risks of water contamination in oil at the inlet of an EHD contact. An original dual experimental and numerical analysis is performed. First, direct observations allowed tracking of the colored water droplet distributions approaching the contact area. Numerical modeling can replicate qualitatively and quantitatively the water droplet distributions observed in experiments. This enables a further parametric study on the impacts of various operating parameters on the water-in-oil emulsion flow. The potential risks of water droplet contamination were evaluated by comparing the distance between the closest water droplets and the contact center with the critical meniscus position at which starvation occurs in pure oil conditions. When water droplets penetrate this critical area, the contact area is no longer under a full oil supply but rather a water-in-oil mixture supply. As a result, the film-forming ability may be affected. Finally, a semi-analytical expression for the inlet distance of water droplets is proposed. It is found in the present study that water droplets are more likely to approach the contact area with an increase in the rolling velocity, applied load, and lubricant viscosity.

Oil/refrigerant solution and water droplet in oil emulsion, as two typical industrial mixtures, are thoroughly explored in this thesis. The distinct research methodologies and analysis methods developed in this work for these two mixtures can be applied to other miscible and immiscible fluids, providing a general solution of lubrication with a mixture of oil and operating fluids.

Furthermore, while the solubility-based cavitation model proposed in this work was originally developed to explore the oil/refrigerant solution, it can also be used for other solutions consisting of lubricant and volatile liquid or non-condensable gas (such as air, carbon dioxide, argon, and helium dissolved in oil). Additionally, the two-phase flow approach was initially proposed in this work to investigate the cavitation area, but it also provides a general numerical procedure for modeling the liquid-gas phase change that accounts for the interaction of the liquid and gas phases (phase transition, heat transfer, and variations in liquid-gas mixture properties).

Besides, the experimental and numerical methodologies proposed for water droplets in oil emulsion offer a new direction of exploration for immiscible mixtures in EHL contact. They can be adapted and extended to various mixtures involving a dispersed phase (liquid droplets, solid particles, and gaseous bubbles) in a continuous phase.

Perspectives

This thesis presents a thorough work addressing the current industrial challenge of lubrication with a mixture of oil and operating fluids in the framework of an EHD contact. Despite all of the results provided in this study for both miscible and immiscible lubricant mixtures, there are still many topics to be investigated and new difficulties to be solved.

Oil/refrigerant solution is regarded as a typical example of miscible fluids. The present work can be extended as follows:

- First, from an experimental point of view, the length and location of refrigerant cavitation can be measured to give further validation to the proposed numerical model. The measurement of the cavity length and flow patterns have been reported for pure oil cavitation at the atmospheric pressure [45–47]. However, no such measurement exists for oil/refrigerant solution since a pressurized environment is required. As a result, developing an optical interferometry ball on disc apparatus capable of measuring the refrigerant cavity under pressure may be a suggestion for future work.

- Besides, additional investigations should be conducted to determine the real rate of absorption of refrigerant in oil. On this basis, a model for refrigerant absorption by oil may be added to the current numerical model. Indeed, the potential risks on the next contact caused by refrigerant cavitation may be evaluated in a time-dependent scenario by taking into account the rate of refrigerant absorption and the duration the oil/refrigerant solution travels between two successive contacts.

- Furthermore, the 'flashing' phenomenon observed in the industry, in which a part of the oil becomes attached to the refrigerant gaseous phase and is rejected, was not represented in the current work. The rejected sample may be examined further to see if the chemical structure changes. If this is the case, this phenomenon may be investigated using for example molecular modeling.

- In addition, the current model focused mainly on the interaction between the oil and the dissolved refrigerant in the cavitation region. However, a three dimensional description of the cavitation zone (across the gap) may also be of interest. It can be realized by tracing the interface of these two phases using for example the phase field method. The estimation of the position of the outlet meniscus can be studied together with the size and

location of the cavitation area obtained in the present work to determine the flow pattern of oil/refrigerant solution at the contact outlet.

Research may also be extended concerning the investigation of water droplets in oil emulsion at the contact inlet.

- Other factors on water droplet trajectories in oil such as water concentration, surface geometry, and surface tension (different types of oils and contacting surfaces) can be further investigated experimentally and numerically.

- The present model can be further completed to allow the change of the size of the water droplets (water droplets break up) under pressure and shear. By assuming that a droplet will break up when the droplet Weber number We is larger than a critical value, the maximum stable droplet size can be estimated using surface tension and density of the continuous phase. The consideration of droplet break-up allows for investigations of large water droplets with a more accurate and physical prediction.

- Additionally, the present model considered only the influence of oil flow on water droplets. However, particle-particle interactions, particle-surface interactions, and particle-fluid interactions may also be taken into account for a more rigorous investigation. The phenomenon of water droplet accumulation leading to water-in-oil mixture supply at the contact inlet region may then be numerically reproduced. On this basis, the moving mesh approach [183] might be used to predict the film thickness under such circumstances. The major drawback of this method is that high computational cost and long computation time would be expected.

Appendices

A Governing equations for oil/refrigerant lubricated EHD line contacts

As discussed in Chapter 2 (Section 2.2.3), the geometry of EHL point contact can be reduced to a contact between a plane and a sphere of radius R (see Figure 2.2 (b)). If the curvature radii of the contacting bodies differ greatly in the x and y directions (for example, if $R_x << R_y$), it can be approximated by an infinitely long line contact problem (considering $R_y = \infty$). The geometry can be reduced to a contact between a rigid plane and an elastic cylinder.

The Reynolds equation adapted for a two-phase flow for the steady-state line contact case is derived from the generalized point contact equation (Eq. (2.12) in Chapter 2), by neglecting corresponding field variable variations in the y direction:

$$-\frac{\partial}{\partial x}\left[\left(\frac{\rho_m}{\mu_m}\right)_e \frac{\partial p(x)}{\partial x}\right] + \frac{\partial \rho^*_{x,m}}{\partial x} = 0 \tag{A.1}$$

where the integral terms are written as follows:

$$\begin{aligned}
\left(\frac{\rho_m}{\mu_m}\right)_e &= \frac{\mu_{e,m}}{\mu^{'}_{e,m}}\rho^{'}_{e,m} - \rho^{''}_{e,m} \\
\rho^*_{x,m} &= \rho^{'}_{e,m}\mu_{e,m}(u_{2x} - u_{1x}) \\
\rho_{e,m} &= \int_0^{h(x)} \rho_m(p,T,w)\, dz \\
\rho^{'}_{e,m} &= \int_0^{h(x)} \rho_m(p,T,w) \left(\int_0^z \frac{1}{\mu_m(p,T,w)}\, dz^{'}\right) dz \\
\rho^{'}_{e,m} &= \int_0^{h(x)} \rho_m(p,T,w) \left(\int_0^z \frac{z^{'}}{\mu_m(p,T,w)}\, dz^{'}\right) dz \\
\frac{1}{\mu_{e,m}} &= \int_0^{h(x)} \frac{1}{\mu_m(p,T,w)}\, dz \\
\frac{1}{\mu^{'}_{e,m}} &= \int_0^{h(x)} \frac{z}{\mu_m(p,T,w)}\, dz
\end{aligned} \tag{A.2}$$

However, isothermal and Newtonian fluid conditions are assumed for the line contact case study (Section 3.5 in Chapter 3), and density and viscosity

variations across the film thickness (in the z direction) are neglected. Thus Eq. (A.1) can be simplified to:

$$-\frac{\partial}{\partial x}\left(\frac{\rho_m h^3}{\mu_m}\frac{\partial p(x)}{\partial x}\right) + 12u_m\frac{\partial \rho_m h}{\partial x} = 0 \tag{A.3}$$

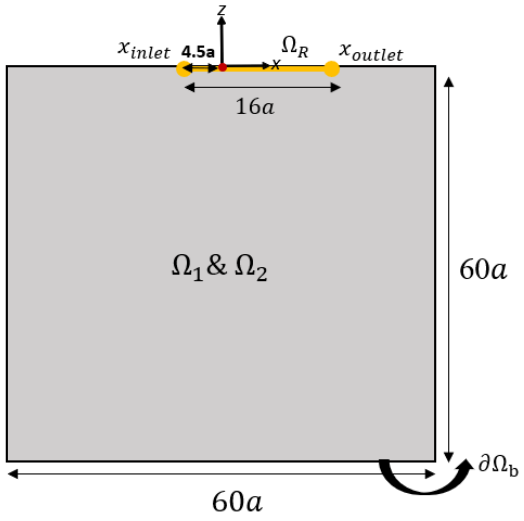

Figure A.1: Geometries used for EHL line contact problem

Equation (A.3) completed with the novel cavitation model is solved on the one-dimensional contact area Ω_R defined for $x \in [-4.5a, 11.5a]$ (see Figure A.1) with the following boundary condition:

$$\begin{aligned} &\boldsymbol{U} = 0 \quad \text{at the bottom boundary } \partial\Omega_b \\ &\sigma_n = -p \quad \text{at the contact area } \Omega_R \\ &\sigma_n = 0 \quad \text{elsewhere} \end{aligned} \tag{A.4}$$

Accordingly, the film thickness equation for the line contact becomes:

$$h(x) = h_0 + \frac{x^2}{2R} - \delta(x) \tag{A.5}$$

The general numerical framework remains the same as for the point contact problem described in Chapter 2.

B Adaptation of the Bayada cavitation model

According to Bayada [40], the volume fraction of gas can be expressed as:

$$\alpha_g = \frac{\rho - \rho_l}{\rho_g - \rho_l}. \tag{B.1}$$

Assuming that the entropy produced during the phase transition is zero, the relationship between density and pressure is given by [184]:

$$\frac{dp}{d\rho} = c_f^2, \tag{B.2}$$

with c_f the speed of sound in the medium expressed as [185]:

$$\frac{1}{c_f^2} = \rho \left(\frac{\alpha_g}{c_g^2 \rho_g} + \frac{1 - \alpha_g}{c_l^2 \rho_l} \right). \tag{B.3}$$

Finally, after integration, three relations are obtained in function of the volume fraction of gas α_g in the work of Bayada [40]:

$$p(\alpha_g) = c_g^2 \rho \qquad \text{if } \alpha_g \geq 1, \tag{B.4a}$$

$$p(\alpha_g) = p_{ml} + (\rho - \rho_l)\, c_l^2 \qquad \text{if } \alpha_g \leq 0, \tag{B.4b}$$

$$p(\alpha_g) = p_{ml} + N \log \left(\frac{\rho_g c_g^2 \rho}{\rho_l \left[\rho_g c_g^2 (1 - \alpha_g) + \rho_l c_l^2 \alpha_g \right]} \right) \qquad \text{if } 0 \leq \alpha_g \leq 1. \tag{B.4c}$$

where p_{ml} is the bubble point (see Section 3.3.2 in Chapter 3).

Equation (B.4) is rewritten using Eq. (B.1) to represent ρ as a function of p to facilitate implementation and comparison with the present solubility-based cavitation model [120]:

$$\rho\,(p) = \frac{p}{c_g^2} \qquad \text{if } \rho \leq \rho_g \tag{B.5a}$$

$$\rho\,(p) = \frac{p - p_{ml}}{c_l^2} + \rho_l \qquad \text{if } \rho \geq \rho_l \tag{B.5b}$$

$$\rho\,(p) = \frac{\left(\rho_l \rho_g^2 c_g^2 - \rho_l^3 c_l^2 \right) \exp\left(\frac{p - P_{ml}}{N} \right)}{\rho_g c_g^2 (\rho_g - \rho_l) - \left(\rho_l^2 c_g^2 - \rho_l \rho_g c_g^2 \right) \exp\left(\frac{p - P_{ml}}{N} \right)} \qquad \text{if } \rho_g \leq \rho \leq \rho_l. \tag{B.5c}$$

C Choice of the water droplet tracing techniques

During the preparation of water-in-oil emulsion, water droplets and air bubbles were both detected in the mixture (see microscopic visualization in Figure C.1), disrupting the trace of water droplets.

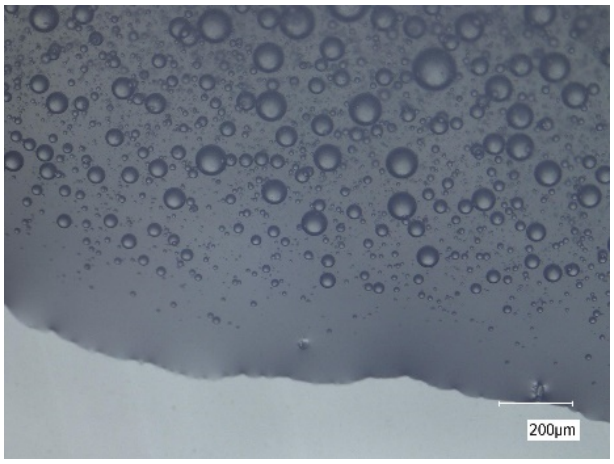

Figure C.1: Microscopic visualization of emulsion after stirring under digital microscope KEYENCE

Fluorescence technique

To visualize and identify the water droplets in oil as presented in Chapter 2, an appropriate particle tracing technique is required. Different water tracing dyes and techniques have been tested. First, a fluorescent water dye (Rhodamine 6G-red) was tested. It is known to react to a laser excitation of wavelength at 555 nm, an induced emission is recorded around 630 nm [186]. The experiments have been performed by Ana-Maria SFARGHIU under the Confocal microscope. However, air bubbles were observed to be colored as well and to collapse during the observation as presented in Figure C.2. It can be explained by the highly inflected oil-air interface, which may react to laser excitation as well. As a result, the fluorescent approach is unable to differentiate between water drops and air bubbles.

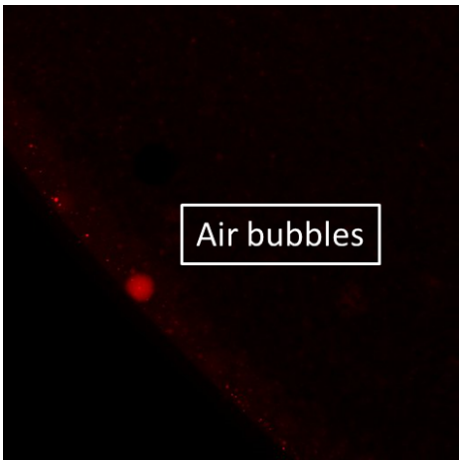

Figure C.2: Visualization of emulsion with Rhodamine 6G under Confocal microscope

Classical optical technique

An optical microscope technique was then used, and several hydrophilic dyes were tested to color the water droplets. Finally, a food coloring dye composed of dextrose, and a mixture dye of culvert 4R (E124) and brilliant blue FCF (E133) is chosen as it shows the best contrast and can distinguish water droplets from air bubbles (see Figure 2.5). Figure C.3 (a) is a microscope picture of the chosen food coloring powder. Furthermore, preliminary evidence suggests that this water dye does not dissolve in the oil and is not attached to the oil-air interface (see Figure C.3 (b)).

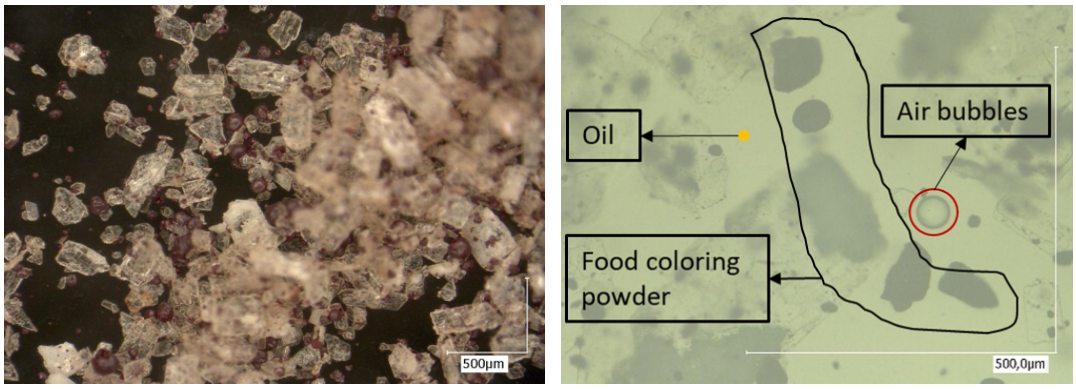

(a) (b)

Figure C.3: Water dye powder (a) and its mixture with oil and air bubbles (b) observed with an optical microscope

D Interface representation techniques for immiscible fluids

The two main interface representation techniques are interface-tracking methods and interface-capturing methods [187, 188].

In interface-tracking methods, the interface is represented explicitly and the Lagrangian approach is used. These methods can successfully locate the position of the interface by tracking the interface markers. However, they are limited when treating topology changes and large interface deformations [189]. Adaptations were then developed using ALE (Arbitrary Lagrangian Eulerian) methods, to model free surface flows by including surface tension effects. In this method, the interface is represented by resolved mesh, and this mesh moves and deforms with the flow. It has been proved that such an ALE technique can obtain the position of the interface with high precision when no topological changes happen. Thus, it is widely applied to solve Fluid-Structure Interaction (FSI) problems, where the flow boundary changes slightly. The ALE method for one phase-flow with a free interface or two-phase flow has also been broadly used by many authors [190–192].

In interface-capturing methods, the location of the interface is captured implicitly by a scalar function on a fixed Eulerian mesh. The main advantage of these methods compared to the interface-tracking methods is that the topology changes are treated naturally. The most common interface-tracking methods that has been applied include Volume-Of-Fluid (VOF) method [193], level-set method [194] and phase field method [195]. VOF method can conserve the mass exactly, but the reconstruction of the interface is difficult. Furthermore, the computations of the location of curvature are less accurate because the interface is smeared by the numerical diffusion. The level-set method can represent the curvature of the interface and the surface tension with high accuracy with the level-set function. However, the main drawback of this method is the lack of mass conservation [196]. In the phase field method, a conserved order parameter or phase field parameter ϕ is introduced to represent the interface. This method can capture complex interfacial shapes. It has been mainly used for two-phase flows from different species where the predominant physical phenomena are governed by the interface and capillary effects. However, the results are significantly affected by the mesh and the interface thickness. Furthermore, the scale of the studied interface is required to be comparable to the computational domain.

As is described in Chapter 2, these methods are not suitable for the water droplets in oil emulsion flow in the present study, where the size of the individual droplets is much smaller than the computational domain containing a large zone upstream of the contact. They can, however, be used to explore free water in

oil flow in EHL contacts where the shape of water droplets must be specified in detail and the impact of surface wettability and water-oil interfacial tension can no longer be neglected. To develop a general approach to accurately describe the behavior of the free water in and around a lubricated contact under the action of capillary effects, the phase field method is used in the following.

The phase field method uses the Cahn-Hilliard equation [197, 198] coupled with the Navier-Stocks equation to solve the two-phase flow problem. The two-phase flow dynamics are governed by the Cahn-Hilliard equation, which tracks a diffuse interface with limited thickness separating the oil/water phase [199]:

$$\frac{\partial \phi}{\partial t} + \boldsymbol{u} \cdot \nabla \phi = \nabla \cdot \frac{\gamma \lambda}{\epsilon^2} \nabla \psi \tag{D.1}$$

$$\psi = -\nabla \cdot \epsilon^2 \nabla \phi + (\phi^2 - 1)\phi \tag{D.2}$$

where ϕ is the dimensionless phase field variable varying from -1 to 1. It represents pure oil when it equals -1, pure water when it is 1, and the interface of the water droplets in oil when it equals 0. The volume fraction of water and oil can be expressed with the phase field variable ϕ:

$$V_{f,w} = \frac{1 - \phi}{2} \tag{D.3}$$

$$V_{f,o} = \frac{1 + \phi}{2} \tag{D.4}$$

This approach involves two numerical parameters which are the interface thickness ϵ and the mobility parameter γ proportional to the relaxation time of the interface. The interface thickness ϵ should, by definition, be small enough in comparison to the characteristic scales of the problem to assure the convergence of the method [199]. The mobility parameter γ can be related to ϵ through [200, 201]:

$$\gamma = \chi \epsilon^2 \tag{D.5}$$

Where χ is the mobility tuning parameter and is set to 1 by default.

The mixing energy density λ and ϵ are related to the surface tension coefficient, σ, through the following equation:

$$\sigma = \frac{2\sqrt{2}}{3} \frac{\lambda}{\epsilon} \tag{D.6}$$

The Navier-Stokes equations are used here to describe the transport of mass and momentum for fluids:

$$\rho_{mix}\frac{\partial \boldsymbol{u}}{\partial t} + \rho_{mix}(\boldsymbol{u}\cdot\nabla)\boldsymbol{u} = \nabla\cdot[-p\boldsymbol{I} + \mu_{mix}(\nabla\boldsymbol{u} + (\nabla\boldsymbol{u})^T)] + \rho_{mix}\boldsymbol{g} + \boldsymbol{F_{st}} \tag{D.7}$$

$$\nabla\cdot(\rho_{mix}\boldsymbol{u}) = 0 \tag{D.8}$$

with

$$\rho_{mix} = \rho_w + (\rho_o - \rho_w)V_{f,o} \tag{D.9}$$

$$\mu_{mix} = \mu_w + (\mu_o - \mu_w)V_{f,o} \tag{D.10}$$

The surface tension force acting at the oil/water interface is introduced as a source term $\boldsymbol{F_{st}} = \boldsymbol{G}\cdot\nabla\phi$ in the Navier-Stokes equations. Where $\boldsymbol{G}$ is the chemical potential close to the oil/water interface defined as:

$$\boldsymbol{G} = \lambda\left(-\nabla^2\phi + \frac{\phi(\phi^2-1))}{\epsilon^2}\right) \tag{D.11}$$

As previously stated, this method is capable of capturing the location of the interfaces when the scale is comparable to that of the computational domain. A preliminary study using this method was performed to calculate the detailed shape of several large water droplets in the oil while flowing towards the EHL contact. The operating and numerical conditions are described in Table D.1:

Table D.1: Operating and numerical conditions for interface-capturing of water in oil flow using the phase-field method

Reduced radius R_x	1.27×10^{-2} m
Load w	40 N
Entrainment speed u_1, u_2	0.1 m/s
Density of the oil ρ_o	850 kg/m^3
Density of the water ρ_w	1000 kg/m^3
Viscosity of the oil μ_o	1.754 Pa $\cdot$ s
Viscosity of the water μ_w	10^{-3} Pa $\cdot$ s
Surface tension σ	10^{-1} N $\cdot$ m^{-1}

The computational domain constructed for phase-field method calculations is demonstrated in Figure D.1.

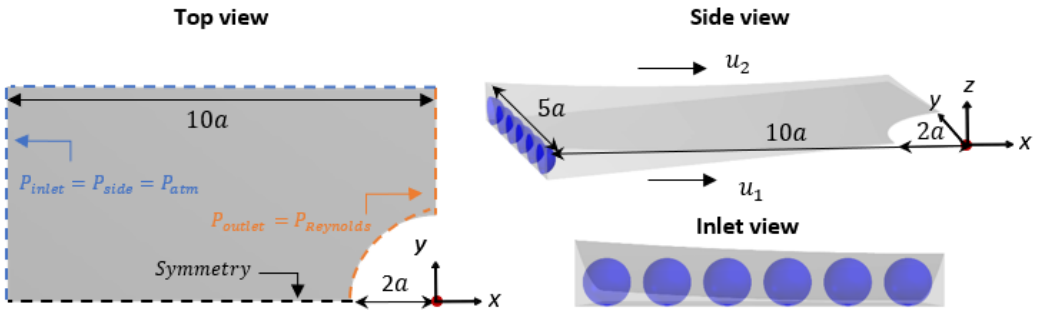

Figure D.1: Geometries used for water droplet in oil interface capturing by using the phase-field method and boundary conditions

The geometry of the lubricant layer is generated from the calculated film thickness distribution by using the finite element full system approach developed by Habchi et al. [15]. The inlet boundary and the outlet boundary are placed at $10a$ and $2a$ upstream from the contact center, respectively (the circular Hertzian contact area is not studied in detail). Pressure boundary conditions are imposed at the inlet and outlet boundary as shown in Figure D.1. Symmetry condition on the x-z plane at y=0 is applied to reduce computational efforts.

Several semi-spheres, each 120 µm in diameter and separated from the others in the center by 120 µm are arranged at the inlet. At the inlet boundary, it is assumed that the water phase enters continuously through the blue circles as shown in Figure D.1 and the oil phase enters through the remaining surfaces.

Figure D.2 shows a preliminary numerical result representing the interface of water phases in oil ($\phi = 0$). As can be seen, the deformation, break up, and coalescence of water droplets as they flow towards the contact region may be estimated numerically with the phase-field method.

Figure D.2: Numerical result of water droplets in oil interface by using the phase-field method

However, additional experimental work is required to validate the numerical results. Also, it should be notice that this approach requires high computational cost and long computation time. Furthermore, a predefined geometry of the water-oil interface at the contact inlet is required for this method, which would be problematic.

E Surface tension and wettability

Wetting is the ability of a liquid to maintain contact with a solid surface, which can be measured by the contact angle between the liquid and the surface [202]. A low contact angle stands for high wettability, whereas a high contact angle infers low wettability. Figure E.1 illustrates the vapor–liquid-solid interfaces where θ_w, γ_{lv}, γ_{sv}, γ_{ls}, are the contact angle, interfacial free energies of liquid/vapor, solid/vapor, solid/liquid respectively.

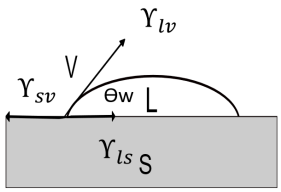

Figure E.1: Schematic of the solid–liquid interface showing the interfacial free energies of liquid/vapor (γ_{lv}), solid/vapor (γ_{sv}), solid/liquid (γ_{ls})

The contact angle can be related to interfacial energies through Young's equation [203]:

$$\gamma_{lv} \cos \theta_w = \gamma_{sv} - \gamma_{ls} \tag{E.1}$$

The contact angle and surface energy measurements were carried out using the Video Goniometer Tensiometer Dataphysics OCA20. Figure E.2 shows the measured contact angles of water, water with water dye, and oil on a 100Cr6 steel surface.

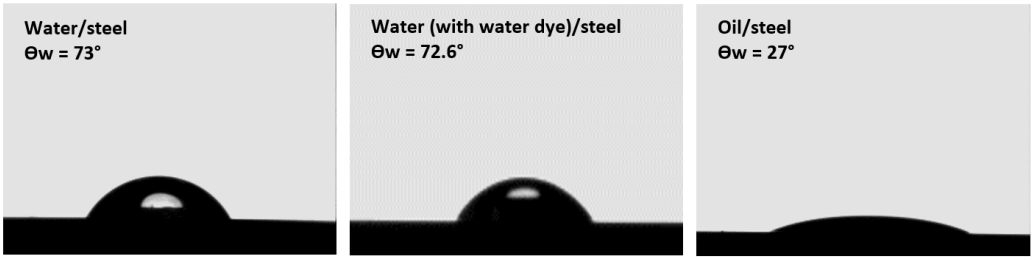

Figure E.2: Water, water with water dye and oil contact angles obtained on a 100Cr6 steel surface

It can be derived from the results that the water dye used in the present study does not influence the surface tension of water and the wettability of water on the testing surface is much smaller than that of oil.

F Direct observations of 60 µm water droplets at the contact inlet

Results of direct observations on water droplets (with initial size of 60 µm) in oil at the contact inlet under rolling speed u_m (see Table 4.1) can be found in Figure F.1.

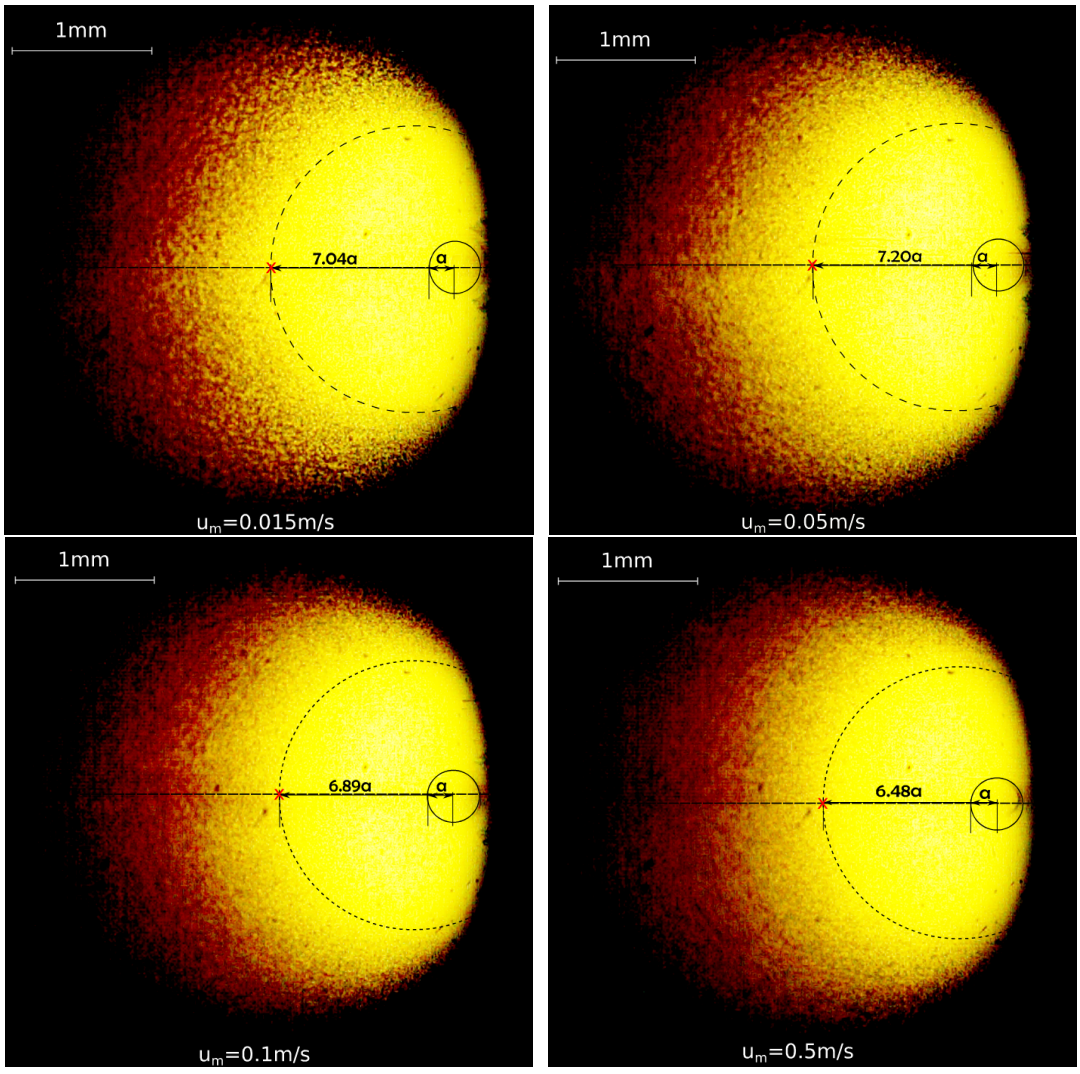

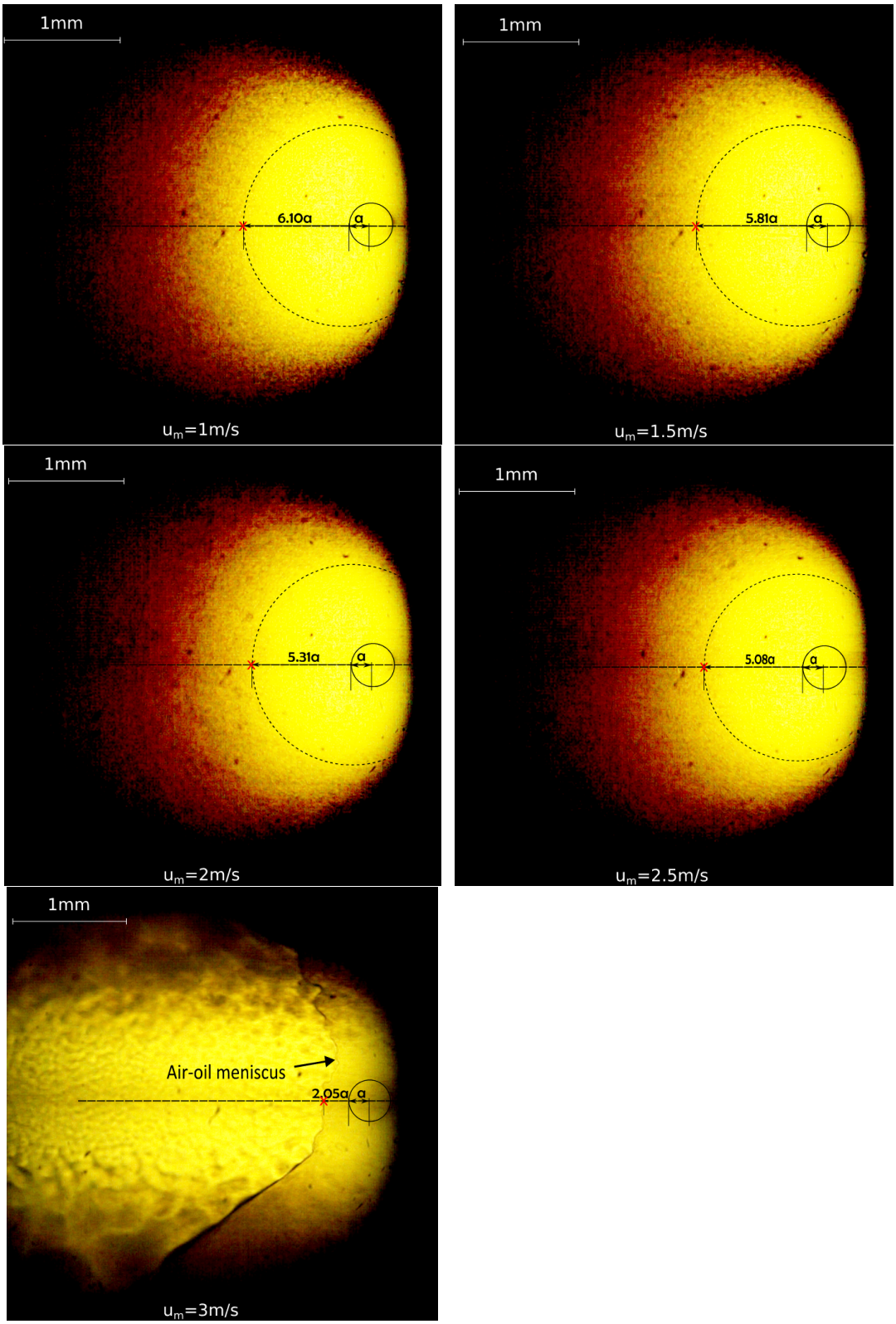

Figure F.1: Distributions of water droplets in oil at the inlet of an EHL contact and estimation of inlet distance with characteristic droplet diameter of 60 µm

Bibliography

[1] S. Seireg. *Friction and lubrication in mechanical design*. New York: Marcel Dekker, 1998, pp. 310–336.

[2] B. Tower. "First Report on Friction Experiments (Friction of Lubricated Bearings)". *Proc. Instn. Mech.Engrs*, 1883, pp. 632–659.

[3] N. P. Petrov. "Friction in Machines and the Effect of the Lubricant". *Inzh. Zh., St-Peterb.* 1, 1883, pp. 71–140.

[4] O. Reynolds. "IV. On the theory of lubrication and its application to Mr. Beauchamp tower's experiments, including an experimental determination of the viscosity of olive oil". *Philosophical transactions of the Royal Society of London* 177, 1886, pp. 157–234.

[5] R. Stribeck and M Schröter. *Die wesentlichen Eigenschaften der Gleit- und Rollenlager: Untersuchung einer Tandem-Verbundmaschine von 1000 PS*. Springer, 1903.

[6] A. Ertel. "Hydrodynamic lubrication based on new principles". *Akad. SSR Prikadnaya Mathematica i Mekhanika* 2, 1939, pp. 41–52.

[7] A. Grubin. "Fundamentals of the hydrodynamic theory of lubrication of heavily loaded cylindrical surfaces". *Investigation of the Contact Machine Componets* 2, 1949.

[8] H. Hertz. "Ueber die Berührung fester elastischer Körper." *J. für die reine und Angew. Math. (Crelle's Journal)* 92, 1882, pp. 156–171.

[9] C. Barus. "Isothermal, Isopiestics and Isometrics Relative to Viscosity". *Am. J. Sci.* 45, 1893, pp. 87–96.

[10] D. Dowson and G. Higginson. *Elastohydrodynamic Lubrication, The Fundamentals of Roller and Gear Lubrication*. New York: Pergamon Press, Oxford, 1966.

[11] B. J. Hamrock and D. Brewe. "Isothermal Elastohydrodynamic Lubrication of Point Contacts, part I, Theoretical Formulation". *ASME J. Lub. Tech.* 105, 1976, pp. 171–177.

[12] A. Lubrecht, W. Ten Napel, and R Bosma. "Multigrid, and alternative method for calculating film thickness and pressure profiles in elastohydrodynamically lubricated line contacts". *Journal of tribology* 108.4, 1986, pp. 551–556.

[13] C. Venner. "Multilevel solution of the EHL line and point contact problems(Ph. D. Thesis)". PhD thesis. University of Twente, 1991.

[14] H. Evans and R. Snidle. "The Isothermal Elastohydrodynamic Lubrication of Spheres". *ASME J Lubric Technol* 103, 1981, pp. 57–547.

[15] W. Habchi, D. Eyheramendy, P. Vergne, and G. Morales. "A Full-System Approach of the Elastohydrodynamic Line / Point Contact Problem". *Trans. ASME, Journal of Tribology* 130 (2), 2008, pp. 1–10.

[16] D. Dowson. "A generalized Reynolds equation for fluid-film lubrication". *International Journal of Mechanical Sciences* 4.2, 1962, pp. 159 –170.

[17] H. S. Cheng and B. Sternlicht. "A Numerical Solution for the Pressure, Temperature, and Film Thickness Between Two Infinitely Long, Lubricated Rolling and Sliding Cylinders, Under Heavy Loads". *Journal of Basic Engineering* 87.3, 1965, pp. 695–704.

[18] H. S. Cheng. "A Refined Solution to the Thermal-Elastohydrodynamic Lubrication of Rolling and Sliding Cylinders". *ASLE Trans.* 8, 1965, pp. 397–410.

[19] W. Habchi, D. Eyheramendy, S Bair, P Vergne, and G Morales-Espejel. "Thermal elastohydrodynamic lubrication of point contacts using a Newtonian/generalized Newtonian lubricant". *Tribology letters* 30.1, 2008, pp. 41–52.

[20] R. Gohar and A. Cameron. "The Mapping of Elastohydrodynamic Contacts". *ASLE Transactions* 10.3, 1967, pp. 215–225.

[21] C. A. Foord, W. C. Hammann, and A. Cameron. "Evaluation of Lubricants Using Optical Elastohydrodynamics". *ASLE Transactions* 11.1, 1968, pp. 31–43.

[22] H. S. Cheng. "Isothermal elastohydrodynamic theory for the full range of pressure-viscosity coefficient". *ASLE Transactions* 8, 1972, pp. 397–410.

[23] A. P. Vazquez. "Lubricant starvation in elastohydrodynamic large-size spinning contacts". PhD thesis. Université de Lyon, 2020.

[24] L. Wedeven, D. Evans, and A. Cameron. "Optical analysis of ball bearing starvation". *Trans. ASME, J. Lubric. Technol.* 93, 1971, pp. 349–363.

[25] Y. P. Chiu. "An Analysis and Prediction of Lubricant Film Starvation in Rolling Contact Systems". *ASLE Transactions* 17.1, 1974, pp. 22–35.

[26] G. Guangteng and H. Spikes. "Fractionation of liquid lubricants at solid surfaces". *Wear* 200.1-2, 1996, pp. 336–345.

[27] J. J. Coy and E. V. Zaretsky. "Some limitations in applying classical EHD film thickness formulas to a high-speed bearing". *J. of Lubr. Technol.* 2.103, 1981, pp. 295–304.

[28] P. E. Wolveridge, K. P. Baglin, and J. F. Archard. "The starved lubrication of cylinders in line contact". *ARCHIVE: Proceedings of the Institution of Mechanical Engineers 1847-1982 (vols 1-196)* 185, 1970, pp. 1159–1170.

[29] B. J. Hamrock and D. Dowson. "Isothermal Elastohydrodynamic Lubrication of Point Contacts: Part III—Fully Flooded Results". *Journal of Lubrication Technology* 99.2, 1977, pp. 264–275.

[30] H. G Elrod. "A cavitation algorithm". *J. Lubr. Technol.* 103(3), 1981, pp. 350–54.

[31] F. Chevalier. "Modélisation des conditions d'alimentation dans les contacts Elastohydrodynamiques ponctuels". PhD Thesis. Insa de Lyon, 1996.

[32] B. Damiens. "Modéisation de la lubrification sous -alimentée dans les contacts elastohydrodynamiques elliptiques". PhD Thesis. Insa de Lyon, 2003.

[33] M. Van Zoelen. "Thin layer flow in rolling element bearings". PhD Thesis. University of Twente, 2009.

[34] D. Dowson and T. C.M. *Fundamental aspects of cavitation on bearings.* 1st Leeds-Lyon Symposium: Ed. by Dowson, Godet and Taylor, 1975.

[35] D. Brewe, J. Ball, and M. Khonsari. "Current research in cavitating fluid films". *NASA STI/Recon Technical Report N* 90, 1990, p. 28791.

[36] L. Floberg. "On hydrodynamic lubrication with special reference to subcavity pressures and number of streamers in cavitation regions". *Acta. Poly. Scan* M.E.19, 1965, pp. 3–35.

[37] L. Floberg. "On journal bearing lubrication considering the tensile strength of the liquid lubricant". *Transactions of the Machine Elements Division*, 1973, pp. 1–26.

[38] L. Floberg. "Sub-cavity pressure and number of oil streamers in cavitation regions with special reference to the infinite". *Journal Bearing Mech. Engng.: Acta Polytechnica Scandinavica.–1968.–Ser* 37, 1968.

[39] M. Hopkins. "Viscous flow between rotating cylinders and a sheet moving between them". *Brit. Jour. Appl. Phys.* 8, 1957, pp. 442–444.

[40] G. Bayada and L. Chupin. "Compressible Fluid Model for Hydrodynamic Lubrication Cavitation". *Journal of Tribology* 135.4, 2013, p. 041702.

[41] L Gümbel. "Das problem der Lagerreibung". *Mbl. Berlin. Bez. Ver. dtsch. Ing* 5, 1914, pp. 87–104.

[42] W. Stieber. *Das schwimmlager: Hydrodynamische Theorie des Gleitlagers.* V.D.I. Verlag GMBH, Berlin, 1933.

[43] B. Jakobsson, L. Floberg, and L. Floberg. "The Finite Journal Bearing, Considering Vaporization". *Transaction of Chalmers University of Technology*, 1957, pp. 1–117.

[44] K.-O. Olsson. "Cavitation in dynamically loaded bearings". *Transactions of Chalmers University of Technology* 308, 1965.

[45] V. Bruyere, N. Fillot, G. E. Morales-Espejel, and P. Vergne. "A Two-Phase Flow Approach for the Outlet of Lubricated Line Contacts". *Journal of Tribology* 134.4, 2012, p. 041503.

[46] K. Stadler, N. Izumi, T. Morita, J. Sugimura, and B. Piccigallo. "Estimation of Cavity Length in EHL Rolling Point Contact". *Journal of Tribology* 130.3, 2008, p. 031502.

[47] E. van Emden, C. Venner, and G. Morales-Espejel. "Aspects of flow and cavitation around an EHL contact". *Tribology International* 95, 2016, pp. 435–448.

[48] T. Otsu, H. Tanaka, N. Izumi, and J. Sugimura. "Effect of Surrounding Gas on Cavitation in EHL". *Tribology Online* 4.2, 2009, pp. 50–54.

[49] E. Harika, J. Bouyer, M. Fillon, and M. Hélène. "Effects of Water Contamination of Lubricants on Hydrodynamic Lubrication: Rheological and Thermal Modeling". *Journal of Tribology* 135.4, 2013, p. 041707.

[50] H. Bai, Y. Wang, Y. Ma, Q. Zhang, and N. Zhang. "Effect of CO2 partial pressure on the corrosion behavior of J55 carbon steel in 30% crude oil/brine mixture". *Materials* 11.9, 2018, p. 1765.

[51] G. E. Morales-Espejel, H. H. Wallin, R. Hauleitner, and M. Arvidsson. "Progress in rolling bearing technology for refrigerant compressors". *Proceedings of the Institution of Mechanical Engineers, Part C: Journal of Mechanical Engineering Science* 232.16, 2018, pp. 2948–2961.

[52] G. Morales-Espejel, A Gabelli, and C Vieillard. "Hybrid bearings lubricated with pure refrigerants". *SRM Technical Screw Compressor Conference*. 2001, pp. 4–7.

[53] G. Morales-Espejel, R Hauleitner, and H. Wallin. "Pure Refrigerant Lubrication Technology in Oil Free Centrifugal Compressors". *SKF Evolution* 1, 2017, pp. 26–30.

[54] X. Wu, Z. Xing, Z. He, X. Wang, and W. Chen. "Effects of lubricating oil on the performance of a semi-hermetic twin screw refrigeration compressor". *Applied Thermal Engineering* 112, 2017, pp. 340–351.

[55] M. Akei and K. Mizuhara. "The Elastohydrodynamic Properties of Lubricants in Refrigerant Environments". *Tribology Transactions* 40.1, 1997, pp. 1–10.

[56] M. Akei, K Mizuhara, T Taki, and T Yamamoto. "Evaluation of film-forming capability of refrigeration lubricants in pressurized refrigerant atmosphere". *Wear* 196.1-2, 1996, pp. 180–187.

[57] F. P. Wardle, B. Jacobson, H. Dolfsma, E. Hoglund, and U. Jonsson. "The effect of refrigerants on the lubrication of rolling element bearings used in screw compressors". *Proceedings of the 1992 International Compressor Engineering Conference at Purdue*. 1992, pp. 523–534.

[58] U. Jonsson. "Elastohydrodynamic lubrication and lubricant rheology in refrigeration compressors". PhD thesis. Luleå tekniska universitet, 1998.

[59] U. Jonsson and E. Höglund. "Determination of viscosities of oil-refrigerant mixtures at equilibrium by means of film thickness measurements". *Ashrae transactions* 99.2, 1993, pp. 1129–1136.

[60] M. Muraki and T. Sano. "Determination of Film Thickness and Traction of Polyol Ester under an EHD Contact in Some Refrigerant Environments". *Tribology Transactions* 43.1, 2000, pp. 15–20.

[61] S. Bair, W. Habchi, M. Baker, and D. M. Pallister. "Quantitative Elastohydrodynamic Film-Forming for an Oil / Refrigerant System". *Journal of Tribology* 139.6, 2017, p. 061501.

[62] U. J. Jonsson and K. C. Lilje. "Elastohydrodynamic lubrication properties of polyol ester lubricants-R134a mixtures". *Tribologia: Finnish Journal of Tribology* 18.1, 1999, pp. 31–37.

[63] S. Bair, M. Baker, and D. M. Pallister. "The high-pressure viscosity of refrigerant/oil systems: The High-pressure viscosity of refrigerant/oil systems". *Lubr. Sci.* 29.6, 2017, pp. 377–394.

[64] M. Leung, C. K. Jotshi, D. Y. Goswami, D. O. Shah, and A. Gregory. "Measurements of Absorption Rates of HFC Single and Blended Refrigerants in POE Oils". *HVAC&R Res.* 4.2, 1998, pp. 141–151.

[65] U. J. Jonsson. "Lubrication limits of rolling element bearings in refrigeration compressors". *Tribologia: Finnish Journal of Tribology* 18.1, 1999, pp. 23–30.

[66] S. Bair. "A critical evaluation of film thickness-derived pressure–viscosity coefficients". *Lubrication Science* 27.6, 2015, pp. 337–346.

[67] S. Bair, L. Martinie, and P. Vergne. "Classical EHL Versus Quantitative EHL: A Perspective Part II—Super-Arrhenius Piezoviscosity, an Essential Component of Elastohydrodynamic Friction Missing from Classical EHL". *Tribol Lett* 63.3, 2016, p. 37.

[68] R Larsson, P. O. Larsson, E Eriksson, M Sjöberg, and E Höglund. "Lubricant properties for input to hydrodynamic and elastohydrodynamic lubrication analyses". *Proceedings of the Institution of Mechanical Engineers, Part J: Journal of Engineering Tribology* 214.1, 2000, pp. 17–27.

[69] D. E. P. Gonçalves, J. M. Liñeira del Rio, M. J. P. Comuñas, J. Fernández, and J. H. O. Seabra. "High Pressure Characterization of the Viscous and Volumetric Behavior of Three Transmission Oils". *Ind. Eng. Chem. Res.* 58.4, 2019, pp. 1732–1742.

[70] V. Geller, M. Paulaitis, D. Bivens, and A Yokozeki. "Viscosities of HFC-32 and HFC-32/lubricant mixtures". *International journal of thermophysics* 17.1, 1996, pp. 75–83.

[71] M. J. Comuñas, A. Baylaucq, C. Boned, and J. Fernandez. "Dynamic viscosity for HFC-134a+ polyether mixtures up to 373.15 K and 140 MPa at low polyether concentration. Measurements and modeling". *Industrial & engineering chemistry research* 43.3, 2004, pp. 804–814.

[72] M. A. Monsalvo, A. Baylaucq, P. Reghem, S. Quiñones-Cisneros, and C. Boned. "Viscosity measurements and correlations of binary mixtures: 1, 1, 1, 2-tetrafluoroethane (HFC-134a)+ tetraethylene glycol dimethylether (TEGDME)". *Fluid phase equilibria* 233.1, 2005, pp. 1–8.

[73] M. A. Monsalvo, A. Baylaucq, S. E. Quiñones-Cisneros, and C. Boned. "High-pressure viscosity behavior of x 1, 1, 1, 2-tetrafluoroethane (HFC-134a)+(1- x) triethylene glycol dimethylether (TriEGDME) mixtures: Measurements and modeling". *Fluid phase equilibria* 247.1-2, 2006, pp. 70–79.

[74] S. Gunsel and M. Pozebanchuk. "Elastohydrodynamic Lubrication With Polyolester Lubricants and HFC Refrigerants". *Air Conditioning and Refrigeration Technology Institute, Arlington, VA* 1, 1999, pp. 23810–102.

[75] S. Bair. "A New High-Pressure Viscometer for Oil/Refrigerant Solutions and Preliminary Results". *Tribology Transactions* 60.3, 2017, pp. 392–398.

[76] S. Bair and A. Laesecke. "Viscosity measurements of R32 and R410A to 350 MPa". *International Journal of Refrigeration* 83, 2017, pp. 157–167.

[77] S. Bair, M. Baker, and D. M. Pallister. "Revisiting the Compressibility of Oil/Refrigerant Lubricants". *Journal of Tribology* 139.2, 2017, p. 024501.

[78] V. Lacerda, A. Prata, and F. Fagotti. "Experimental characterization of oil-refrigerant two-phase flow". *American Society of Mechanical Engineers, Advanced Energy Systems Division (Publication) AES* 40, 2000, pp. 101–109.

[79] E. Poiate Jr. and J. L. Gasche. "Foam flow of oil-refrigerant R12 mixture in a small diameter tube". *J. Braz. Soc. Mech. Sci. & Eng.* 28.4, 2006, pp. 390–398.

[80] H. O. S. Castro, J. L. Gasche, and A. T. Prata. "Pressure drop correlation for oil–refrigerant R134a mixture flashing flow in a small diameter tube". *International Journal of Refrigeration* 32.3, 2009, pp. 421–429.

[81] H. O. S. Castro, J. L. Gasche, W. P. Conti, and E. D. R. Vieira. "Flow patterns of the ester oil-refrigerant R134a mixture flashing flow through a small diameter tube". *RETERM* 7.1, 2008, p. 41.

[82] H. O. S. Castro and J. L. Gasche. "Foam flow of oil-refrigerant R134a mixture in a small diameter tube". *International Heat Transfer Conference 13*. Begel House Inc. 2006.

[83] J. P. Dias, J. L. Gasche, and A. L. Seixlack. "Mathematical Modeling of the Ester Oil-Refrigerant R134a Mixture Two-Phase Flow with Foam Formation Through a Small Diameter Tube". *J. Braz. Soc. Mech. Sci. & Eng.* 33.3, 2011, pp. 314–323.

[84] J. Barbosa, V. Lacerda, and A. Prata. "Prediction of pressure drop in refrigerant–lubricant oil flows with high contents of oil and refrigerant outgassing in small diameter tubes". *International Journal of Refrigeration* 27.2, 2004, pp. 129–139.

[85] F. P. Grando, M. Priest, and A. T. Prata. "A two-phase flow approach to cavitation modelling in journal bearings". *Tribol Lett* 21.3, 2006, pp. 233–244.

[86] F. P. Grando, M Priest, and A. T. Prata. "Lubrication in refrigeration systems: Numerical model for piston dynamics considering oil-refrigerant interaction". *Proceedings of the Institution of Mechanical Engineers, Part J: Journal of Engineering Tribology* 220.3, 2006, pp. 245–258.

[87] J. L. Gasche, T. Andreotti, and C. R. M. Maia. "A model to predict R134a refrigerant leakage through the radial clearance of rolling piston compressors". *International Journal of Refrigeration* 35.8, 2012, pp. 2223–2232.

[88] J. Lancaster. "A review of the influence of environmental humidity and water on friction, lubrication and wear". *Tribology International* 23.6, 1990, pp. 371–389.

[89] J. Fitch and S. Jaggernauth. "Moisture–The second most destructive lubricant contaminate, and its effects on bearing life". *P/PM Technology* 12, 1994, pp. 1–4.

[90] W. M. Needelman, M. A. Barris, G. L. LaVallee, et al. "Contamination control for wind turbine gearboxes". *Power Engineering* 113.11, 2009, p. 112.

[91] X. Liu, J. Wang, L. Huang, J. Zhang, C. Xu, L. Tong, and D. Guo. "Direct observation of the impact of water droplets on oil replenishment in EHD lubricated contacts". *Friction* 10.3, 2022, pp. 388–397.

[92] G. T. Y. Wan and H. A. Spikes. "The Elastohydrodynamic Lubricating Properties of Water-Polyglycol Fire-Resistant Fluids". *A S L E Transactions* 27.4, 1984, pp. 366–372.

[93] H. Cen. *Effect of water on the performance of lubricants and related tribochemistry in boundary lubricated steel/steel contacts*. University of Leeds, 2012.

[94] D. C. Barker, G. J. Johnston, H. A. Spikes, and T. F. Bünemann. "EHD Film Formation and Starvation of Oil-in-Water Emulsions". *Tribology Transactions* 36.4, 1993, pp. 565–572.

[95] J. Hili, C. Pelletier, L. Jacobs, A. Olver, and T. Reddyhoff. "High-Speed Elastohydrodynamic Lubrication by a Dilute Oil-in-Water Emulsion". *Tribology Transactions* 61.2, 2018, pp. 287–294.

[96] H. Liang, D. Guo, L. Ma, and J. Luo. "Increased Film Thickness of Oil-in-Water (O/W) Emulsions at High Speed". *Tribol Lett* 65.2, 2017, p. 68.

[97] S.-W. Lo, T.-C. Yang, Y.-A. Cian, and K.-C. Huang. "A Model for Lubrication by Oil-in-Water Emulsions". *Journal of Tribology* 132.1, 2010, p. 011801.

[98] W. Wilson, Y. Sakaguchi, and S. Schmid. "A dynamic concentration model for lubrication with oil-in-water emulsions". *Wear* 161.1-2, 1993, pp. 207–212.

[99] H. Yang, S. R. Schmid, T. J. Kasun, and R. A. Reich. "Elastohydrodynamic Film Thickness and Tractions for Oil-in-Water Emulsions". *Tribology Transactions* 47.1, 2004, pp. 123–129.

[100] D. Zhu, G Biresaw, S. Clark, and T. Kasun. "Elastohydrodynamic Lubrication With 0/W Emulsions". *Journal of tribology* 116.2, 1994, pp. 310–320.

[101] E. Harika, M. Helene, J. Bouyer, and M. Fillon. "Impact of lubricant contamination with water on hydrodynamic thrust bearing performance". *Mécanique & Industries* 12.5, 2011, pp. 353–359.

[102] "Chapter 21 Lubricant contamination". *Rheology and Elastohydrodynamic Lubrication*. Ed. by B. O. Jacobson. Vol. 19. Tribology Series. Elsevier, 1991, pp. 341 –356.

[103] R. E. Cantley. "The effect of water in lubricating oil on bearing fatigue life". *ASLE transactions* 20.3, 1977, pp. 244–248.

[104] D. S. Kolotova, Y. A. Kuchina, L. A. Petrova, N. G. Voron'ko, and S. R. Derkach. "Rheology of Water-in-Crude Oil Emulsions: Influence of Concentration and Temperature". *Colloids and Interfaces* 2.4, 2018, p. 64.

[105] H. Hamaguchi, H. A. Spikes, and A. Cameron. "Elastohydrodynamic properties of water in oil emulsions". *Wear* 43.1, 1977, pp. 17 –24.

[106] W. Liu, D. Dong, Y. Kimura, and K. Okada. "Elastohydrodynamic lubrication with water-in-oil emulsions". *Wear* 179.1-2, 1994, pp. 17–21.

[107] J. J. Benner, F. Sadeghi, M. R. Hoeprich, and M. C. Frank. "Lubricating Properties of Water in Oil Emulsions". *Journal of Tribology* 128.2, 2006, pp. 296–311.

[108] G. Dalmaz and M. Godet. "Film Thickness and Effective Viscosity of Some Fire Resistant Fluids in Sliding Point Contacts". *Journal of Lubrication Technology* 100.2, 1978, pp. 304–307.

[109] G. Dalmaz. "Traction and film thickness measurements of a water glycol and a water in oil emulsion in rolling-sliding point contacts". *Friction and Traction, Proc. of the 7th Leeds-Lyon Symp.* 1981, pp. 231–242.

[110] M. Ratoi-Salagean and H. A. Spikes. "The lubricant film-forming properties of modern fire resistant hydraulic fluids". *ASTM special technical publication* 1310, 1997, pp. 21–37.

[111] T. Nakahara. "Observations of Liquid Droplet Behavior and Oil Film Formation in O/W Type Emulsion Lubrication". *Trans. ASME, J. of Trib.* 110, 1988, p. 348.

[112] H. Yang, S. R. Schmid, R. A. Reich, and T. J. Kasun. "Direct Observations of Emulsion Flow in Elastohydrodynamically Lubricated Contacts". *Journal of Tribology* 128.3, 2006, pp. 619–623.

[113] L. Ma, C. Zhang, and J. Luo. "Direct observation on the behaviour of emulsion droplets and formation of oil pool under point contact". *Appl. Phys. Lett.* 101.24, 2012, p. 241603.

[114] A. Al-Sharif, K. Chamniprasart, K. R. Rajagopal, and A. Z. Szeri. "Lubrication With Binary Mixtures: Liquid-Liquid Emulsion". *Journal of Tribology* 115.1, 1993, pp. 46–55.

[115] S. H. Wang, A. Al-Sharif, K. R. Rajagopal, and A. Z. Szeri. "Lubrication With Binary Mixtures: Liquid-Liquid Emulsion in an EHL Conjunction". *Journal of Tribology* 115.3, 1993, pp. 515–522.

[116] S. Yan and S. Kuroda. "Lubrication with emulsion: first report, the extended Reynolds equation". *Wear* 206.1-2, 1997, pp. 230–237.

[117] W. R. D. Wilson, Y. Sakaguchi, and S. R. Schmid. "A Mixed Flow Model for Lubrication with Emulsions". *Tribology Transactions* 37.3, 1994, pp. 543–551.

[118] F. Cyriac, P. M. Lugt, R. Bosman, and C. H. Venner. "Impact of Water on EHL Film Thickness of Lubricating Greases in Rolling Point Contacts". *Tribol Lett* 61.3, 2016, p. 23.

[119] M. Youbi-Idrissi. "Impact de l'huile de lubrification sur les performances thermodynamiques des pompes à chaleur réversibles". PhD thesis. Conservatoire national des arts et metiers-CNAM, 2003.

[120] F. Zhang, N. Fillot, R. Hauleitner, and G. Morales Espejel. "Thermal-EHD contacts lubricated with oil/refrigerant solutions: a new cavitation modeling approach based on refrigerant solubility". *Journal of Tribology*, 2022, pp. 1–19.

[121] M. A. K. Mizuharab and T Yamamoto. "Evaluation of film-forming capability of refrigeration lubricants in pressurized refrigerant atmosphere". *wear* 196, 1996, pp. 180–187.

[122] M. J. Braun and W. M. Hannon. "Cavitation formation and modelling for fluid film bearings: A review". *Proceedings of the Institution of Mechanical Engineers, Part J: Journal of Engineering Tribology* 224.9, 2010, pp. 839–863.

[123] H. Elrod and M. Adams. "Cavitation and related phenomena in lubrication". *Proceedings - Mech. Eng. Publ. ltd*, 1975, pp. 37–42.

[124] D. Vijayaraghavan and T. G. Keith Jr. "An efficient, robust, and time accurate numerical scheme applied to a cavitation algorithm". *Journal of Tribollogy* 112(1), 1990, pp. 44–51.

[125] D. BREWE. "Theoretical modeling of the vapor cavitation in dynamically loaded journal bearings". *Journal of tribology* 108.4, 1986, pp. 628–638.

[126] F. Sahlin, A. Almqvist, R. Larsson, and S. Glavatskih. "A cavitation algorithm for arbitrary lubricant compressibility". *Tribology International* 40.8, 2007, pp. 1294–1300.

[127] A. Kumar and J. F. Booker. "A Finite Element Cavitation Algorithm". *Journal of Tribology* 113.2, 1991, pp. 276–284.

[128] S. Boedo, J. F. Booker, and M. J. Wilkie. "A mass conserving modal analysis for elastohydrodynamic lubrication". *Tribology Series*. Vol. 30. Elsevier, 1995, pp. 513–523.

[129] D. Bonneau, D. Guines, J. Frene, and J. Toplosky. "EHD analysis, including structural inertia effects and a mass-conserving cavitation model". *Journal of tribology* 117.3, 1995, pp. 540–547.

[130] K. G. Murty et al. "Note on a Bard-type scheme for solving the complementarity problem". *Opsearch* 11.2-3, 1974, pp. 123–130.

[131] F. Grando, M. Priest, and A. Prata. "Lubrication in Refrigeration Systems: Performance of Journal Bearings Lubricated with Oil and Refrigerant Mixtures". *Tribology and Interface Engineering Series*. Vol. 48. Elsevier, 2005, pp. 481–491.

[132] D. E. A. van Odyck and C. H. Venner. "Compressible Stokes Flow in Thin Films". *Journal of Tribology* 125.3, 2003, pp. 543–551.

[133] E. van Emden, C. Venner, and G. Morales-Espejel. "A challenge to cavitation modeling in the outlet flow of an EHL contact". *Tribology International* 102, 2016, pp. 275–286.

[134] A. Porras-Vazquez, N. Fillot, P. Vergne, D. Philippon, and G. E. Morales-Espejel. "Influence of spin on film thickness in elastohydrodynamic starved point contacts". *Tribology International* 156, 2021, p. 106825.

[135] C. Xing, M. J. Braun, and H. Li. "A Three-Dimensional Navier-Stokes–Based Numerical Model for Squeeze-Film Dampers. Part 1—Effects of Gaseous Cavitation on Pressure Distribution and Damping Coefficients without Consideration of Inertia". *Tribology Transactions* 52.5, 2009, pp. 680–694.

[136] X.-s. Li, Y. Song, Z.-r. Hao, and C.-w. Gu. "Cavitation Mechanism of Oil-Film Bearing and Development of a New Gaseous Cavitation Model Based on Air Solubility". *Journal of Tribology* 134.3, 2012, p. 031701.

[137] W. Martz, C. Burton, and A. Jacobi. "Local composition modelling of the thermodynamic properties of refrigerant and oil mixtures". *International Journal of Refrigeration* 19.1, 1996, pp. 25–33.

[138] L. Tao, S. Diaz, L. S. Andre´s, and K. R. Rajagopal. "Analysis of Squeeze Film Dampers Operating With Bubbly Lubricants". *Journal of Tribology* 122.1, 2000, pp. 205–210.

[139] E. W. Llewellin, H. M. Mader, and S. D. R. Wilson. "The rheology of a bubbly liquid". *Proc. R. Soc. Lond. A* 458.2020, 2002, pp. 987–1016.

[140] Y. Murai and H. Oiwa. "Increase of effective viscosity in bubbly liquids from transient bubble deformation". *Fluid Dyn. Res.* 40.7-8, 2008, pp. 565–575.

[141] T. N. Wong and K. T. Ooi. "Refrigerant flow in capillary tube: an assessment of the two-phase viscosity correlations on model prediction". *International communications in heat and mass transfer* 22.4, 1995, pp. 595–604.

[142] W. L. Owens. "Two-phase pressure gradient". *Int. Dev. in heat transfer*, 1961.

[143] A. Cicchitti, C. Lombardi, M. Silvestri, G. Soldaini, and R. Zavattarelli. *Two-phase cooling experiments: pressure drop, heat transfer and burnout measurements*. Tech. rep. Centro Informazioni Studi Esperienze, Milan, 1959.

[144] A. E. Dukler, M. Wicks, and R. G. Cleveland. "Frictional pressure drop in two-phase flow: A. A comparison of existing correlations for pressure loss and holdup". *AIChE J.* 10.1, 1964, pp. 38–43.

[145] W. H. McAdams. "Vaporization inside horizontal tubes-II, Benzene oil mixtures". *Trans. ASME* 64, 1942, pp. 193–200.

[146] D. R. Beattie and P. B. Whalley. "Simple two-phase frictional pressure drop calculation method". *Int. J. Multiphase Flow;(United Kingdom)* 8.1, 1982.

[147] S. Lin, C. C. K. Kwok, R.-Y. Li, Z.-H. Chen, and Z.-Y. Chen. "Local frictional pressure drop during vaporization of R-12 through capillary tubes". *International Journal of Multiphase Flow* 17.1, 1991, pp. 95–102.

[148] A. Asnaghi, A. Feymark, and R. Bensow. "Improvement of cavitation mass transfer modeling based on local flow properties". *International Journal of Multiphase Flow* 93, 2017, pp. 142–157.

[149] D. D. Joseph. "Cavitation and the state of stress in a flowing liquid". *Journal of Fluid Mechanics* 366.-1, 1998, pp. 367–378.

[150] Y. Yang, W. Li, W. Shi, W. Zhang, and M. A. El-Emam. "Numerical Investigation of a High-Pressure Submerged Jet Using a Cavitation Model Considering Effects of Shear Stress". *Processes* 7.8, 2019, p. 541.

[151] P. Yang and S. Wen. "A Generalized Reynolds Equation for Non-Newtonian Thermal Elastohydrodynamic Lubrication". *Journal of Tribology* 112.4, 1990, pp. 631–636.

[152] R. L. Panton and S. Berger. "Incompressible Flow". *Journal of Applied Mechanics* 52.2, 1985, p. 500.

[153] W Habchi. "Coupling strategies for finite element modeling of thermal elastohydrodynamic lubrication problems". *Journal of Tribology* 139.4, 2017, p. 041501.

[154] V. Strubel, S. Simoens, P. Vergne, N. Fillot, F. Ville, M. El Hajem, N. Devaux, A. Mondelin, and Y. Maheo. "Fluorescence tracking and μ-PIV of individual particles and lubricant flow in and around lubricated point contacts". *Tribology Letters* 65.3, 2017, pp. 1–15.

[155] R. Abu-Much, S. Basheer, A. Basheer, and M. Hugerat. "Going inside Colored Solutions: The Optical Microscope as a Tool for Studying the Chemistry of Hydrophilic and Hydrophobic Materials". *J. Chem. Educ.* 90.9, 2013, pp. 1207–1211.

[156] J Molimard, M Querry, and P Vergne. "New tools for the experimental study of EDH and limit lubrications". *Tribology series*. Vol. 36. Elsevier, 1999, pp. 717–726.

[157] V. Strubel, N. Fillot, F. Ville, J. Cavoret, P. Vergne, A. Mondelin, and Y. Maheo. "Particle entrapment in hybrid lubricated point contacts". *Tribology Transactions* 59.4, 2016, pp. 768–779.

[158] C. Roelands, J. Vluger, and H. Waterman. "Correlational Aspects of the Viscosity-Temperature-Pressure Relationship of Lubricating Oils and in Correlation with Chemical Constitution". *Trans. ASME., J.Basic Eng.* 11, 1963, pp. 601–619.

[159] R. Clift, J. R. Grace, and M. E. Weber. *Bubbles, drops, and particles*. San Diego: Academic Press, 1978.

[160] G. G. Stokes. "Report on recent researches in hydrodynamics". *Brit. Assoc. Rep* 1, 1846, pp. 1–20.

[161] J. Sivasamy, T.-N. Wong, N.-T. Nguyen, and L. T.-H. Kao. "An investigation on the mechanism of droplet formation in a microfluidic T-junction". *Microfluidics and nanofluidics* 11.1, 2011, pp. 1–10.

[162] F. Bai, X. He, X. Yang, R. Zhou, and C. Wang. "Three dimensional phase-field investigation of droplet formation in microfluidic flow focusing devices with experimental validation". *International Journal of Multiphase Flow* 93, 2017, pp. 130–141.

[163] A. Laesecke and S. Bair. "High-Pressure Viscosity Measurements of 1,1,1,2-Tetrafluoroethane". *Int J Thermophys* 32.5, 2011, pp. 925–941.

[164] E. d. C. Andrade. "The viscosity of liquids". *Nature* 125.3148, 1930, pp. 309–310.

[165] E. McEwen. "The effect of variation of viscosity with pressure on the load-carrying capacity of the oil film between gear-teeth". *J. Inst. Pet* 38.344-345, 1952, pp. 646–672.

[166] M. R. Conde. "Estimation of thermophysical properties of lubricating oils and their solutions with refrigerants: An appraisal of existing methods". *Applied Thermal Engineering* 16.1, 1996, pp. 51–61.

[167] Y Mermond, C Marvillet, and M Feidt. "Thermodynamic and physical properties of mixtures of refrigerants and oils; Proprietes thermodynamiques et physiques des melanges de fluides frigorigenes et d'huiles". *International Journal of Refrigeration* 22, 1999.

[168] G. Totten, R. Shah, and D. Forester. *Fuels and Lubricants Handbook: Technology, Properties, Performance, and Testing 2nd Edition*. West Conshohocken, PA: ASTM International, 2019.

[169] Y. Zhang and M. He. "Kinematic viscosity of R410A and R407C refrigerant- oil mixtures in the saturated liquid phase with lubricant mass fraction in the range of (0 to 0.0001)". *Journal of Chemical & Engineering Data* 55.8, 2010, pp. 2886–2889.

[170] A. Laesecke, R. Perkins, and C. Nieto de Castro. "Thermal conductivity of R134a". *Fluid Phase Equilibria* 80, 1992, pp. 263–274.

[171] M. McLinden, S. Klein, E. Lemmon, and A. Peskin. "REFPROP—thermodynamic and transport properties of refrigerants and refrigerant mixtures, version 6.0". *Washington (DC): NIST*, 1998.

[172] *DuPont HFC-134a Properties, Uses, Storage, and Handling. (Accessed 2020-04-03)*.

[173] J. Raisin, N. Fillot, P. Vergne, and D. Dureisseix. "Numerical simulation of lubricated DLC-coated point contacts under infinite sliding conditions". *Tribology International* 133, 2019, pp. 136–151.

[174] W. Habchi and S. Bair. "The role of the thermal conductivity of steel in quantitative elastohydrodynamic friction". *Tribology International* 142, 2020, p. 105970.

[175] I. Etsion. "Observation of Pressure Variation in the Cavitation Region of Submerged Journal Bearings". *J. Lub. Tech.* 104, 1982, p. 157.

[176] M. Braun and R. Hendricks. "An experimental investigation of the vaporous/gaseous cavity characteristics of an eccentric journal bearing". *ASLE transactions* 27.1, 1984, pp. 1–14.

[177] J. P. Dias, J. R. Barbosa Jr., and A. T. Prata. "Dynamics of gas bubble growth in oil-refrigerant mixtures under isothermal depressurization". *J. Braz. Soc. Mech. Sci. & Eng.* 34.2, 2012, pp. 155–166.

[178] G. Nijenbanning, C. Venner, and H. Moes. "Film thickness in elastohydrodynamically lubricated elliptic contacts". *Wear* 176.2, 1994, pp. 217–229.

[179] B. Meziane, P. Vergne, N. Devaux, L. Lafarge, G. E. Morales-Espejel, and N. Fillot. "Film thickness build-up in zero entrainment velocity wide point contacts". *Tribology International* 141, 2020, p. 105897.

[180] Y. Kimura and K. Okada. "Lubricating Properties of Oil-In-Water Emulsions". *Tribology Transactions* 32.4, 1989, pp. 524–532.

[181] S. G. Oh and D. O. Shah. "Effect of counterions on the interfacial tension and emulsion droplet size in the oil/water/dodecyl sulfate system". *J. Phys. Chem.* 97.2, 1993, pp. 284–286.

[182] A. M. Kabir, D. Inoue, Y. Kishimoto, J.-i. Hotta, K. Sasaki, N. Kitamura, J. P. Gong, H. Mayama, A. Kakugo, et al. "Drag force on micron-sized objects with different surface morphologies in a flow with a small Reynolds number". *Polymer Journal* 47.8, 2015, pp. 564–570.

[183] V. Bruyere, N. Fillot, G. E. Morales-Espejel, and P. Vergne. "Computational fluid dynamics and full elasticity model for sliding line thermal elastohydrodynamic contacts". *Tribology International* 46, 2012, pp. 3 –13.

[184] D. P. Schmidt, C. Rutland, and M. L. Corradini. "A fully compressible,two-dimensional model of small, high-speed, cavitating nozzles". *Atomization and sprays* 9-3, 1999, pp. 255–276.

[185] J.-B. Moreau. "Modélisation de l'écoulement polyphasique à l'intérieur et en sortie des injecteurs diesel". PhD thesis. Institut National Polytechnique de Toulouse-INPT, 2005.

[186] G. Aubry. "Microresonateurs optiques à etat liquide et microfluidique digitale: applications aux lasers à colorant en gouttes pour les laboratoires-sur-puce". PhD thesis. Université Paris Sud-Paris XI, 2011.

[187] J. Luo, X. Hu, and N. Adams. "A conservative sharp interface method for incompressible multiphase flows". *Journal of Computational Physics* 284, 2015, pp. 547–565.

[188] J. Kim. "Phase-Field Models for Multi-Component Fluid Flows". *Commun. comput. phys.* 12.3, 2012, pp. 613–661.

[189] S. Gross and A. Reusken. *Numerical methods for two-phase incompressible flows*. Vol. 40. Springer Science & Business Media, 2011.

[190] T. J. Hughes, W. K. Liu, and T. K. Zimmermann. "Lagrangian-Eulerian finite element formulation for incompressible viscous flows". *Computer Methods in Applied Mechanics and Engineering* 29.3, 1981, pp. 329–349.

[191] S. Ganesan and L. Tobiska. "Computations of flows with interfaces using arbitrary Lagrangian Eulerian method". *ECCOMAS CFD 2006: Proceedings of the European Conference on Computational Fluid Dynamics, Egmond aan Zee*. The Netherlands, 2006.

[192] B. Maury. "Characteristics ALE Method for the Unsteady 3D Navier-Stokes Equations with a Free Surface". *International Journal of Computational Fluid Dynamics* 6.3, 1996, pp. 175–188.

[193] C. Hirt and B. Nichols. "Volume of fluid (VOF) method for the dynamics of free boundaries". *Journal of Computational Physics* 39.1, 1981, pp. 201–225.

[194] S. Osher and J. A. Sethian. "Fronts propagating with curvature-dependent speed: Algorithms based on Hamilton-Jacobi formulations". *Journal of Computational Physics* 79.1, 1988, pp. 12–49.

[195] D. Jacqmin. "Contact-line dynamics of a diffuse fluid interface". *J. Fluid Mech.* 402, 2000, pp. 57–88.

[196] A.-K. Tornberg and B. Engquist. "A finite element based level-set method for multiphase flow applications". *Computing and Visualization in Science* 3.1, 2000, pp. 93–101.

[197] J. Cahn and J. Hilliard. "Free Energy of a Nonuniform System. I. Interfacial Free Energy". *The Journal of chemical physics* 28, 1957, pp. 258–267.

[198] J. Cahn and J. Hilliard. "Free Energy of a Nonuniform System. III. Nucleation in a Two-Component Incompressible Fluid". *The Journal of chemical physics* 31, 1959, pp. 688–699.

[199] P. Yue, J. Feng, C. Liu, and J. Shen. "A diffuse interface method for simulating two-phase flows of complex fluids". *Journal of Fluid Mechanics* 515, 2004, pp. 293–317.

[200] D. Jacqmin. "Calculation of Two-Phase Navier-Stokes Flows Using Phase-Field Modeling". *Journal of Computational Physics* 155, 1999, pp. 96–127.

[201] H. D. Ceniceros, R. L. Ns, and A. M. Roma. "Three-dimensional, fully adaptive simulations of phase-field fluid models". *Journal of Computational Physics* 229.17, 2010, pp. 6135 –6155.

[202] K. Praveen, C. Pious, S. Thomas, and Y. Grohens. "Relevance of plasma processing on polymeric materials and interfaces". *Non-Thermal Plasma Technology for Polymeric Materials*. Elsevier, 2019, pp. 1–21.

[203] T. Young. "III. An essay on the cohesion of fluids". *Philosophical transactions of the royal society of London* 95, 1805, pp. 65–87.

FOLIO ADMINISTRATIF

THESE DE L'INSA LYON, MEMBRE DE L'UNIVERSITE DE LYON

NOM : ZHANG DATE de SOUTENANCE : 08/12/2022

Prénoms : Fan

TITRE : Elastohydrodynamic lubrication with mixtures of oil and operating fluids: an industrial challenge

NATURE : Doctorat Numéro d'ordre : 2022ISAL0121

Ecole doctorale : Mécanique, Energétique, Génie civil, Acoustique (MEGA)

Spécialité : Génie Mécanique

RESUME : Le fluide qui sépare les éléments en contact dans de nombreuses applications industrielles est souvent un mélange d'huile et de fluides environnants. Ce travail vise à fournir une meilleure compréhension de la lubrification avec des mélanges dans les contacts élastohydrodynamiques afin d'anticiper les performances du système. Le mélange huile/réfrigérant et le mélange huile/eau, représentant respectivement des fluides miscibles et des fluides non miscibles, sont étudiés de manière approfondie dans cette étude. Les questions essentielles diffèrent en fonction des caractéristiques des mélanges.

Dans le cas d'une solution huile/réfrigérant, la principale question se pose à la sortie du contact, où le réfrigérant peut s'évaporer. Une modélisation originale de la cavitation incluant des effets thermiques est rapportée dans ce travail. Une comparaison avec d'autres modèles de cavitation de la littérature est proposée, soulignant la nécessité de considérer la solubilité du réfrigérant dans l'huile pour de tels problèmes. En effet, les mélanges huile/réfrigérant peuvent réduire considérablement la quantité d'huile liquide pour le prochain contact par rapport à la cavitation de l'huile pure.

De manière tout à fait différente, le problème des gouttelettes d'eau dans l'émulsion d'huile est abordé à l'entrée du contact pour évaluer les risques de contamination. Des gouttelettes d'eau dans l'huile de tailles microscopiques sont observées directement à l'entrée du contact EHL. Une approche numérique a été développée pour étudier les impacts de divers paramètres de fonctionnement sur l'écoulement de l'émulsion. Les résultats de ce travail donnent une explication possible aux conclusions parfois contradictoires de la littérature, et révèlent les conditions critiques dans lesquelles l'émulsion « eau-dans-huile » influencerait les contacts EHD.

MOTS-CLÉS : Dynamique des fluides numérique, Mécanique des fluides, Ecoulement diphasique, Effets thermiques, Modélisation numérique, Emulsion, Mélange lubrifiant, Cavitation, Lubrification, Elastohydrodynamique

Laboratoire (s) de recherche : Laboratoire de mécanique des Contacts et des Structures (LaMCoS)

Directeur de thèse: FILLOT Nicolas

Président de jury : CAYER-BARRIOZ Juliette

Composition du jury : ARGHIR Mihaï, HARTL Martin, BRUYERE Vincent, FILLOT Nicolas, MORALES-ESPEJEL Guillermo